LAPPEENRANTA UNIVERSITY OF TECHNOLOGY
LUT School of Energy Systems
LUT Mechanical Engineering

Joni Reijonen

UTILIZING METALLIC WASTE STREAMS AS RAW MATERIAL FOR POWDER-BASED ADDITIVE MANUFACTURING

Examiners: Prof. Antti Salminen
M.Sc. (Tech.) Pasi Puukko

Supervisor: M.Sc. (Tech.) Antero Jokinen

TIIVISTELMÄ

Lappeenrannan teknillinen yliopisto
LUT School of Energy Systems
LUT Kone

Joni Reijonen

Metallisten jätevirtojen hyödyntäminen jauhetta käyttävän lisäävän valmistuksen raaka-aineena

Diplomityö

2016

131 sivua, 69 kuvaa, 13 taulukkoa ja 3 liitettä

Tarkastajat: Professori Antti Salminen
DI Pasi Puukko

Hakusanat: Jauheen karakterisointi, kaasuatomisointi, kierrätys, kiertotalous, lisäävä valmistus, metallijäte, mekaaninen jauhatus, plasmapyöristys

Diplomityö on tehty osana VTT:n Mineraaliekonomia-hanketta, joka tähtää teknologisiin innovaatioihin, joilla edesautetaan kannattavaa kiertotaloutta. Työssä tutkittiin mahdollisuuksia käyttää valmistavan teollisuuden metallijätettä jauhepetitekniikkaan perustuvan lisäävän valmistuksen raaka-aineena. Tavoitteena on soveltaa kiertotalouden ajatusta lisäävään valmistukseen. Pyrkimyksenä oli yhtäaikaisesti tuottaa ratkaisuja konventionaalisen kierrätyksen ongelmiin ja lisäävän valmistuksen raaka-aineen korkeaan hintaan. Tutkimus koostuu kirjallisuuskatsauksesta ja kokeellisesta osuudesta. Kirjallisuuskatsauksessa kartoitettiin ehdotettujen kierrätysreittien soveltamismahdollisuuksia ja hyötyjä. Katsauksen perusteella valittiin eräät soveltuvat jauheenvalmistusreitit ja jätevirrat kokeelliseen osuuteen testattaviksi.

Kokeissa valmistettiin jauhepetitekniikkaan soveltuvaa metallijauhetta sata prosenttisesta kierrätysromusta. Jauhetta valmistettiin kahdella eri prosessilla: 1) agglomeroituneen jätejauheen mekaaninen jauhatus yhdistettynä tarvittaessa plasma pyöristykseen sekä 2) tukirakenteiden ja viallisten komponenttien kaasuatomisointi. Hyödynnetyt jätteet olivat peräisin tuotteiden valmistuksesta jauhepetitekniikalla. Romusta valmistettujen jauheiden ominaisuuksia verrattiin kaupallisen jauheen ominaisuuksiin. Molemmista jauheista valmistettiin koekappaleita mekaanisten ominaisuuksien määrittämiseksi jauhepetisulatukseen perustuvalla SLM 125 HL laitteella. Kirjallisuuskatsauksen perusteella työssä ehdotetut kierrätysreitit kuluttavat vähemmän energiaa kuin konventionaalinen kierrätys. Lisäävä valmistus myös synnyttää lähtökohtaisesti vähemmän jätettä kuin nykyisin yleisesti käytetty materiaalia poistava valmistus. Kokeet osoittivat kiinteästä jätteestä kaasuatomisoinnilla ja agglomeroituneesta jauhejätteestä suihkujauhamisella valmistetun jauheen soveltuvuuden jauhepetitekniikan raaka-aineeksi ja täten näiden kierrätysreittien teknologisen toteutettavuuden. Näin ollen siirtyminen kohti lisäävää valmistusta tulee parantamaan valmistavan teollisuuden kestävyyttä.

ABSTRACT

Lappeenranta University of Technology
LUT School of Energy Systems
LUT Mechanical Engineering

Joni Reijonen

Utilizing metallic waste streams as raw material for powder-based additive manufacturing

Master's thesis

2016

131 pages, 69 figures, 13 tables and 3 appendices

Examiners: Professor Antti Salminen
M. Sc. (Tech.) Pasi Puukko

Keywords: additive manufacturing, circular economy, gas atomization, mechanical milling, metallic waste, recycling, plasma spheroidization, powder characterization

This study is done as a part of VTT's Mineral Economy innovation programme, which aims at developing technological innovation for a profitable circular economy. The possibilities of enhancing the sustainability of the manufacturing industry are studied by utilizing metallic waste streams from the manufacturing industry as feedstock material for powder bed fusion (PBF) additive manufacturing (AM). The goal is to apply the concept of circular economy into AM, in attempt to provide solutions simultaneously for issues regarding conventional recycling of scrap and the high price of feedstock material used in PBF AM.

This study consists of a literature review and experimental part. In the literature review the possibilities and potential benefits of the proposed recycling methods are explained. Based on the findings from the literature, suitable waste streams and powder preparation technologies were selected for a case study. In the experiments the objective was to prepare spherical powder from 100 % scrap feedstock following two routes: 1) mechanical milling and further plasma spheroidization (if needed) of agglomerated residue powder, and 2) gas atomization of solid scrap. These were scrap generated as a side stream during the PBF process. The powder properties were analysed and test specimens for the determination of mechanical properties were made from the prepared powders and commercial reference powder with SLM 125 HL powder bed fusion machine. Based on the literature review, the proposed recycling routes use less energy than the conventional recycling. Additive manufacturing also inherently generates less waste than the conventional manufacturing of today. The experimental work proved the technical feasibility of recycling new scrap into suitable powder for PBF via gas atomization of solid scrap and jet milling of agglomerated residue powder. Therefore shifting from subtractive towards additive manufacturing will enhance the sustainability of the manufacturing industry.

ACKNOWLEDGEMENTS

Firstly, I would like to thank VTT Technical Research Centre of Finland for the opportunity to do my master's thesis on such an interesting topic. I would like to express my gratitude to my supervisors Prof. Antti Salminen from Lappeenranta University of Technology and Pasi Puukko and Antero Jokinen from VTT for their guidance and feedback during the thesis work. Special thanks go to all those at VTT who helped in conducting the experiments, especially to Kimmo Kaunisto for the help with PSD, SEM and XRD equipment and also to Antti Heikkinen at LUT for the help with preparing metallographic specimens.

During the five years of study in Lappeenranta I made a lot of new friends who made the experience special. In the presence of the great members of KRK it was never boring. Before going to the university I knew nothing, now I've at least seen it all.

Last and foremost, I would like to thank my family for all the support during my studies. To Sanni, thank you for being there for me, pushing me forward and supporting me.

Joni Reijonen

Espoo 14.12.2016

TABLE OF CONTENTS

LIST OF SYMBOLS AND ABBREVIATIONS

A	Elongation after fracture [%]
h	Hatch spacing [µm]
LT	Layer thickness [µm]
R_m	Tensile strength [MPa]
$R_{p0.2}$	Yield strength [MPa]
v	Scanning speed [mm/s]
VED	Volumetric energy density [J/mm^3]

AM	Additive manufacturing
BCC	Body-centred cubic
BCT	Body-centred tetragonal
D10	10 % of particles in a population have a smaller diameter than this value
D50	50 % of particles in a population have a smaller diameter than this value
D90	90 % of particles in a population have a smaller diameter than this value
DMLS	Direct metal laser sintering
EAF	Electric arc furnace
EBM	Electron beam melting
EDS	Energy dispersive x-ray spectroscopy
EIGA	Electrode induction melting gas atomization
E-PBF	Electron beam-powder bed fusion
FCC	Face-centred cubic
GA	Gas atomization
GHG	Greenhouse gas
HIP	Hot isostatic pressing
HRC	Hardness, Rockwell C
L-PBF	Laser-powder bed fusion
MIM	Metal injection moulding
MM	Mechanical milling
MV	Mean volume diameter
OM	Optical microscopy

PA	Plasma atomization
PBF	Powder bed fusion
PH	Precipitation hardening
PM	Powder metallurgy
Ppm	Parts per million
PREP	Plasma rotating electrode process
PS	Plasma spheroidization
PSD	Particle size distribution
REP	Rotating electrode process
RF	Radio frequency
SD	Standard deviation
SEC	Specific energy consumption
SEM	Scanning electron microscope
SLM	Selective laser melting
SS	Stainless steel
XRD	X-ray diffraction

1 INTRODUCTION

This master's thesis is done at VTT Technical Research Centre of Finland as a part of the spearhead Mineral Economy innovation programme, which aims at developing technological innovation for a profitable circular economy. One of the main targets of the programme is closing the loop of mineral based materials with low energy, material efficient solutions. Among others, powder based additive manufacturing is seen as a potential technology for the efficient utilization of secondary raw materials recycled from waste. (VTT 2015.)

1.1 Background

Recently, there has been increasing concern about the sustainability of the manufacturing industry, a major consumer of energy and raw materials, and therefore, a major producer of greenhouse gas (GHG) emissions and waste. The manufacturing industry is estimated to account for 18.8 % of GHG emissions and 11 % of waste produced in the European Union, equivalent to 860 million tonnes of GHG emissions and 270 million tonnes of waste annually. The statistics are from year 2013 for GHG emissions and from 2012 for waste. (Eurostat 2016; Eurostat 2015.) Sustainable manufacturing is defined by the United States Environmental Protection Agency (2016) as "the creation of manufactured products through economically-sound processes that minimize negative environmental impacts while conserving energy and natural resources. Sustainable manufacturing also enhances employee, community, and product safety."

The EU implemented a Circular Economy Package in 2015, which consists of the EU Action Plan for the Circular Economy with a concrete programme of action to foster sustainable economic growth in the EU. European Commission (2015, p. 12) defines circular economy as a concept "where the value of products, materials and resources is maintained in the economy for as long as possible, and the generation of waste minimised." The first priority is to prevent or minimize waste generation and after that comes efficient reuse and recycling (European Commission 2015, p. 8.) Figure 1 shows the implementation of circular economy concept into the life cycle of steel. Metal ores are extracted from the Earth's crust, refined into ingots of pure metals and alloys from which

products are manufactured. The product is used for some time and once at the end of use phase, the material in the product is recycled and new ingots are made from it, closing the loop. Natural resources, in this case metals, can be preserved by minimizing the need of raw materials coming from outside the circle with the methods inside the circle shown in figure 1. The use phase of a product can be extended by reusing and remanufacturing or repairing, decreasing the demand for new products and therefore new raw materials. Once the product cannot be used anymore, it is recycled as post-consumer scrap (old scrap) to substitute virgin metal ores in steel production. In the same way, pre-consumer scrap that is generated during the manufacturing phase of the product can be recycled to substitute virgin raw materials, which is the focus of this study. (World Steel Association 2016a).

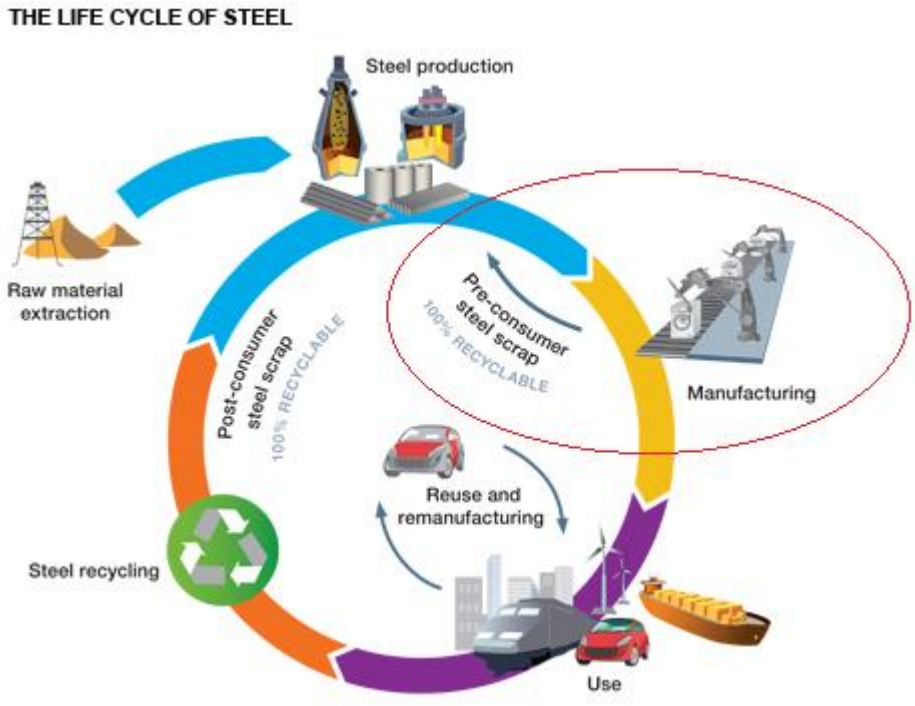

Figure 1. The life cycle of steel (World Steel Association 2016a).

In the manufacturing phase various technologies are used to produce finished products from metals and alloys. Typically the raw materials are in the form of semi-finished bulky products such as plate, bar, wire, ingot and different tube profiles, from which the desired geometry of the finished product is achieved by various forms of cutting, machining, forming and joining. The amount of scrap generated during the manufacturing phase increases along with the geometrical complexity of the product. This waste stream is referred to as new scrap and it can be recycled in the production of new semi-finished raw

materials through re-melting at the metal production process. However, this way of recycling is energy-intensive and in the case of many engineering metals and alloys, expensive and rare alloying elements are lost as a result of non-functional recycling. (Reijnders 2016, p. 76–96; Graedel et al. 2011, p. 14.)

New manufacturing technologies are needed to answer the increasing demand for the production of geometrically complex products from various engineering metals and alloys in a sustainable manner, with optimal resource use and recycling (Commission of the European Communities 2008, p. 8). Additive manufacturing (AM) is a relatively new manufacturing technology developed in the 1980's that has great potential as a more sustainable way of manufacturing products. According to the standard SFS-ISO/ASTM 52900 (2016, p. 5), additive manufacturing is defined as a "process of joining materials to make parts from 3D model data, usually layer upon layer, as opposed to subtractive and formative manufacturing methodologies." This manufacturing methodology means that material is only added where it is needed, enabling the manufacture of geometrically complex near-net-shape products. This means that after AM the product is almost ready for use, requiring only minimal post-processing to achieve the final geometry, surface finish and tolerances, resulting in minimal waste production.

The extraction of metal ores and refining them into semi-finished bulky feedstock for the manufacturing industry has significant environmental impacts in the form of greenhouse gas emissions and solid and toxic wastes (Norgate, Jahanshahi & Rankin, 2007, p. 838–848). Therefore minimizing scrap alone is not enough, as raw materials are still needed for the product itself. Powder-based additive manufacturing technologies use metal and alloy powders consisting of particles with diameters in the range of around 15–106 µm as the raw material from which the products are manufactured (Dawes, Bowerman & Trepleton 2015, p. 246). This granular instead of bulky form of feedstock material enables the consideration of efficient utilization of metallic waste streams instead of virgin ores as the raw material for powder preparation and ultimately product manufacturing.

Recycling new scrap by preparing fine metallic powder from it could avoid the issues related to the conventional recycling of new scrap via re-melting, casting and forming into new ingots, plates and bars at the metal production plant. In addition to the improved

recycling benefits, this way of preparing feedstock for additive manufacturing could provide substantial cost reduction, as the commercially available powders for additive manufacturing are relatively expensive, ranging from around 80 €/kg for stainless steel to 145 €/kg for aluminium alloys and up to 400 €/kg for titanium alloys, other materials used in AM falling in between (Piili et al. 2015, p. 392; Atzeni & Salmi 2012, p. 1154; Froes 2012, p. 18). These values are for relatively small batches of powder and the prices differ depending on the batch size, powder quality and particle size distribution. However, for comparison, titanium alloys costs around 20 €/kg in plate feedstock (Froes 2012, p. 16). If usable powder for AM from metallic scrap can be prepared with relative ease, this could provide substantial economic and environmental benefits for the manufacturing industry.

1.2 Objectives

In this master's thesis the possibilities of utilizing metallic waste streams from the manufacturing industry as feedstock material for powder-based additive manufacturing are studied. The goal is to apply the concept of circular economy into additive manufacturing, in attempt to provide solutions simultaneously for issues regarding conventional recycling of scrap and the high price of feedstock material used in powder-based metal AM.

The objective of the literature review is as follows. Define the sources, types and quantities of the metallic waste streams in the manufacturing industry. Identify the issues regarding conventional handling and recycling of these waste streams and the possible benefits provided by recycling scrap through powder preparation. State of the art studies in preparation of powders from recycled metallic waste are reviewed. In addition, the required properties of powders for AM and the corresponding characterization methods together with the effects of powder variation on the properties of additively manufactured finished parts are defined. Significant consideration is given to the powder characterization, as the main target of the experimental part of this thesis is to prepare powder that meets the requirements for additive manufacturing.

Based on the findings from the literature, one material waste stream is selected for a case study. In the experimental part the aim is to prepare powder having spherical morphology, desired particle size distribution and no impurities. From this powder the objective is to additively manufacture test specimens for mechanical and microstructural evaluation. The

powder is characterized and the mechanical properties of the manufactured test pieces are compared to test pieces made of commercial powder to see if any differences occur. The process of preparing spherical powder from metallic waste is described in detail.

This study seeks answers to the following research questions:

1. What are the benefits of recycling metallic waste as powder for AM?
2. What type of waste streams are most suitable for recycling via the proposed route?
3. Can the powder prepared from the selected material waste stream be used in powder-based AM?
4. What differences are there between the prepared and commercially available powders with the same nominal chemical composition?
5. Are there differences in mechanical properties and microstructures of parts manufactured from the prepared powder, compared to commercial?

1.3 Scope

Regarding waste streams, this study is limited to metallic waste produced in the manufacturing phase of products, referred to as new scrap. From the numerous additive manufacturing processes only those utilizing metallic powder as feedstock are considered. The references used consist mostly of peer-reviewed scientific articles and conference proceedings along with selected books, standards and company web pages. Cross-referencing is used to further enhance the reliability of the information. The experimental part of this study consist of tests in attempt to produce such metallic powder from the selected waste stream, which matches the characteristics required from powders used in additive manufacturing. The waste stream for the experiments is selected based on the findings of the literature review. The powder production methods considered are limited to thermal and mechanical processes capable of utilizing scrap feedstock. The prepared powder and the commercial powder used for comparison is analysed to determine the particle morphology, flowability, density, particle size distribution and chemical composition. Samples for tensile testing, microstructural evaluation, porosity measurements and hardness tests are manufactured from this powder via additive manufacturing with a commercially available SLM 125 HL powder bed fusion machine. The results are compared to a commercially available powder and parts manufactured of the commercial material with the same nominal chemical composition.

2 METAL WASTE STREAMS IN THE MANUFACTURING INDUSTRY

The production of metal parts and components for various engineering and consumer products generates substantial amounts of metallic waste annually. This waste stream can be divided into old, home and new scrap. The part of the initial feedstock material that is included in the finished product becomes old scrap once the product reaches the end of use. Home scrap is such leftover material from the manufacturing process that can be directly used again as raw material for making more products. The third waste stream is referred to as new scrap. It is generated at the manufacturing phase of products from semi-finished bulky raw materials and consists of machining turnings, grindings, cuttings, stampings etc. Although not useable directly as raw material for manufacturing more products, this waste stream can be recycled to the production of new semi-finished bulk raw materials. (Graedel et al. 2011, p. 13–14.)

The amount of new scrap generated in the manufacturing phase of products from semi-finished raw materials has been estimated to be 14.6 % for steel and 13.7 % for aluminium from the input material stream (Cullen, Allwood & Bambach 2012, p. 13051; Stacey 2015, p. 41). These estimates are for the global flows of these materials, therefore including all types of manufacturing methods. At the moment of these studies the share of additive manufacturing in making products is extremely small compared to conventional manufacturing, so these values represent more closely the case of just conventional manufacturing. The amount of scrap generated is almost same for both materials, due to the use of same manufacturing technologies to make similar end-use products. However, if we compare titanium, a material mostly used by the aerospace sector where web-like structures with low weigh and high strength are manufactured mostly by machining from wrought raw materials, the amount of new scrap generated is estimated at 55 % of the input material (Kobryn et al. 2006, p. 3–4; Goonan 2010, p. Y2). Figure 2 shows the material flow for steel, aluminium and titanium in the manufacturing phase. Note that for steel and aluminium the data is global, whereas for titanium only national data of U.S was available. The values are in millions of metric tonnes (Mt).

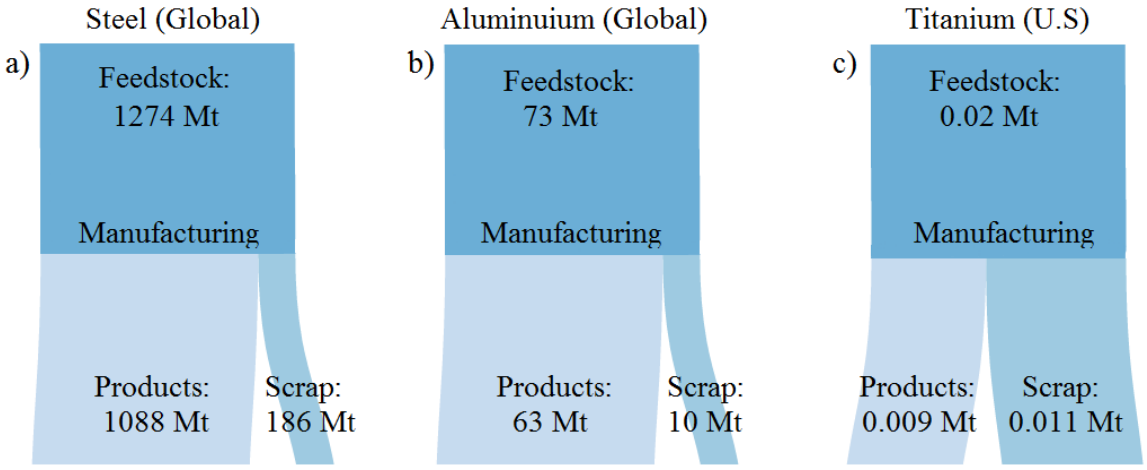

Figure 2. Material flow of a) steel, b) aluminium and c) titanium in the manufacturing phase of finished metal products (re-drawn from: Cullen et al. 2012, p. 13051; Stacey 2015, p. 41; Goonan 2010, p. Y2).

The primary objective in the sustainable material usage in circular economy is to prevent the formation of this scrap (European Commission 2015, p. 8). Only extremely simple products can be manufactured with only minor amounts of waste with conventional manufacturing technologies of forming, joining or subtracting bulky raw materials. Product complexity typically increases waste generation in the manufacturing phase, as is the case with aerospace titanium products described earlier. Shifting from subtractive manufacturing towards additive manufacturing will produce less new scrap, because of the fundamental difference of *adding* material, instead of *removing* it, to achieve the desired shape. With additive manufacturing even complex geometries can be achieved with minimal waste, however not completely without waste, as shown in figure 3. Therefore after minimizing the waste generation by using best available technology in regards of waste generation in the manufacturing phase, such as additive manufacturing, the next step is efficient recycling of the unavoidable new scrap generated in the process. Renvall (2014, p. 1–78) did a master's thesis on the performance of additive manufacturing in the process industry, with a mechanical seal as a case study, which could be considered relatively complex product. Figure 3 shows significant reduction in scrap produced when the product is additively manufactured with powder bed fusion (PBF) together with finishing machining for surfaces with tight tolerances, compared to the conventional way of production by roughing and finishing machining from bar feedstock.

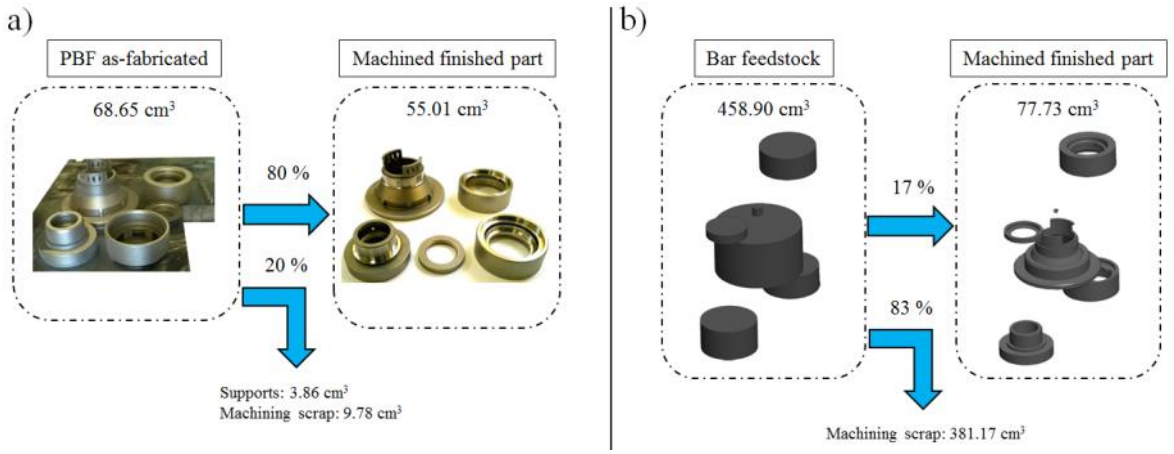

Figure 3. The amount of scrap generated in a) powder bed fusion together with finishing machining, compared to b) completely machining the product from bar feedstock (modified: Renvall 2014, p. 59, 60, 63).

The form of the scrap that is produced depends on the manufacturing process, but can be mostly categorized based on the size of individual pieces of scrap in the waste stream. Scrap particles measured in the range of micrometres are essentially metallic dust or powder, typically produced in finishing operations such as grinding and polishing and in powder metallurgy applications where the feedstock material is initially in the form of fine powder. The second group is small macroscopic scrap particles, typically in the form of chips, stampings and turnings. The third group includes large bulky pieces of scrap, such as cuttings from semi-finished bar or plate feedstock. Figure 4 illustrates the forms of scrap metal typically produced by the manufacturing industry.

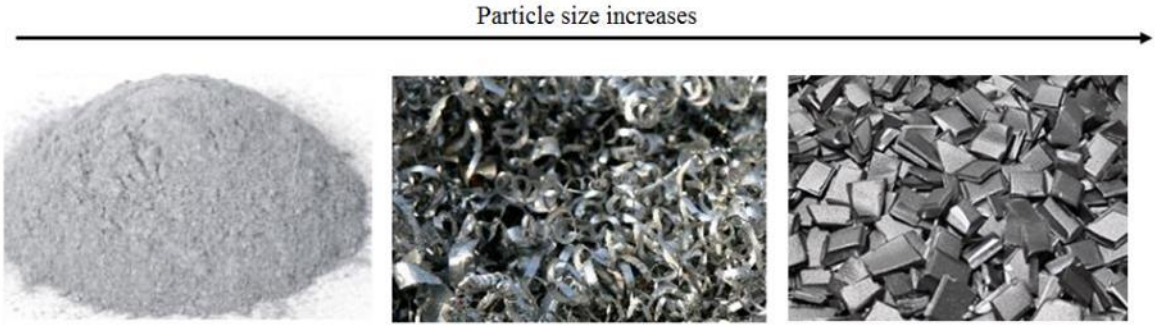

Figure 4. Different forms of scrap metal (modified: The Bermet Company 2016; SJM Alloys & Metals Limited 2014).

2.1 Issues of conventional recycling of scrap metal

In theory, metals are infinitely and 100 % recyclable as their properties do not degrade during the process. This would be easily achievable, if metals were used as pure metals. However, most of the metallic materials used are alloys, consisting of several different metals and other elements mixed together. (Reuter et al. 2013, p. 26; Dubreuil et al. 2010, p. 623.) Alloying is done to enhance the properties or some property of the particular material and there are over 3500 alloys of steel alone (World Steel Association 2016b). Every alloy has a unique chemical composition and set of properties. To conserve these properties after recycling requires every alloy to be separately recycled in their own closed-loop cycle. In the conventional large scale recycling through concentrated re-melting at large processing plants this is not done because of practical and economic difficulties, resulting in open-loop recycling where different metals and alloys are mixed together. (Graedel et al. 2011, p. 13–14; Reijnders 2016, p. 83.)

To recycle a waste stream consisting of mixed scrap there are two options: try to separate specific alloys or melt the mixed scrap and dilute it with virgin materials to achieve the desired alloy composition. In the conventional recycling process both methods are applied to some extent, however effective scrap separation and minimized dilution losses are under constant research efforts, as they are problematic. Separation of metal materials prior re-melting is unfortunately usually done with only basic technologies like magnetic separation where only large material groups, such as ferrous, non-ferrous, can be sorted. To separate specific alloys more advanced technologies such as laser or x-ray based sorting should be applied. However, these technologies are not utilized in industrial scale because of economic reasons. Recovery of specific materials in the melting phase can be also done to some extent. Here thermodynamics ultimately set the limit, as the alloying elements often have similar thermodynamic behaviour, making the separation extremely energy-intensive or in some cases impossible. This means that some amount of dilution and addition of alloying elements in the form of virgin raw materials is necessary in the re-melting phase to get the right composition. This decreases the resource saving benefit and increasing the true specific energy consumption (SEC) of conventional recycling. (Nakamura et al. 2012, p. 9266–9273; Reck & Graedel 2012, p. 692–693.) Cullen & Allwood (2013, p. 3057–3064) mapped the global material flow of aluminium based on the

data of 2007 and found that 25 % of the input material in scrap recycling through the conventional route was actually virgin aluminium used for dilution.

In addition to the need of virgin materials for dilution, the alloying elements can lose their functionality in the material during recycling mixed scrap via re-melting. Functional recycling of a given metal or alloy is such that the intended function of the alloying elements in the material is preserved after recycling. As an example, if austenitic stainless steel is re-melted to make austenitic stainless steel, the nickel and chromium retain their function. Of course there are several different grades of austenitic stainless steels with differences in the chemical composition. However, recycling within a certain class of alloys like austenitic stainless steels, which all have the same main alloying elements, is considered functional recycling. Nevertheless, for example if titanium stabilized austenitic stainless steel is re-melted along with the workhorse alloy 304 to make 304 stainless steel, the titanium loses its function and is considered a tramp element. Non-functional recycling is the case of mixing completely different classes of materials, like the case of mixing copper alloys in the re-melting of steel. The copper alloy loses its function and furthermore is an impurity in the steel, so if present in large enough quantities in the mixed scrap, it has to be diluted with virgin materials to the acceptable level of the given steel alloy. (Graedel et al. 2011, p. 14; Nakamura et al. 2012, p. 9266–9273.)

Recycling via the conventional route of melting, casting and forming into bulky feedstock does save energy and is the primary reason for using scrap in the production of metals and alloys as the extraction and refining of ores can be avoided (Reck & Graedel 2012, p. 691). Most metals are found in Earth’s crust as oxides or other minerals and the separation of the desired metal from other elements is usually energy-intensive and increasingly so when the reactivity of the given metal increases (Reuter et al. 2013, p. 266–273). Table 1 lists values found from the literature for specific energy consumptions to produce bulky semi-finished feedstock of some typical engineering metals from virgin ore and from recycled scrap. When possible, the values are presented as averages with corresponding standard deviations. For some cases only one value was found from the literature.

Table 1. Specific energy consumptions to produce semi-finished bulky materials from virgin and scrap feedstock ([1]Grimes et al. 2008, p. 8, 10, 15, 17; [2]Johnson et al. 2008, p. 187; [3]Norgate et al. 2007, p. 844; [4]Cullen & Allwood 2013, p. 3062; [5]Stacey 2015, p. 53; [6]Denkena, Dittrich, & Jacob 2016, p. 479).

Material	SEC (virgin ore) [MJ/kg]	Reference	SEC (scrap) [MJ/kg]	Reference
Ferrous steel	21.9±5.1	[1]	11.7±2.1	[1]
Stainless steel	77±2.8	[2,3]	11.7±2.1	[1]
Aluminium	184.4±47.3	[1]	7.6±2.5	[1,4,5]
Titanium	326.5±48.8	[3,6]	62.9	[6]

For virgin production the increase in SEC along with the increased reactivity of the material is clearly shown. The extraction and production of titanium feedstock from virgin ores takes over ten times the energy needed in virgin steel production. Aluminium alloys, as low melting temperature materials (pure Al 660 °C), have the largest energy savings of these materials when recycling via the conventional re-melting route. Iron based ferrous and stainless steel requires more energy during the conventional recycling than aluminium, because of the higher melting point (pure Fe 1523 °C) of these materials (Maol 2005, p. 72). SEC of titanium production from scrap is also reduced significantly when compared to virgin production. However, the SEC of the conventional titanium scrap recycling is still relatively high, because of the extreme reactivity of titanium in molten state or even at elevated temperatures. Therefore special re-melting processes are needed, all processing has to be carried under vacuum or inert atmosphere and often multiple re-melting steps are needed to guarantee a homogenous ingot. Furthermore, titanium has poor formability, which makes also the rolling or forging into semi-finished bulky feedstock challenging. (Rotmann, Lochbichler & Friedrich 2011, p. 1466.) All of this contributes to the relatively high SEC, compared to the steel or aluminium.

The SEC of conventional stainless steel scrap recycling is assumed to be the same as ferrous scrap recycling. Both are recycled conventionally via the same electric arc furnace (EAF) re-melting route. For example, Outokumpu produces stainless steel from scrap via the EAF route, and reports a SEC value of 11.2 MJ/kg (Outokumpu 2015, p. 20). This is in

good accordance with the 11.7±2.1 MJ/kg reported for ferrous steel recycling via the EAF route (Grimes, Donaldson & Gomez 2008, p. 17).

It should be noted that the SEC values for scrap feedstock represent cases where high purity scrap is recycled in a closed-loop manner. In the conventional recycling of mixed scrap the virgin materials used for dilution further increase the true SEC values accordingly. The extraction and refining of the virgin materials that were used for dilution has to be taken into consideration. (Johnson et al. 2008, p. 181–192.) Such virgin material dilution is not included in the values for conventional scrap recycling in table 1. Instead, the SEC values represent a best case scenario of using 100 % scrap feedstock to enhance the comparability with the proposed recycling routes.

2.2 Scrap recycling through powder preparation

Because of the issues related to the conventional recycling route, less energy-intensive closed-loop recycling processes are needed. To avoid some of the energy intensive processing steps, such as melting, refining, casting and forming, to produce bulky feedstock, that is used by most conventional manufacturing technologies, manufacturing processes that can utilize feedstock in a different form has to be considered. Powder metallurgy (PM) covers the manufacturing technologies that use metal powders as feedstock for making products. Powder metallurgy techniques include press and sinter, hot isostatic pressing (HIP), metal injection moulding (MIM) and the more recently developed powder-based metal additive manufacturing, which is the focus of this study.

The whole powder metallurgy market produces an estimated 1.5 million metric tonnes of metal powders, valuing at around 8 billion dollars in 2015 (McWilliams 2016, p. 132,134). Metal powder sales for additive manufacturing have been estimated at 88.1 million dollars in 2015, accounting for around 1 % of the whole PM metal powder market (Caffrey, Wohlers & Campbell 2016, p. 154). Therefore AM powders could be regarded at the moment as a niche application in the whole PM market. However, the sales of metal powders for AM have been increasing at an increased pace every year as seen in figure 5. The trend is most likely to remain, as metal AM shifts more from prototyping towards production of final parts. As an example of forthcoming AM mass production, GE

Aviation plans to additively manufacture over 100,000 fuel nozzles for their next generation jet engines by 2020 (Zaleski 2015).

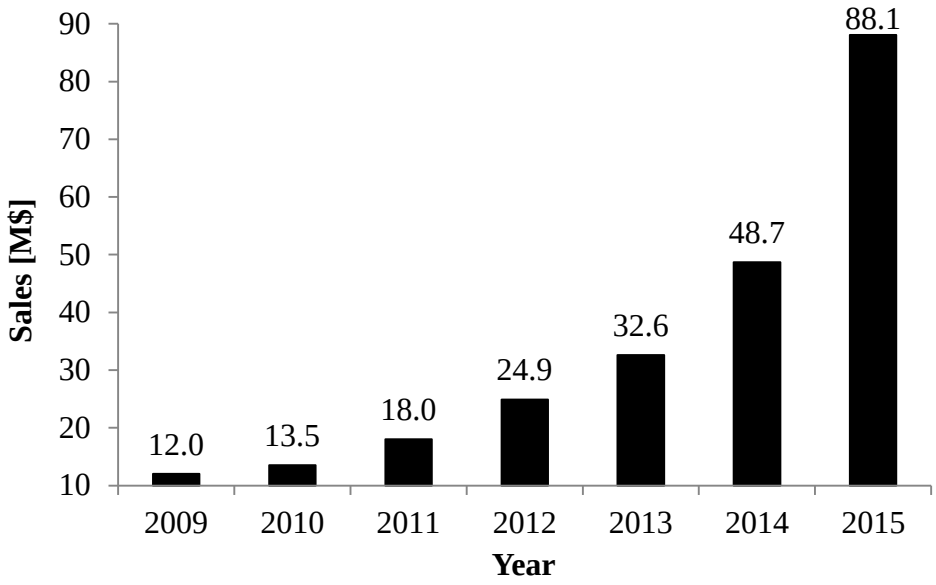

Figure 5. Development of metallic powder sales for additive manufacturing. The estimates are in millions of dollars. (Re-drawn from: Caffrey et al. 2016, p. 154.)

Recycling through powder preparation further increases the energy saving benefit of recycling compared to the conventional route. In this study the methods to produce spherical powder from scrap feedstock are limited to gas atomization (GA) and mechanical milling (MM) combined with plasma spheroidization (PS). Depending on the material and used production method the reported estimates for specific energy consumptions vary accordingly, as seen from table 2. The SEC value for atomization, the most used powder production method, is 6.1±0.6 MJ/kg. Comparison to the SEC of 11.7±2.1 MJ/kg for steel recycling through the conventional route implies larger energy saving potential for the powder preparation recycling route. In plasma spheroidization the SEC is higher than in GA and in some cases even higher than the values for conventional recycling route in table 1. It should be noted that the SEC value for PS is in the case of molybdenum, a material with relatively high melting point of 2623 °C. The SEC might be somewhat lower for materials with lower melting temperatures, such as iron based alloys. However, in addition to the melting temperature, the heat transfer properties of the material are also crucial for the energy needed in PS. Materials with high thermal conductivity, such as molybdenum, receive energy more efficiently from the plasma during the process. (Boulos 2016, p. 12.)

For mechanical milling the values are significantly smaller than for the other methods, as the melting of the material can be avoided. It should be noted that the values found from the literature are for the milling of brittle materials. For engineering metals and alloys with even moderate ductility the values might be higher.

Table 2. Specific energy consumption to produce micron sized metal powders from scrap feedstock ([1]Morrow et al. 2007, p. 938; [2]Kruzhanov & Arnhold 2012, p. 14; [3]Williams 2012, p. 19; [4]Wilson et al. 2013, p. 248; [5]Jankovic 2003, p. 338; [6]Kulu et al. 2003, p. 41; [7]Dietmar 2012, p. 14; [8]Boulos 2016, p. 13).

Material	Production method	SEC [MJ/kg]	Reference
H13 tool steel	Gas atomization	6.45	[1]
Iron	Water atomization	6.48	[2]
Titanium-based alloys	Gas atomization	5.4	[3]
NiAl	Crushing and milling to 100 µm	0.16	[4]
Minerals in general	Ball mill to 30 µm	0.3	[5]
WC-based hardmetal	Disintegrator mill to 100 µm	0.25	[6]
N/A	Air classifier jet mill to 7.5 µm	0.4	[7]
Molybdenum	Plasma spheroidization	24	[8]

2.3 Preparation of spherical powders for additive manufacturing

There are few commercialized methods to produce spherical powders suitable for additive manufacturing. Plasma atomization (PA), rotating electrode process (REP), plasma rotating electrode process (PREP) and electrode induction melting gas atomization (EIGA) can be used to produce highly spherical powders with low levels of impurities, but these processes require the feedstock material to be in the form of high purity bar or wire. Therefore these processes are not considered as viable for powder production from scrap feedstock in this study. This leaves us with water/gas atomization, mechanical milling and plasma spheroidization techniques, where scrap can be used as feedstock to produce spherical powders. (Dawes et al. 2015, p. 245–248; Antony & Reddy 2003, p. 14–18.)

2.3.1 Atomization

The most used method for metal powder production is melt atomization. The feedstock material is melted in a crucible by heat generated with induction or gas furnace and the molten metal stream is forced through a nozzle by gravitation or with the aid of moderate pressure. Atomization can be divided into water or gas atomization, depending on whether gas or water jets of high velocity are used to disintegrate the melt into micron sized droplets of molten metal, which then cool down and solidify in to fine particles during the freefall in the chamber. The produced particles have a spherical morphology, because of the high surface energy of molten metal. The kinetic energy of the jet has to be sufficient to overcome the viscous and surface energy forces of the molten metal stream. Gas atomization produces powders with more spherical morphology as the cooling rate is one or two magnitudes slower than in water atomization, where the rapid cooling provides insufficient time for the droplets to completely spheroidize. In figure 6 is the schematic representation of gas atomization. In water atomization the principle is same, except for the jet being liquid instead of gaseous. (Zheng & Lavernia 2011, p. 837–840; Dawes et al. 2015, p. 246–249.)

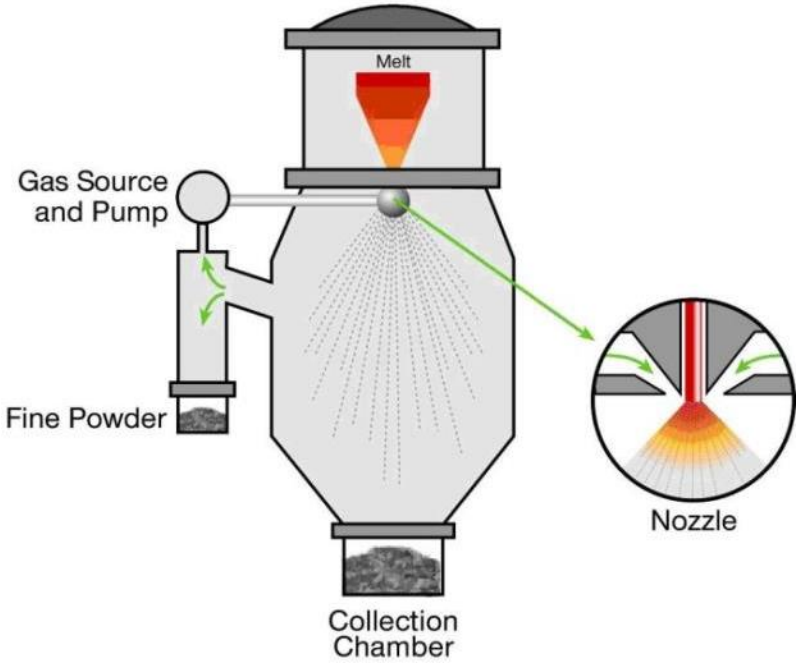

Figure 6. Gas atomization process (LPW Technology 2016a).

Gas atomization with inert gases like argon, nitrogen or helium is more suitable for reactive metals than water atomization. For the most reactive materials like titanium alloys

even inert gas atomization is problematic, as the molten metal is in contact with the ceramic crucible and nozzle, where the extremely reactive molten titanium tends to pick up interstitial impurities. Other disadvantages of the gas atomized powders considering AM include wide particle size distribution, the presence of satellites formed when smaller particles stick to larger ones during solidification and pores inside of particles caused by gas entrapment. (Zheng & Lavernia 2011, p. 837–840; Dawes et al. 2015, p. 246–249.) Caffrey et al. (2016, p. 61) reports that in gas atomization around 70 % of the powder produced can be used in powder bed fusion, regarding the particle size.

2.3.2 Mechanical milling and plasma spheroidization

Mechanical milling of scrap metal to form powder is a more simple way and it uses significantly less energy in the process as no melting of metal is needed, as mechanical force is used in the size reduction. There are various different types of mills commercially available. In figure 7 a planetary ball mill is described. The feedstock is loaded in a vial with steel balls and the vial is rotated so that the collisions between the feedstock material, balls and the vial walls crushes the material, ultimately yielding powder. The black arrows in figure 7 indicate the rotation of the disc and vial, and the red arrow indicates the movement of the grinding balls inside the vial. Unfortunately milling typically results in particles with irregular morphologies and therefore might not be usable as-fabricated in powder based additive manufacturing because of poor flowability and packing density. Other concerns in mechanical milling include contamination from the material of the vial and grinding media due to wear, and oxidation when processing reactive materials. Inert gas shielding can be used to reduce the amount of oxidation during processing. Contamination in the form of unwanted elements from the processing equipment can be avoided by using similar material for the processing equipment and powder. (Antony & Reddy 2003, p. 17; Suryanarayana 2001, p. 23–24.)

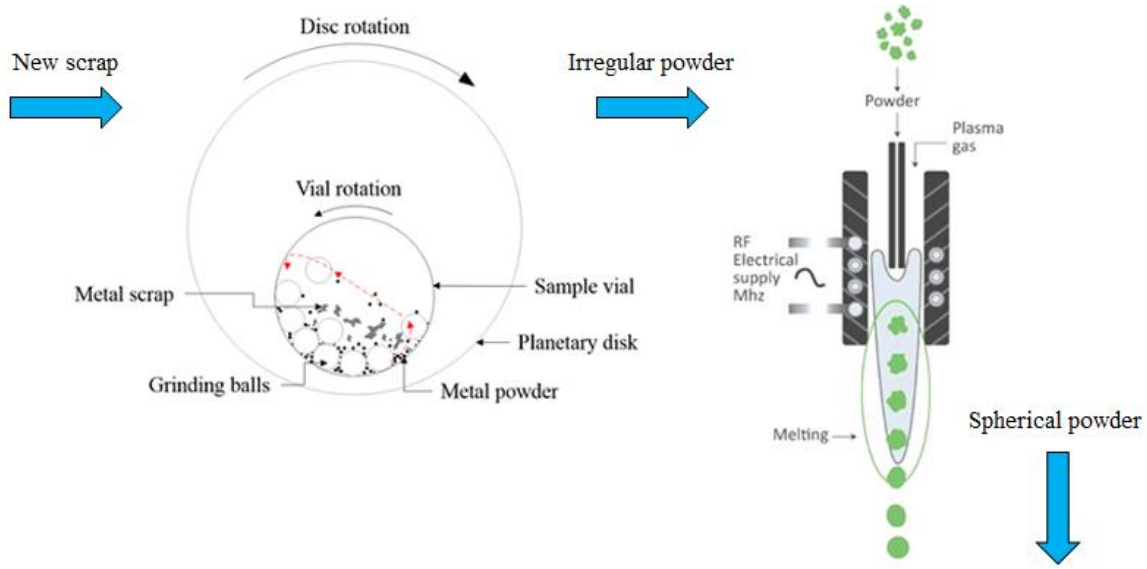

Figure 7. Ball milling and further plasma spheroidization to produce spherical powders from new scrap (modified: LPW Technology 2016b).

Plasma spheroidization (PS) process can be used to further convert the milled powder with irregular morphology into spherical particles, as also seen in figure 7. The irregular particles are fed in an inert gas stream into the atomization chamber through plasma gas, where the intense heat (up to 10000 K) melts the particles in-flight. Once pass the plasma the particles cool down and solidify during freefall before the bottom of the chamber into spherical particles due to surface tension, just like in the atomization process. This technique was quite recently commercialized and has demonstrated the ability to produce extremely spherical high purity powders from granulated feedstock of irregular morphologies. The particle size distributions are close to those of the initial feedstock powder. (Dawes et al. 2015, p. 247; Yang et al. 2013, p. 2313–2316.) This means that the desired particle size has to be achieved prior to the spheroidization, for example during mechanical milling. Other major drawback is the high specific energy consumption of the process as seen in table 2.

Ductile materials are hard to crush mechanically, therefore pre-processing to make the material more brittle may be needed to make the milling process more efficient (Antony & Reddy 2003, p. 17). Example of this is the hydrogen embrittlement of titanium, where the titanium feedstock is heated in a hydrogen atmosphere to produce titanium hydride (TiH_2), which is extremely brittle and therefore easy to crush into fine particles. The resulting TiH_2 powder has to be then dehydrogenated to get titanium powder, which can be achieved

during the plasma spheroidization. (Yang et al. 2013, p. 2313–2316.) However, as the hydrogen embrittlement is done at elevated temperature for quite some time, 1 hour at 600 °C in the study by Yang et al. (2013, p. 2313–2316), this further increases the specific energy consumption and cost of this powder production route. Materials brittle enough to be efficiently milled without additional embrittlement treatments would therefore be ideal for powder preparation through mechanical milling and plasma spheroidization.

3 ADDITIVE MANUFACTURING

Known also as 3D-printing, additive manufacturing is the term used for the process of joining materials layer-upon-layer to form a solid object directly from the 3D-model CAD-data (SFS-ISO/ASTM 52900 2016, p. 5). The workflow of the process is shown in figure 8. In recent years additive manufacturing has received a lot of media attention and hype, some heralding the technology even as the third or fourth industrial revolution, depending on how one defines the earlier industrial revolutions (The Economist 2012). The hype is of course based on the concrete benefits that additive manufacturing offers over conventional manufacturing methods, however the fact that AM technologies also have limitations, is often neglected. In the experimental part of this study PBF is used so the benefits and limitations are considered from the perspective of this AM technology.

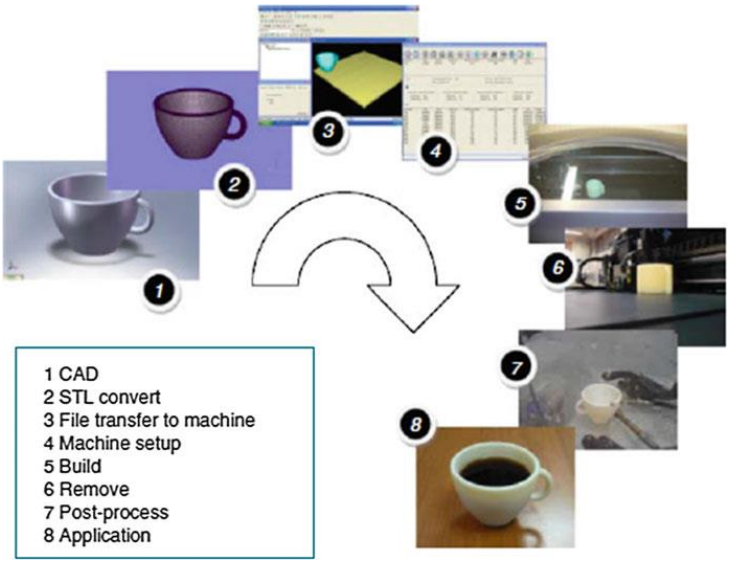

Figure 8. Schematic of the additive manufacturing process (Gibson, Rosen & Stucker 2015, p. 5).

Design freedom provided by the layer-upon-layer manufacturing methodology and tool-less nature of the process is the major benefit of additive manufacturing, as parts can be designed to optimize the geometry for the function, without limitations set by the manufacturing stage. Complex geometries that would otherwise be extremely costly and time-consuming or even simply impossible to manufacture, can be realized with additive manufacturing without any additional cost. Complexity of the part has little to no effect on

the manufacturing cost in additive manufacturing, which is the opposite for conventional subtractive manufacturing. The other major benefit is the mass-customization enabled by the cost-effectiveness of AM with small series production, as size of the production series has little to no effect on the cost of additively manufactured parts. (Gibson et al. 2015, p. 411; Becker 2016, p. 14.) Figure 9 shows the typical trend in cost of production for traditional or conventional manufacturing compared to additive manufacturing.

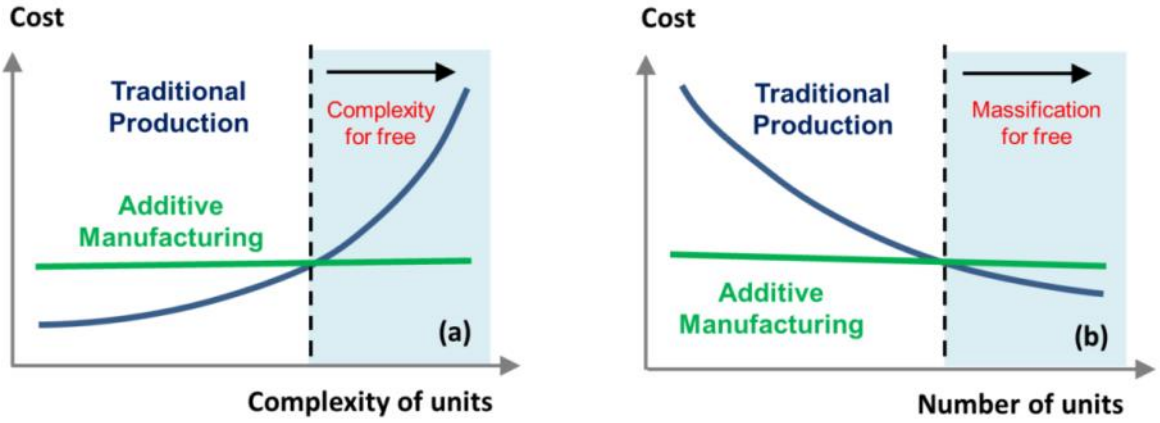

Figure 9. Comparison between the cost of production in traditional production and additive manufacturing, as function of a) complexity of units and b) number of units in production (Becker 2016, p. 14).

As said, there are some limitations to the process as well. The design freedom of AM is somewhat apparent, as support structures are needed for some geometries to be manufactured. Supports are essentially scrap that has to be removed via post-processing, adding extra cost as production time increases and material usage efficiency is decreased. Other concerns are about surface roughness, dimensional accuracy, maximum size of parts produced, the relatively slow production speed and overall cost of production, especially with larger production series. (Gao et al. 2015, p. 65–89.) This study could provide solutions for the cost of production by reducing the feedstock material price. Metal powders used in AM are expensive compared to conventional PM applications like press and sinter, because of the required particle size distribution, high purity and spherical particle morphology of AM powders (Dawes et al. 2015, p. 243–256).

When considering the cost of additively manufactured parts, the metal powder used as feedstock is the most significant variable cost during production. Figure 10 summarizes the

cost structure of parts manufactured via powder bed fusion with varying production parameters. The star marks the base scenario. The highest material price used in the comparison is 600 €/kg, which results in a 46 % share of the whole production cost. To reduce this cost, novel methods of producing spherical powders efficiently are required.

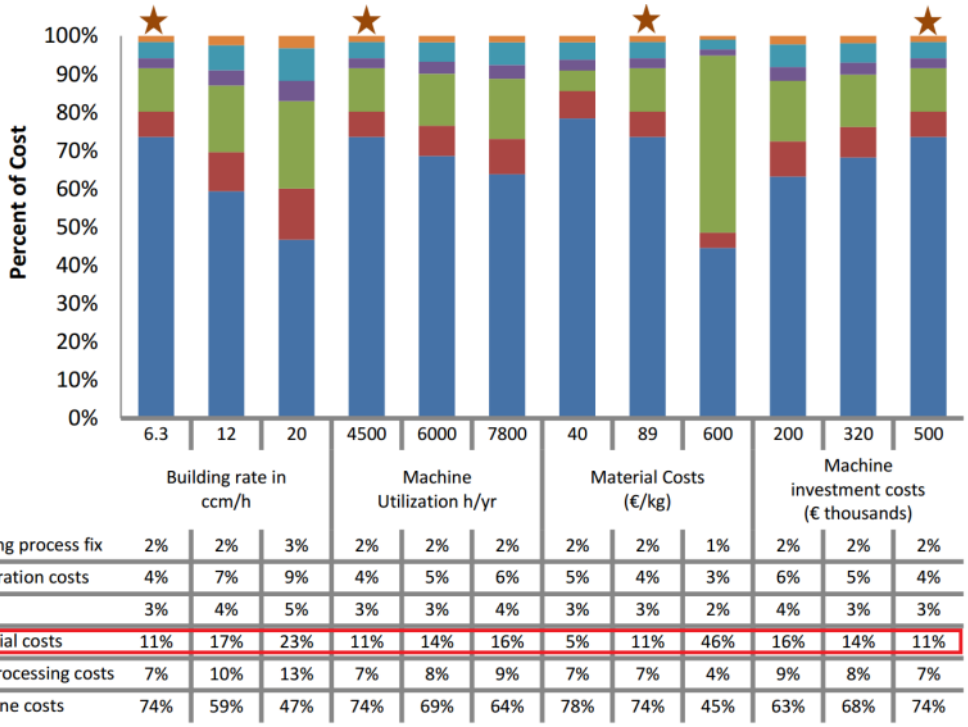

	6.3	12	20	4500	6000	7800	40	89	600	200	320	500
Building process fix	2%	2%	3%	2%	2%	2%	2%	2%	1%	2%	2%	2%
Preparation costs	4%	7%	9%	4%	5%	6%	5%	4%	3%	6%	5%	4%
Oven	3%	4%	5%	3%	3%	4%	3%	3%	2%	4%	3%	3%
Material costs	11%	17%	23%	11%	14%	16%	5%	11%	46%	16%	14%	11%
postprocessing costs	7%	10%	13%	7%	8%	9%	7%	7%	4%	9%	8%	7%
Machine costs	74%	59%	47%	74%	69%	64%	78%	74%	45%	63%	68%	74%

Figure 10. Cost structure of metal AM with varying production parameters and prices (modified: Lindemann et al. 2012, p. 177–188; Thomas & Gilbert 2014, p. 16).

3.1 Powder bed fusion

Powder bed fusion is one of the two powder-based metal additive manufacturing technologies and it is widely regarded as the most prominent one. The other powder based process is directed energy deposition, which is less utilized based on the unit sales, as PBF systems have seven times higher sales (Caffrey et al. 2016, p. 61). A handful of companies develop and sell metal powder bed fusion systems and most of them have different names for the process: selective laser melting (SLM), direct metal laser sintering (DMLS), LaserCUSING and electron beam melting (EBM). During this thesis the terminology used for all of these is powder bed fusion, as they are essentially all the same process of spreading powder in thin layers of few tens of microns and selectively melting and fusing some of the powder particles to form a solid that matches the cross-sectional geometry of the sliced 3D-model. After the first layer is consolidated, the building platform is lowered

by a distance of one layer thickness. A new layer of powder is then spread and again the path corresponding to the cross-sectional geometry of the second slice of the 3D-model is melted and fused together with the previously consolidated geometry. This process of spreading a powder layer and selectively melting the powder particles is repeated until all the sliced layers of the 3D-model are covered and a complete part is consolidated. (Gibson et al. 2015, p. 107–109; Frazier 2014, p. 1918–1919.) Figure 11 shows two schematic representations of the process with different heat source and powder handling configurations.

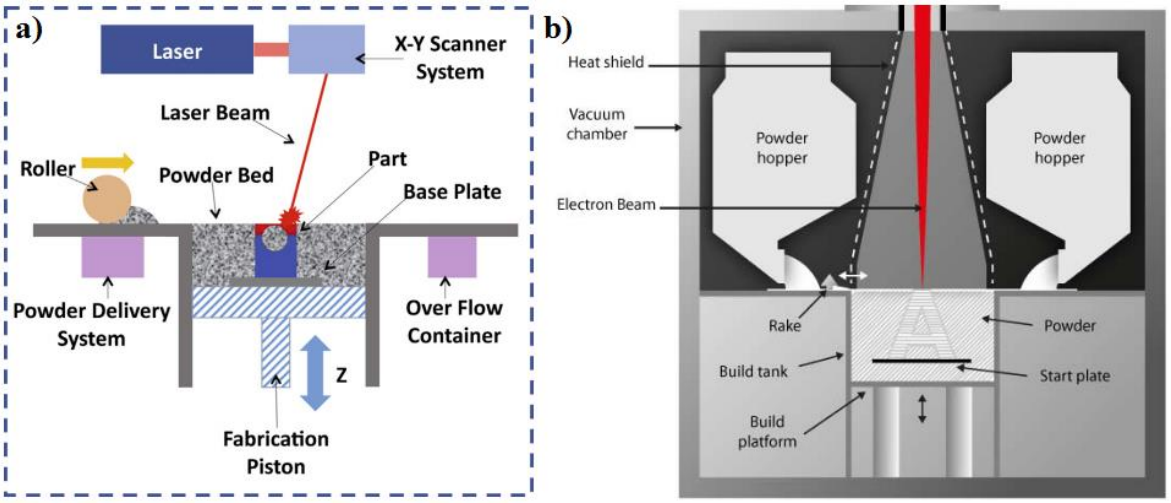

Figure 11. PBF process with a) laser as heat source, roller type spreading mechanism and powder reservoirs next to the building chamber and b) another configuration with electron beam, ruler type spreading and powder hoppers above the powder bed (modified: Thompson et al. 2015, p. 39; Arcam AB 2016).

3.1.1 Heat source

Between different PBF system manufacturers there are some key differences in the machines they provide. Most machines utilize laser beam as a heat source and the process is then called laser powder bed fusion (L-PBF). Electron beam is also used by one machine manufacturer as the heat source and then the process is electron beam powder bed fusion (E-PBF). Depending on the heat source the beam-material interactions differ significantly. The build chamber atmosphere is also affected by this, as electron beam requires a vacuum atmosphere, whereas the laser beam systems use inert gases as protection against melt oxidization. (Gibson et al. 2015, p. 137.) Concerning this study, the most significant difference is that L-PBF uses powders with particle size distributions around 15–45 µm

and E-PBF around 45–106 µm (Dawes et al. 2015, p. 246). The finer particle size distribution (PSD) used in L-PBF enables the use of thinner layers and therefore improving surface finish. E-PBF uses slightly thicker layers and coarser powders, which are usually less expensive, as the conventional powder production methods have higher yield in the particle size range of around 45–106 µm than in the range of 15–45 µm. (Sames et al. 2016, p. 10.) For example, in gas atomization the yield of powder in the desired particle size is around 20 % for L-PBF and 50 % for E-PBF (Caffrey et al. 2016, p. 61).

3.1.2 Powder spreading

The other major variation between different manufacturers is how they incorporate powder handling and spreading mechanisms in the machines. The powder containers prior spreading can be either above or next to the actual powder bed. The coater used to spread the powder from the reservoir to the build chamber is either a ruler or a roller, as seen in figure 12.

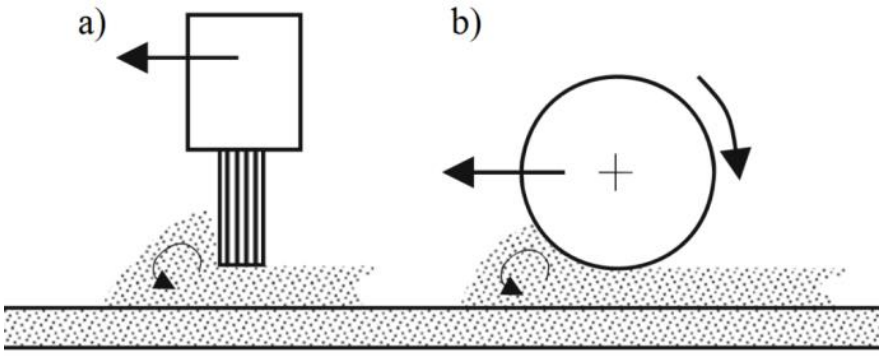

Figure 12. Powder spreading mechanisms used in powder bed fusion: a) ruler and b) counter-rotating roller (Spierings et al. 2016, p. 11).

The applied mechanism is crucial regarding the flowability and the resulting packing density of the powder bed. Nevertheless, the effects of different powder spreading mechanisms on the required flowability and resulting powder bed density have been scarcely studied (Sames et al. 2016, p. 10). Budding & Vaneker (2013, p. 527–532) conducted experiments with a ruler, forward-rotating roller, counter-rotating roller and with the combinations of these to determine the packing density of angular shaped plaster powder consisting of silica, vinyl polymer and sulphate salt. In their study, a counter-rotating roller resulted in a bulk density of 1.2 g/cm^3 and the ruler type spreader resulted in

a bulk density of around 1.0 g/cm^3 for the deposited powder bed. Similar results, indicating higher density powder bed for counter-rotating roller could be expected for metal powders; however this topic should be further studied as the metal powders used in PBF differ from the powder used in the study by Budding & Vaneker (2013, p. 527–532).

3.1.3 Waste in powder bed fusion

AM is often considered to be an extremely resource efficient manufacturing process, producing no waste as the material is only added where it is needed in the product. With powder bed fusion this is not entirely true. After the build, the powder that was not melted to form products is recycled to be reused in the next build, which is the foundation of the resource efficiency in additive manufacturing. The unused powder has to be sieved before reuse to remove any agglomerated particles which form near the part being built, where the temperature is high enough for sintering, but not for melting (Slotwinski et al. 2014, p. 476). The agglomerated particles are sieved out of the powder and left over as waste, referred to as sieve residue, which accounts for around 2–5 % of the powder used in each build (Ford & Despeisse 2016, p. 1575).

Few studies have been conducted to test the effect of recycling the unused powder and they all have concluded that the sieved powder can be reused multiple times without a significant effect to the quality of the parts manufactured (Ardila et al. 2014, p. 99–107; Tang et al. 2015, p. 555–563; Nandwana et al. 2016, p. 754–762). With reactive materials like titanium based alloys, the amount of oxygen increases along with the reuse cycles, which becomes a limiting factor at some stage. However, the oxygen content has been shown to remain under the upper limit of 2000 parts per million (ppm) for Ti-6Al-4V even after 21 reuse times. (Tang et al. 2015, p. 555–563.) These studies were conducted to represent the worst case scenario of not adding any virgin powder between builds. In production virgin powder would be added between builds to account for the material that was melted to form products, which would further reduce the effects of powder reuse. Successful reuse of the powder therefore limits the powder waste to the said 2–5 % sieve residue consisting of oversized particles.

The sieve residue is a constant waste stream in powder bed fusion, but depending on the geometry of the manufactured products, additional waste in the form of support structures

may be generated. Overhanging features that are less than 35 degrees inclined relative to the build platform with only the powder bed beneath are not self-supporting. In addition, such features have limited ability to conduct the extensive heat away from the melt, resulting in dross formation, undesirable microstructures and heat distortions that can ruin the part being built. Additional support structures are therefore needed beneath such features to anchor the part to the build platform, providing mechanical support and a way for the heat to conduct to the base plate. After the build these supports need to be removed and they are regarded as scrap metal, comparable to the new scrap described in chapter 2.1. The amount of supports needed depends entirely on the part geometry. Sometimes only small amounts are needed beneath the part to ease the removal from the platform, while in other cases the powder needed to manufacture the supports is more than the powder that goes in to the final product. (Gibson et al. 2015, p. 143; Cloots, Spierings & Wegener 2013, p. 631–643.) Figure 13a shows geometries where support structures (red arrows) are needed. Figure 13b shows a additively manufactured removable partial denture, with high amount of material needed for support structures compared to the actual finished product.

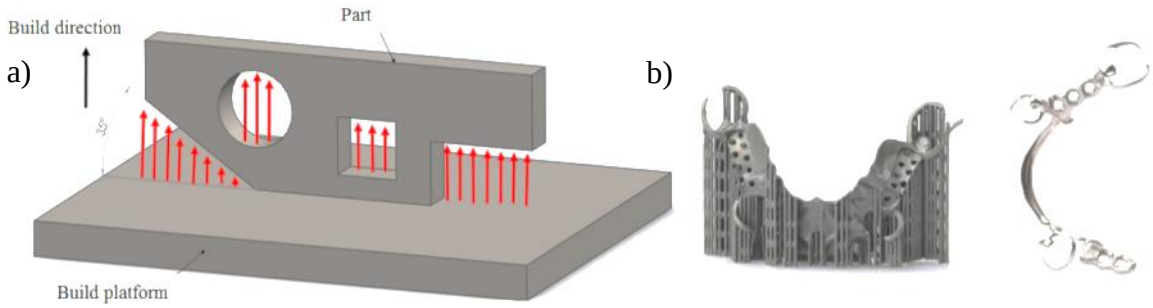

Figure 13. a) Geometries that need support structures and b) a removable partial denture manufactured with PBF (EOS 2013).

The third form of scrap that might be produced, but should be avoidable entirely is rejected parts due to some defect introduced during the powder bed fusion process. A defected part may be caused by flawless design, incorrect parameters or by some error or fault in the machine that causes the build to cease before the part is finished.

3.2 Characteristics of metal powders for powder bed fusion

The following characteristics are for powders used in L-PBF because this AM technology is used in the experimental part of this thesis. The metal powders used as feedstock for

PBF AM have unique requirements from the powder properties. It is crucial that each spread powder layer is uniform. This requires robust powder feeding and spreading mechanisms, but more importantly the powder properties have to be such, that the powder spreads evenly and packs dense enough. These features of the powder bed affect the melting and solidification behaviour of the powder and ultimately the final part's properties. (Strondl et al. 2015, p. 549–554.) To assure in advance that the powder can be used in powder bed fusion a few key properties of the powder can be analysed and based on this characterization the powder can be validated for use without costly and time consuming test runs (Clayton, Millington-Smith & Armstrong 2015, p. 544).

3.2.1 Particle morphology

The powders used in powder metallurgy applications consist of individual particles which can be characterized not only by size, but also by shape. Regarding powders used in additive manufacturing, the particle morphology can be defined either as irregular or spherical. Powders that consist of particles with random geometries and where one cannot distinguish a particular recurring shape are regarded as irregular or random. This is usually the case with metal powders manufactured by mechanical crushing or milling. With thermal processes like gas atomization and plasma spheroidization it is possible to prepare metal powders with spherical powder morphologies. Depending on the manufacturing method and the processing conditions, the sphericality of the particles varies from completely spherical to somewhat elongated or otherwise deformed shapes, with the nominal shape still being a sphere. (Benson & Snyders 2015, p. 109.) Such particle morphology is referred to as quasi-spherical during this thesis.

Particle morphologies of powders used in additive manufacturing are determined via scanning electron microscopy (SEM), by scanning a focused electron beam on the powder particles. The electrons are scattered from the particle surfaces and a high resolution image is constructed based on the electron beam-particle interactions. SEM images are representations of the topography of the particles, resulting in images from which the shape of the particles is easy to determine visually. (Slotwinski et al. 2014, p. 464.) Figure 14 shows metal powders with three different particle morphologies from irregular to quasi-spherical and highly spherical.

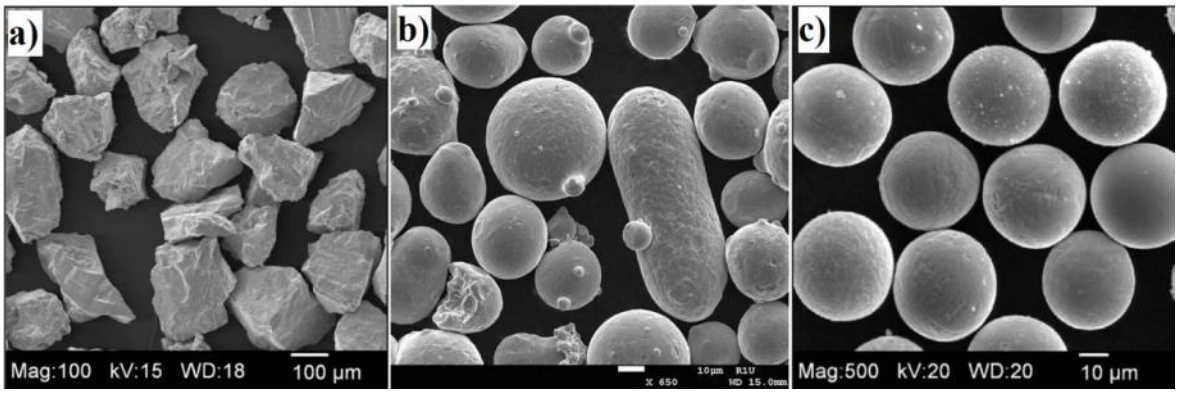

Figure 14. SEM images of a) irregular, b) quasi-spherical and c) highly spherical particle morphologies (Slotwinski & Garboczi 2015, p. 539; McCracken, Motchenbacher & Deeter 2012).

Additive manufacturing, especially powder bed fusion, favours powders with spherical particle morphology to assure good flowability, dense packing of the powder bed and predictable beam-powder material interactions. Fully sph erical particles would be ideal, but in most cases the powder is gas atomized which yields only quasi-spherical powder as seen in figure 14b. Fine spherical particles agglomerating to form so called satellites are more problematic, as they essentially become particles with irregular morphology and therefore reduce the flowability and packing density of the powder. The effect of particle morphology on the flowability and packing density of powder is shown in figure 15, which clearly shows increasing trend for both properties as the powder approach spherical morphology. A spherical particle corresponds to the blockiness value N=2 in figure 15.

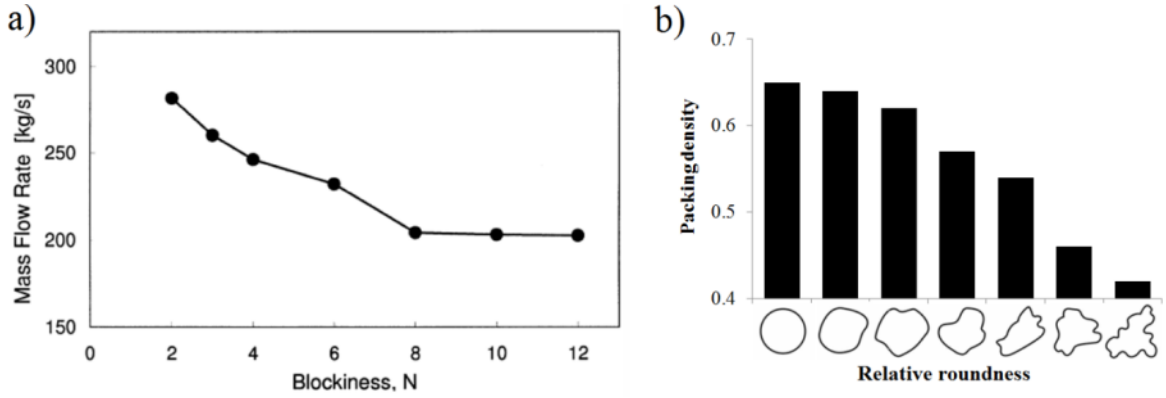

Figure 15. Effect of particle morphology on a) flowability and b) packing density (modified: Cleary & Sawley 2002, p. 99; German 1989, p. 123).

3.2.2 Flowability

Flowability is the parameter used to describe AM powders for how well the powder layers can be generated from that powder. As the powder consists of large amounts of fine particles (diameters less than 100 µm), the inter-particle forces such as Van der Waals attractive forces and electrostatic forces become substantial, gravitation attributing less to the behaviour of the powder. Increase in the particle size increases the role of gravity, which changes the flow and packing behaviour of the powder. In addition, moisture content in the powder limits the flowability. For polydisperse powders, consisting of particles with various sizes, particle shape and size distribution control flowability. Spherical particle shape is ideal for good flow. As for the particle size, increasing the volume fraction of fine particles in the powder reduces flow as the inter-particle forces increase resulting in agglomeration of particles. This is problematic for powder bed fusion, because for other reasons (see chapter 3.3) finer powders would be desirable. Therefore one must compromise with the particle size distribution of the powder to assure sufficient flowability, without making the powder too detrimental for other prospects, like powder layer quality and ultimately finished part quality. (Spierings et al. 2016, p. 9–20; Vlachos & Chang 2011, p. 71–80.)

There are different methods of analysing powder flowability and it is important to choose a technique that represents most accurately the way that the powder flows in the given application (Krantz, Zhang & Zhu 2009, p. 239–245). Hall flowmeter is widely used because it is a simple technique and the same equipment is used in the determination of apparent and tap densities of the powder. Hall flowmeter measures the time it takes for 50 grams of powder to flow through the standardized funnel with a 2.5 mm opening (SFS-EN ISO 4490 2014, p. 1–4). This test method is recommended for AM powders by ASTM (ASTM F3049-14 2014, p. 3). However, limitations in using the Hall flowmeter for characterising PBF powders has been identified and there is a need for a flowability measurement method where the flow state of the powder is closer to that of the PBF machines (Slotwinski & Garboczi 2015, p. 539–540). It is clear that during the powder spreading in the PBF machine the powder flows in a different manner than it does in the Hall flowmeter. However, the method is suitable for comparing the flowability between different powders. First hand flowability estimation is typically done optically, as to define

whether the powder might have sufficient flowability for powder bed fusion. Figure 16 shows optical evaluation done for four different powders by five experienced people.

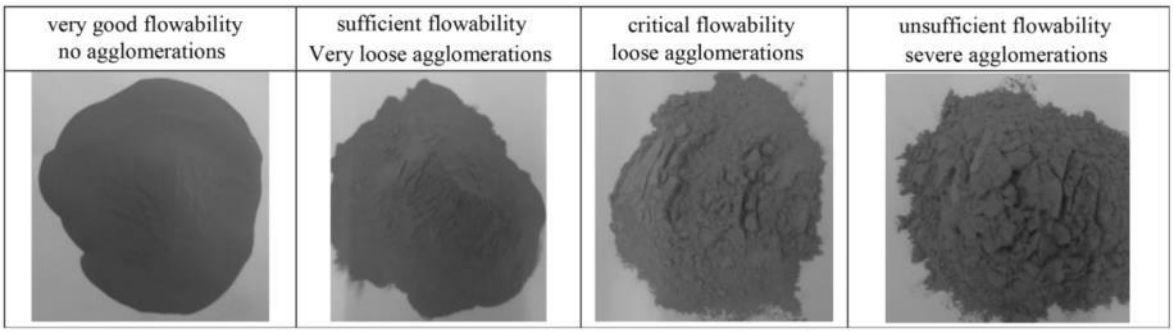

Figure 16. Optical evaluation of powder flowability (modified: Spierings et al. 2016, p. 14).

3.2.3 Density

Density of powder material can be understood in many different ways, so a clear distinction is needed. Particle density means the true density of the powder and is the density of the material itself. Here we are interested in the packing density of the powder material. In standards for determining the packing density of powder material, two different packing densities, apparent and tap density, are considered. Apparent density is used to determine how well the powder fills a given volume. Powder with good apparent density has fewer voids between the particles. According to standard SFS-EN ISO 3923-1 (2008, p. 1), apparent density is the loose packing density of the powder, obtained by measuring "the mass of a certain quantity of powder, which in loose condition exactly fills a cup of know volume". The cup is filled by running the powder through a funnel above the cup, resulting in loose packing of the powder. Dividing the measured mass with the known volume of the cup gives us apparent density of the powder. (SFS-EN ISO 3923-1 2008, p. 1.) Tap density is determined by tapping a specified quantity of the powder in a container until the volume no longer decreases. The tap density is given by dividing mass of the powder quantity with the volume it occupies after the tapping. (SFS-EN ISO 3953 2011, p. 1.)

As the powder is tapped it packs more tightly, therefore the tap density of a given powder is higher than the apparent density. In powder bed fusion the powder flows upon the previously spread powder layers and the spreading mechanism compacts the powder with

some force. However, the resulting packing density of the powder bed is not as tight as with the apparatus in the tap density standard, nor is it as loose as with the apparent density standard, it is somewhere in between these two values (as seen later in figure 21). For comparison of packing behaviours between different powders these test methods are however sufficient. In powder bed fusion powders with high packing densities are preferred. High packing density has a positive impact on laser absorption and thermal conductivity of the powder bed and it also produces more dense finished parts with better mechanical properties. (Boley, Khairallah & Rubenchik 2015, p. 2478; Liu et al. 2011, p. 232; Gibson et al. 2015, p. 124.) The packing density of the powder bed in turn depends on the particle shape, particle size distribution and the powder spreading mechanism used (Gibson et al. 2015, p. 124).

3.2.4 Particle size distribution

The diameter of the particles and the volume fraction that each particle size accounts for in the powder can be defined from the particle size distribution. In PBF thin layers of powders have to be generated so that accurate parts can be produced. Typically the layer thicknesses vary from 20 to 150 µm (Gibson et al. 2015, p. 124). This sets the upper limit for the particle size in the powders. However, it has been shown that the effective or real layer thickness is around 1.5–2 times the set layer thickness (distance that the platform lowers between layers), depending on the set layer thickness and packing density of the powder bed (Spierings & Levy 2009, p. 348). Some of the particles larger than the layer thickness are pushed down to the powder bed by the spreader, but most are just swept to the used powder's reservoir (Slotwinksi et al. 2014, p. 475–476). Extremely fine particles on the other hand, tend to agglomerate as a result of the increased role of the Van der Waals and electrostatic forces, therefore limiting the particle size distribution from the other direction. Agglomerated particles reduce the flowability and packing density of the powder. Typical particle size distribution curves are shown in figure 17.

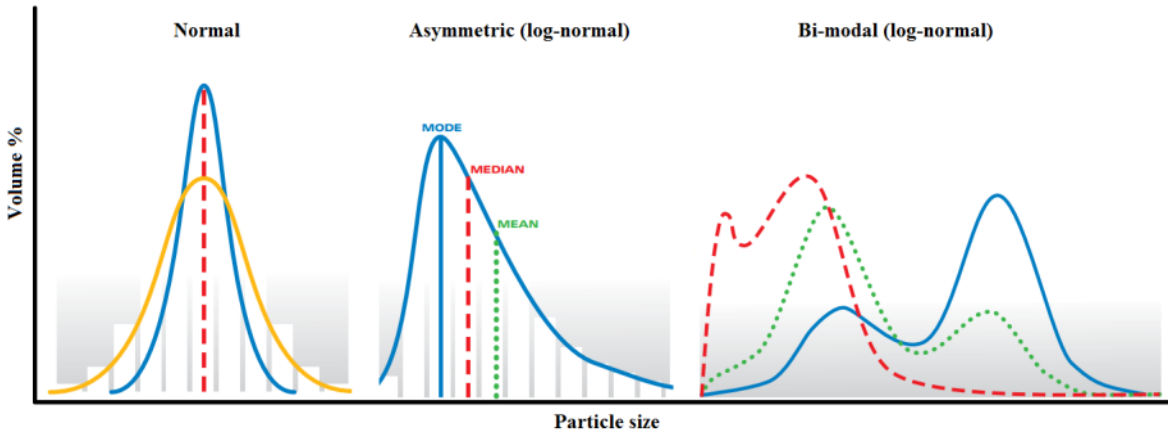

Figure 17. Different particle size distribution curves (modified: Horiba 2016, p. 3, 5, 9).

For normal distribution the mode, the median and the mean value is equal. A normal distribution is often referred to as Gaussian distribution. Asymmetric distribution has median and mean particle sizes shifted either left or right from the highest peak in the distribution, which is the mode. Bi-modal distribution has two distinctive modes and distributions with even more modes are referred to as multi-modal. For powder bed fusion a narrow Gaussian distribution or bi-modal distribution are preferred to achieve good flowability, packing density and desired finished part properties. Powders with Gaussian particle size distributions in the range of 15–45 µm are typically used, because the powder production processes produce powders with variable particle sizes. (Spierings, Herres & Levy 2010, p. 397–406; Shi & Zhang 2008, p. 621–626; Caffrey et al. 2016, p. 60–61.)

In addition to the graphical particle size distribution, values of D10, D50 and D90 can be used to define the width of the distribution. D50 is the median meaning that 50 % (volumetric or mass percent) of the particles have a smaller diameter than this value. D10 means that 10 % are below this value and D90 means that 90 % of the population have diameters less than this. An example of this imposed on the graphic distribution curve is shown in figure 18. (Slotwinski et al. 2014, p. 467; Horiba 2016, p. 6)

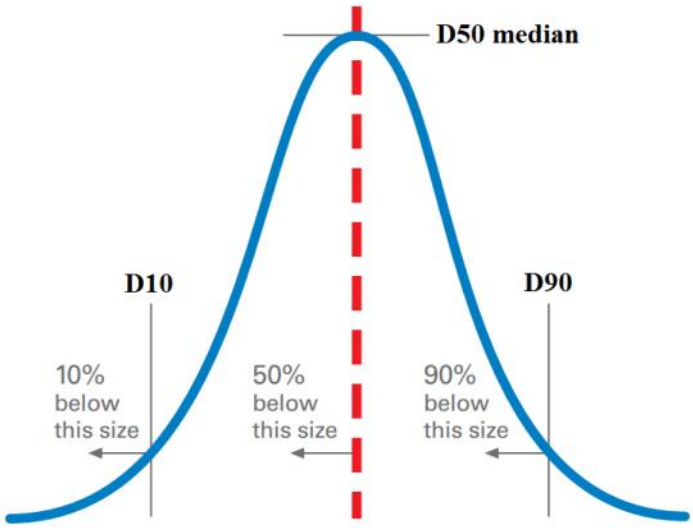

Figure 18. D10, D50 and D90 values of a particle size distribution (modified: Horiba 2016, p. 6).

For powders used in additive manufacturing the commonly used measuring method is laser diffraction, which calculates the particle size distribution from the diffraction pattern produced by a laser beam passing through the particles in the powder batch. Laser diffraction requires that the particles to be analysed are dispersed either in air (dry method) or in liquid (wet method), so that a diffraction pattern can be produced. There are some concerns about the accuracy of laser diffraction in defining the particle size distribution; mostly because the calculations used to convert the diffraction pattern into particle size distribution assumes all particles to be completely spherical. (Slotwinski & Garboczi 2015, p. 540; Slotwinski et al. 2014, p. 462.) As seen in the SEM images of powder that is used in additive manufacturing (figure 14), some particles are only near-spherical, also with obvious irregularities among them. However, the aim of the AM metal powder industry is to produce more spherical powders, as seen in the plasma spheroidized powder figure 14c), which will provide more accurate particle size distributions measured with laser diffraction. Figure 19 shows the PSD curve and corresponding data of laser diffraction analysis for commercially available 17-4 stainless steel (SS) powder used for powder bed fusion. SEM image of the analysed powder is also included. In this case the median particle size is 36.5±0.2 µm and the log-normal distribution is slightly asymmetric towards coarse particles. (Slotwinksi et al. 2014, p. 467, 468.)

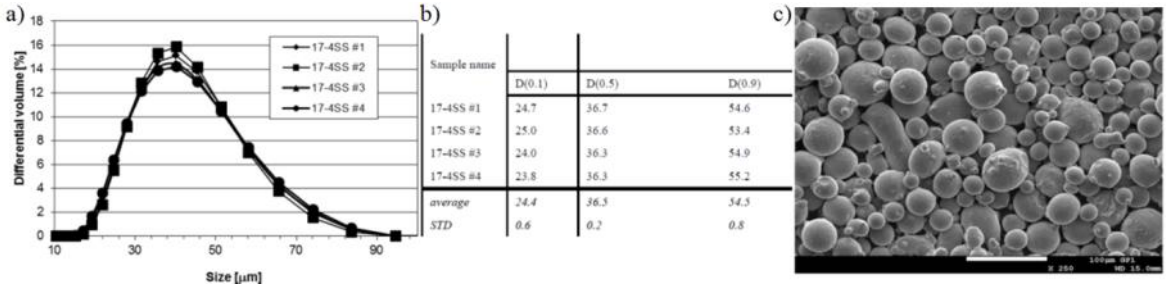

Sample name	D(0.1)	D(0.5)	D(0.9)
17-4SS #1	24.7	36.7	54.6
17-4SS #2	25.0	36.6	53.4
17-4SS #3	24.0	36.3	54.9
17-4SS #4	23.8	36.3	55.2
average	*24.4*	*36.5*	*54.5*
STD	*0.6*	*0.2*	*0.8*

Figure 19. A) PSD curve, b) numerical PSD and c) SEM image of 17-4 SS powder used in AM (modified: Slotwinski et al. 2014, p. 467, 468, 475).

Particle size distribution effects on how the powder flows and how the powder packs, therefore it is a crucial parameter for PBF AM powders, where good flowability and high packing density is required to produce uniform layers of powders. Extremely fine particles with diameters less than 10 µm fill in the voids between the larger particles, increasing the packing density of the powder bed and therefore affect positively to the density of the finished parts. (Slotwinksi et al. 2014, p. 475–476; Gu et al. 2014, p. 470–483.) From figure 20 it can be seen that volume fraction of around 30 % of small particles in a bi-modal size distribution is favoured to achieve good packing and flow. With higher amounts of fine particles the flow and density starts to decrease as the fine particles agglomerate to each other.

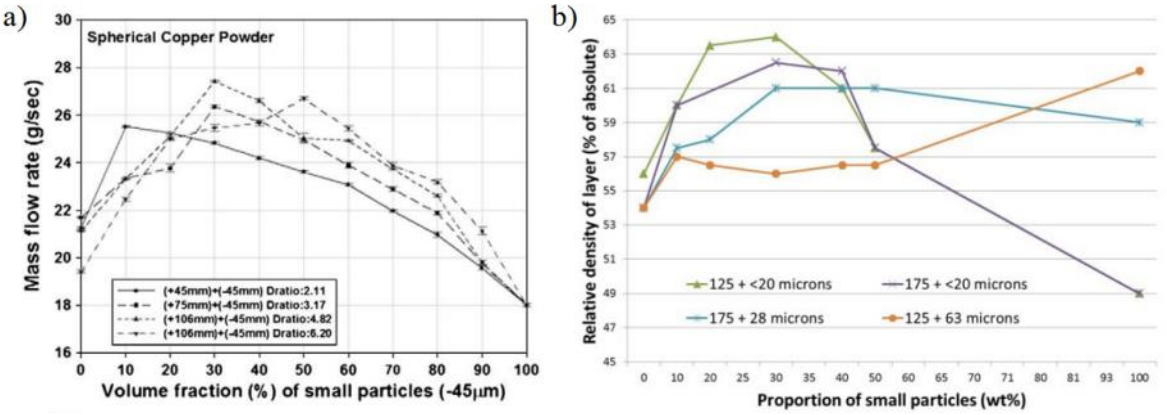

Figure 20. Effect of the volume fraction of small particles in a bi-modal particle size distribution on a) flow of copper powder and b) packing of nickel powder (Benson & Snyders 2015, p. 108; Vlachos & Chang 2011, p. 76).

For normal- and log-normal particle size distributions, including Gaussian distribution, the width, absolute particle size and asymmetry have been shown to have an effect on the

packing density and flow of the powders. The optimal distribution has to be a compromise between flow and packing density properties. For distributions with D50 values close to each other a narrow distribution promotes good flowability whereas a wider distribution with asymmetry towards the finer particles promotes good packing density, as seen from figure 21 (Liu et al. 2011, p. 231–232). In log-normal distributions, when the shape of the distribution is constant the increase in absolute particle size increases the packing density (Zou, Gan & Yu 2011, p. 4719). As explained earlier, increase in particle size decreases the role of inter-particle forces in the powder and therefore the particles form less agglomerates and the particles pack more efficiently.

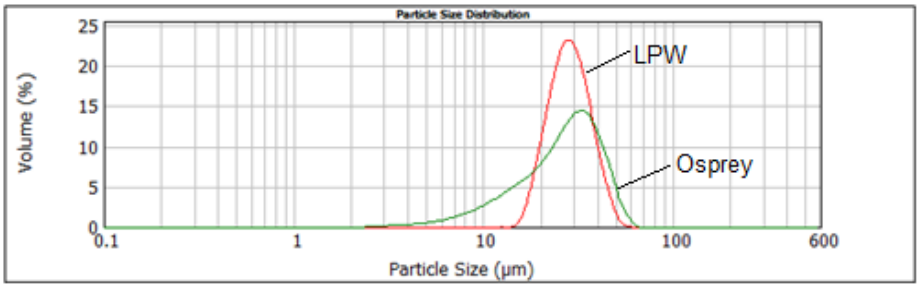

Brand [-]	Apparent density [g/cm^3]	Powder bed density [g/cm^3]	Tap density [g/cm^3]	Hausner ratio [-]
Osprey	4.54	5.312	5.54	1.22
LPW	4.33	4.88	5.03	1.16

Figure 21. Effect of particle size distribution on powder packing and flowability (modified: Liu et al. 2011, p. 231–232).

In the study by Liu et al. (2011, p. 227–238) two 316L stainless steel powders with different size distributions were compared. In addition to the standardized apparent and tap density measurements, they defined experimentally the actual powder bed density for the specific machine (SLM-Realizer 100) they used. A hollow container with defined volume was manufactured with the powder bed fusion system and the unfused powder filling the container after the build was weighted to get the density. For flowability evaluation Hausner ratio was used, which is the ratio between tapped and apparent density values of the powder. Higher Hausner ratio indicates poorer flowability.

In laser-based AM, PSD also has an effect on how the laser beam interacts with the powder. Boley et al. (2015, p. 2477–2482) numerically estimated the laser absorption by metal powders in PBF AM. It was shown that powders with bi-modal PSD's with larger amount of fine particles have higher absorptivity than powders with mono-modal Gaussian distribution. The absorption by the powder particles, referred to as spheres in figure 22, accounts for less with Gaussian distribution than bi-modal distribution. In powders with Gaussian distribution more of the incident laser energy is absorbed by the substrate, which is either the building platform or the previously solidified layer in case of PBF. It can also be noted that there is significant variation in the absorption values during the distance that the beam travels on the powder bed, which may cause non-uniform melting behaviour.

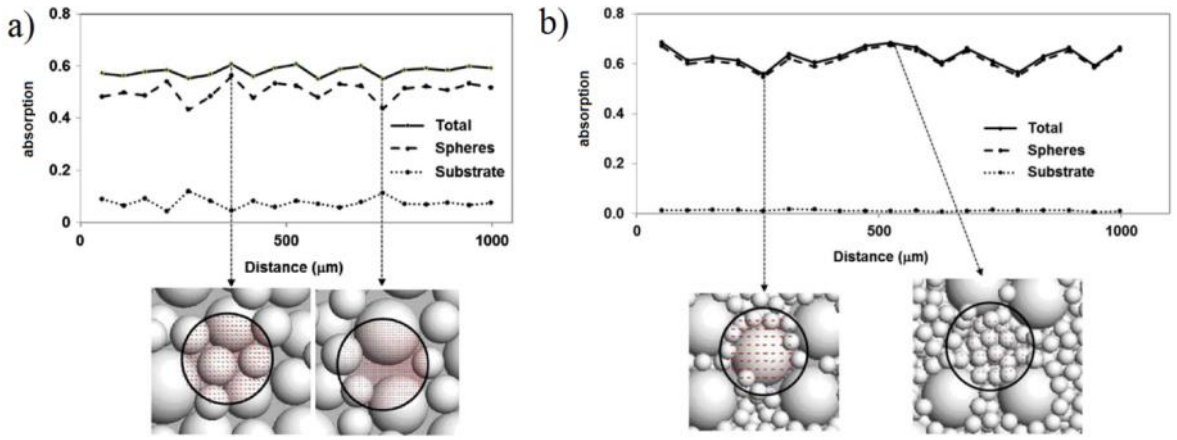

Figure 22. Absorption at 1 μm wavelength calculated for spherical stainless steel powders with a) Gaussian and b) bi-modal particle size distributions (Boley et al. 2015, p. 2481).

3.2.5 Chemical composition and microstructure

Desired physical properties of engineering metals and alloys such as high strength, ductility, toughness and hardness are governed by the microstructure of the material, which in turn depends on the chemical composition and processing history of the material. First of all, to achieve the desired physical properties to the finished parts in PBF AM, the chemical composition of the feedstock powder has to remain in the limits defined for each specific alloy. Secondly, the processing history, in this case the powder manufacturing and the melting and multiple re-heating steps during the additive manufacturing process, affect the microstructure of the finished parts. Thirdly, the chemical composition may change during the additive manufacturing process because of reactions between the material and the gases in the build atmosphere and also, because of evaporation of volatile alloying

elements, such as aluminium from Ti-6Al-4V alloy during E-PBF (Sames et al. 2016, p. 325; Juechter et al. 2014, p. 256). These changes depend on the material, as the affinity towards gas pickup and the evaporation temperatures are always material specific.

The chemical composition of metal powders can be measured with the scanning electron microscope coupled with energy dispersive elemental analysis. As the electrons interact with the sample material, X-rays unique to each element are produced. These X-rays can be detected and analysed with proper instrumentation and calibration to provide qualitative bulk chemistry of the sample material. This technique is called energy-dispersive X-ray spectroscopy (EDS). Accurate and quantitative bulk chemistry analysis requires that the sample surface is flat and polished. Even with such samples, the EDS chemistry analysis is a surface sensitive method as the penetration of the electrons at a typical acceleration voltage of 15 kV is a single crystal layer in steel. (Slotwinski et al. 2014, p. 464.) This means that, for example EDS analysis of a material that forms oxide layers upon the surface would result in bulk chemistry values where the amount of oxygen is too high and does not represent the true amount of oxygen in the bulk of the sample.

Microstructure of metals refers to the crystal phases that are present and their volume in the material. Microstructure of bulky specimens is typically determined by polishing and etching the sample surface with an alloy specific etching reagent, which will bring out the different crystal structures to be distinguished visually with the aid of microscopy. For fine particles in metal powders, X-ray diffraction analysis (XRD) is more suitable method for determining the crystal phases present in the powder material. The diffraction patterns produced by each crystal phase in the material are unique, shown as diffraction peaks in the pattern, as in figure 23. The powder material in question is 17-4 precipitation hardening (PH) stainless steel, with face-centred cubic (FCC) and body-centred cubic (BCC) structures present. (Slotwinski et al. 2014, p. 464.) The FCC is austenite but it should be noted that the XRD analysis denotes both ferritic and martensitic structures in this case as BCC, because of the very low tetragonality of the actually body-centred tetragonal (BCT) structure of martensite in 17-4 PH stainless steel (Cheruvathur, Lass & Campbell 2016, p. 932).

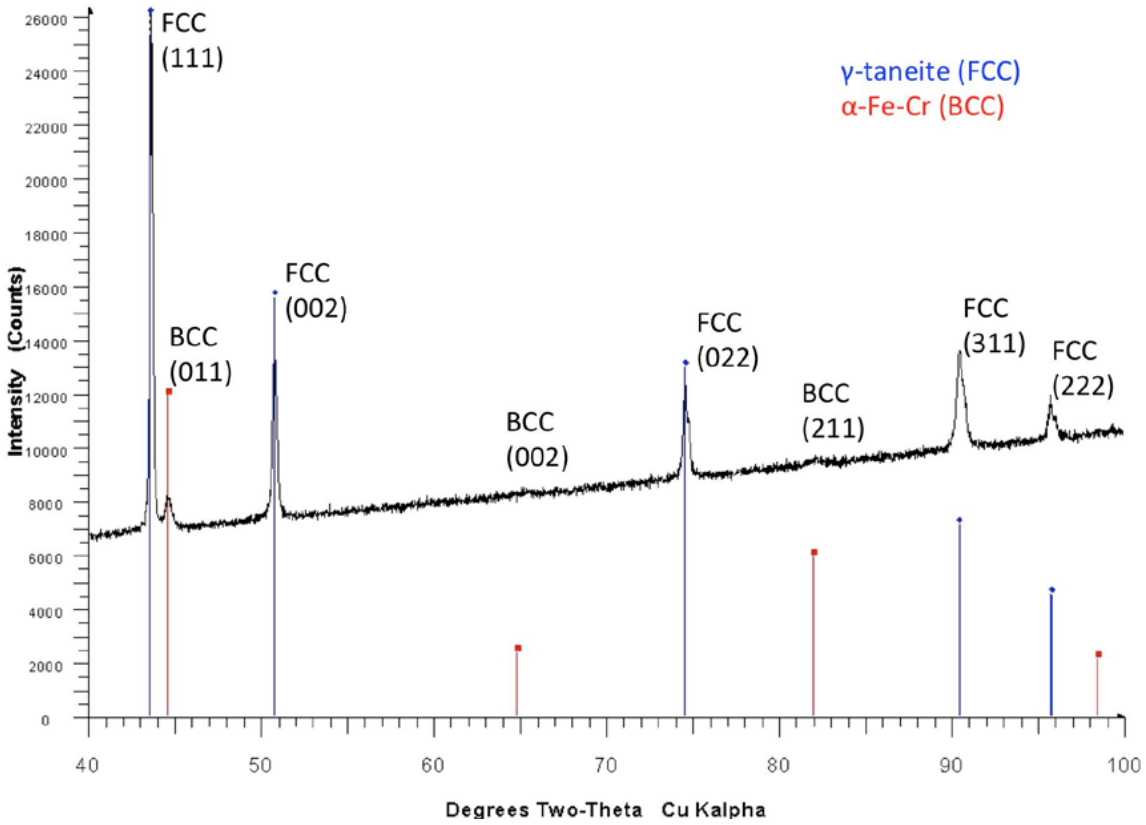

Figure 23. X-ray diffraction pattern of 17-4 stainless steel powder, showing diffraction patterns corresponding to FCC (dominant phase) and BCC crystal structures (Slotwinski et al. 2014, p. 470).

Impurities in the form of unwanted elements in the powder can alter the microstructures and mechanical properties of the finished parts. Solid impurities can be introduced to the powder in the form of dust or other small particles mixing to the powder from the surroundings. The other source is from reactions with solid surfaces that the powder is in contact with, for example during atomization. Gaseous elements like oxygen, nitrogen and hydrogen are picked up by the powder from the atmosphere. Oxygen pickup by the powder is one of the major concerns with materials having a high reactivity and solid solubility towards oxygen, which is the case with titanium, where increased oxygen contents decrease ductility (Lütjering & Williams 2007, p. 15, 50.) As the particle size in the powder decreases, the surface area to volume ratio increases, meaning that there is more surface of the material susceptible to oxidation, increasing the overall oxygen content in the powder. The linear increase in oxygen content as a function of specific surface area of the powder is shown in figure 24. In addition, the melt tends to pick up more oxygen from

the build atmosphere, as there is always a minor amount of oxygen present even with inert gas protection.

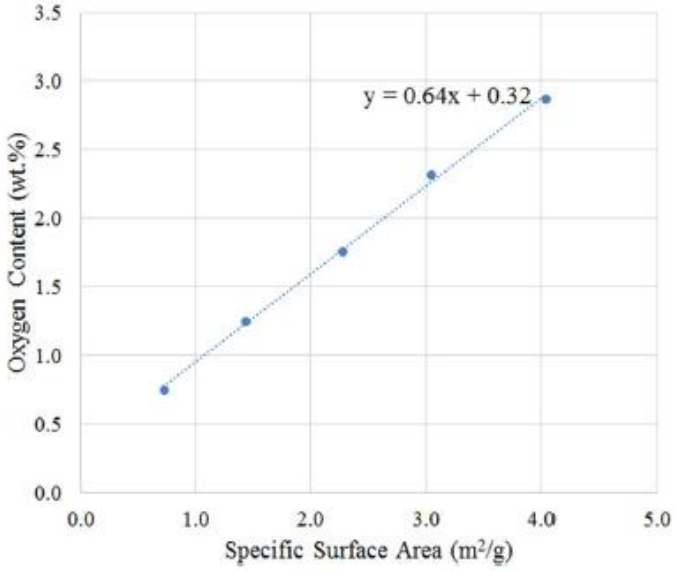

Figure 24. Oxygen content of ball-milled Ti-6Al-4V hydride powder as a function of specific surface area (Sun et al. 2016, p. 334).

3.3 Effects of powder properties on the finished part

Even if the powder is characterized to be usable in the AM machine in terms of how it behaves during the spreading and packing, it is only half the truth. Usability in the machine does not guarantee that the final parts produced from the powder meet the required specifications for mechanical properties. Therefore the effect of varying powder properties on the properties of the finished part has to be known.

3.3.1 Porosity and mechanical properties

Porosity, or the relative density of the parts that have been manufactured by additive manufacturing, is crucial for the mechanical and functional properties of the finished part. Since the powder bed fusion process is a full melting, not sintering process, near fully dense parts can be manufactured with the right set of parameters. However, it has been shown that parts manufactured with the same machine and constant parameters, but from powders with different particle size distributions and morphologies, result in different levels of porosity in the finished parts. Gu et al. (2014, p. 470–483) studied the effects of powder variation on the properties of additively manufactured parts. Three gas atomized Ti-6Al-4V powders provided by three different suppliers (EOS, LPW and Raymor) were

analysed and the tensile properties and microstructures of the manufactured test pieces were compared. With constant parameters that were optimized for the Raymor powder, it was shown that severe porosity was present in the parts manufactured from EOS and LPW powders, which had particle size distributions with larger volume mean diameter. Figure 25 shows SEM images of the three powders, with the mean volume diameter values (MV) and corresponding standard deviation values (SD) from the PSD analysis.

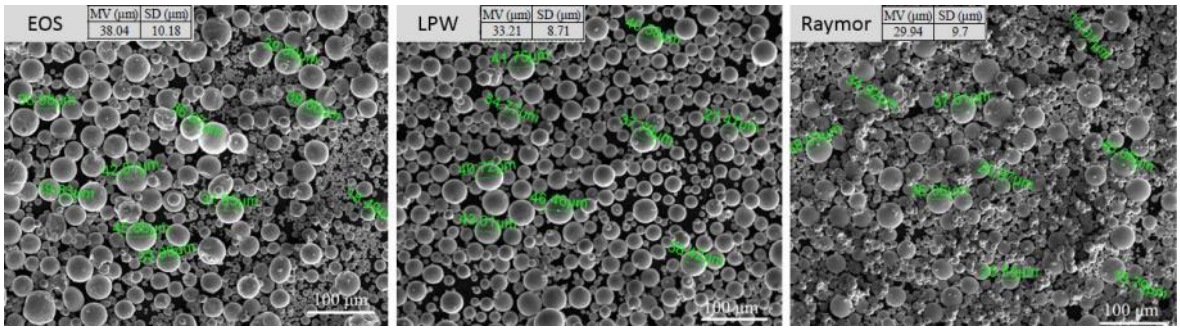

Figure 25. SEM images of Ti-6Al-4V powders from three different manufacturers (modified: Gu et al. 2014, p. 476–477).

From the SEM images it can be seen that the Raymor powder has the most and LPW powder the least amount of extremely fine (<10 µm) particles. Figure 26 shows the cross-sections of the manufactured tests pieces. Raymor test piece c) is almost fully dense, whereas EOS a) and LPW b) show multiple pores, marked with red circles. Manufacturing almost fully dense parts from all three powders was achieved by adjusting the hatch spacing between the melted tracks. Decreasing the distance between adjacent tracks allows for more melt overlapping, filling the pores that formed between the tracks with constant parameters. (Gu et al. 2014, p. 470–483.)

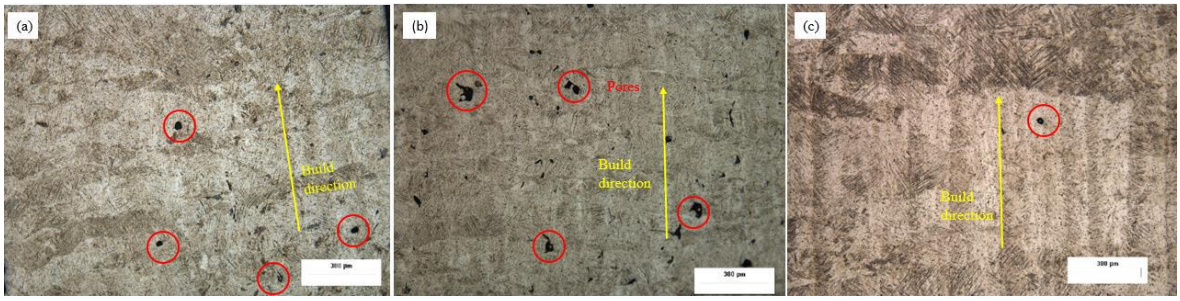

Figure 26. Cross-sections showing the microstructure of Ti-6Al-4V test pieces manufactured from a) EOS, b) LPW and c) Raymor powders (Gu et al. 2014, p. 480).

Other experimental studies by Liu et al. (2011, p. 227–238) and Strondl et al. (2015, p. 549–554) and numerical simulations together with experimental confirmation test by Gürtler et al. (2014, p. 1099–1117) have come to the same conclusion that the particle size distribution of the powder used has an effect on the density of PBF AM parts. Powders with coarser particles and less fine particles result in increased porosity in the finished parts.

In the study by Gu et al. (2014, p. 470–483) no significant difference in tensile properties between the test specimens manufactured from the different powders was seen, all providing yield strengths around 1100 MPa and tensile strengths around 1200 MPa. However, as it was shown, there was significant increase in porosity as the volume mean diameter of the powder increased, which could be detrimental to the fatigue performance of the manufactured parts. In a study by Strondl et al. (2015, p. 549–554) is was also concluded for additive manufactured Ti-6Al-4V and nickel alloy parts that variations in the physical properties of the powder have no significant effect to the tensile properties of the manufactured parts. However, it was shown that increase in the oxygen content of the powder, considered as an impurity in the studied material Inconel 718, leads to decrease in the ductile properties of the additively manufactured parts. 58.8 % increase in the powder oxygen content resulted in 11.1 % decrease in elongation in tensile testing and the impact energy decreased from 109 J to 93.7 J in Charpy V impact toughness test. In another study by Tang et al. (2015, p. 555–563) increase in oxygen content from 800 ppm to 1900 ppm of the studied Ti-6Al-4V powders resulted in an increase on the yield strength from 834 MPa to 960 MPa and tensile strength from 920 MPa to 1039.3 MPa in the additively manufactured parts. In their study the effect of oxygen increase on ductility was insignificant, however it was noted that with higher oxygen content of around 3300 ppm the ductility is known to drop sharply.

Liu et al. (2011, p. 227–238) studied two different powders, one with a narrow Gaussian PSD and the other significantly asymmetric towards fine particles as already seen in figure 21. In their study the powder with wide PSD produced parts with higher densities but with lower tensile strength and hardness than the narrow PSD powder. This indicates that the PSD of the powder has an effect on the mechanical properties of PBF parts.

A recent study by Irrinki et al. (2016, p. 860–868) reports similar results regarding part density: powder consisting of finer particles resulted in higher density parts with low energy densities, as seen in figure 27. The differences in porosity were significantly reduced with higher energy densities. However in their study, where four different 17-4 PH stainless steel powders were compared, significant differences in mechanical properties were found supporting the results by Liu et al. (2011, p. 227–238) but opposed to the findings by Strondl et al (2015, p. 549–554) and Gu et al. (2014, p. 470–483). The results indicated reduced mechanical properties for water atomized powders with larger median particle sizes compared to the gas atomized powder with smaller median particle size. The water atomized powders had irregular morphology whereas the gas atomized powder was spherical. It should be noted that with the high energy densities the irregularly shaped powders yielded comparable densities with higher tensile strength and hardness values than the spherical gas atomized powder, indicating the possibility of using poorer quality powders with acceptable results in powder bed fusion.

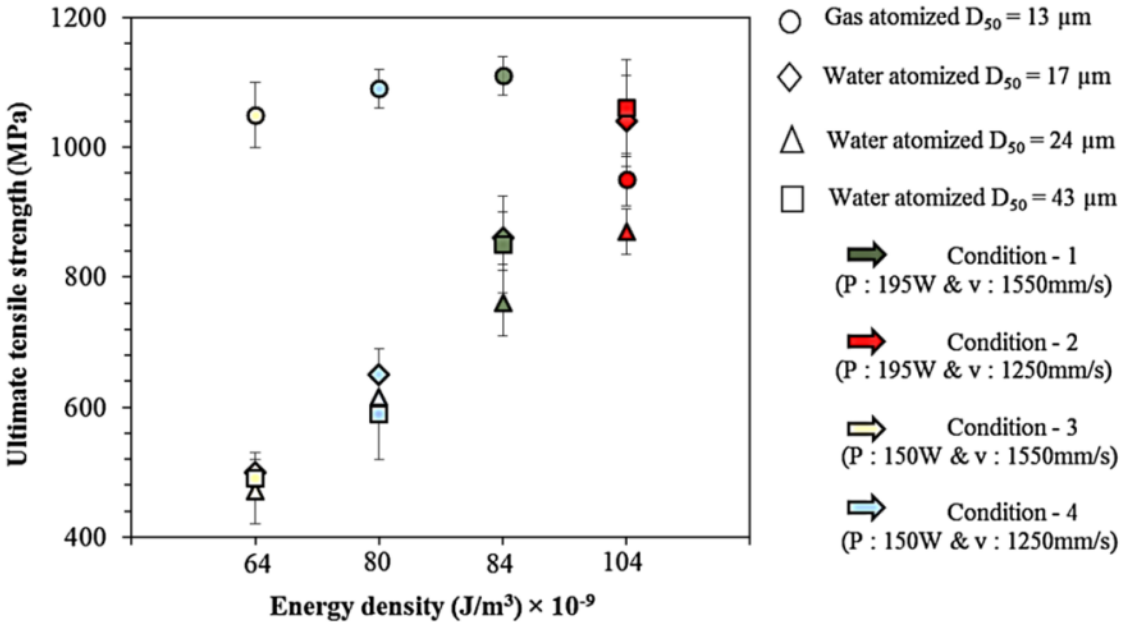

Figure 27. Effect of varying powders and energy densities on ultimate tensile strength of additively manufactured 17-4 PH stainless steel parts (Irrinki et al. 2016, p. 865).

Even with comparable part densities the variations in mechanical properties were relatively large in the study by Irrinki et al. (2016, p. 860–868). This indicates differences in the elemental composition of the powders and/or microstructures of the finished parts. In their

study the chemical compositions were not reported. The water atomized powders could have higher levels of impurities to degrade the mechanical properties. Water atomization is known to produce powders with higher levels of impurities compared to gas atomization. In addition, microstructures of the resulting parts were not reported. Variation in the microstructure is most likely the cause for the variation in mechanical properties. The melting and solidification behaviour of the powders with smaller particles is different than for the coarser powders, which could result in different microstructures in the 17-4 PH stainless steel. The hardness measured in Rockwell C (HRC) varied from 25 to 39 HRC depending on the energy densities. Figure 28 shows clear trend in the increase of hardness while increasing energy density, however between the powders there is no clear connection, as no single powder constantly yields higher or lower hardness values than the others with varying energy densities.

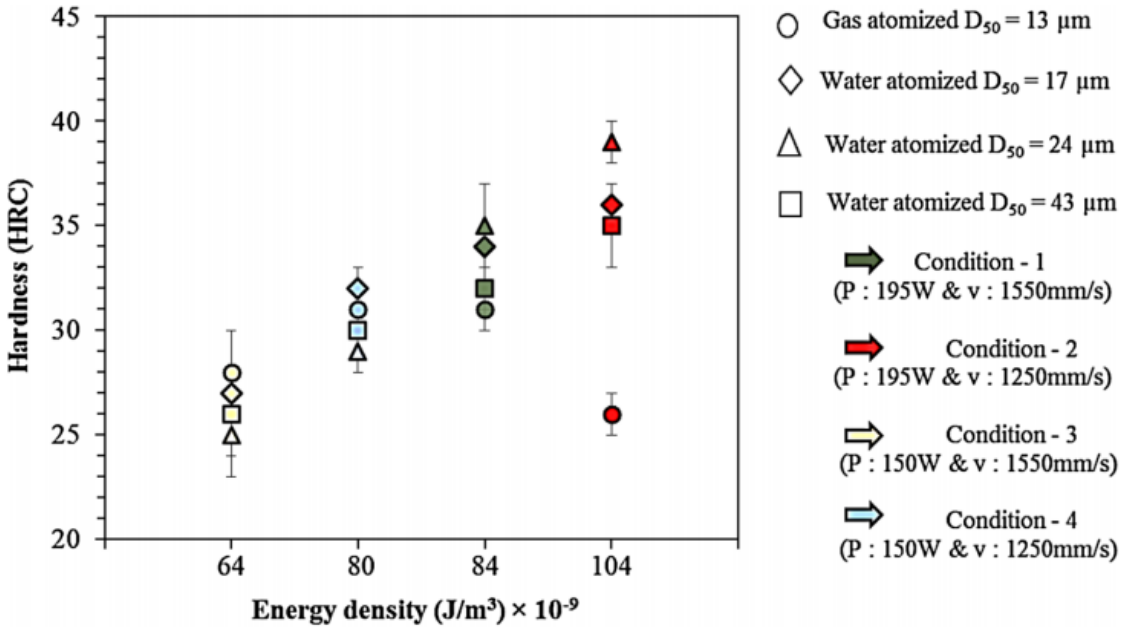

Figure 28. Effect of varying powders and energy densities on hardness of additively manufactured PH 17-4 stainless steel parts (Irrinki et al. 2016, p. 866).

3.3.2 Microstructure

The initial powder material together with the processing conditions during the additive manufacturing process defines the microstructure of the finished parts, which ultimately controls the mechanical properties if no significant porosity is present. The microstructures of parts produced with additive manufacturing differ from those produced by conventional

methods. This is due to the multiple heating and cooling cycles that the part experiences during the melting and solidification of the various layers. The cooling rate is also extremely fast, around 10^4 K/s, resulting in fine grained microstructures. (Vilaro, Coling & Bartout 2011, p. 3192.) Small variations in the physical properties of the powder including PSD and morphology have been shown to have no effect on the resulting microstructure of the finished parts. This is typically the case with used powders recycled between the builds in the AM machine, where slight changes in the powder's PSD and morphology takes place due to agglomeration of fine particles. (Ardila et al. 2014, p. 99–107; Strondl et al. 2015, p. 549–554.) As was seen in figure 26 Ti-6Al-4V powders from different vendors with the same nominal chemical composition but different particle size distributions resulted in similar microstructures apart from the porosity.

Variations in the initial chemistry and microstructure of the powder may result in completely different microstructures on the finished parts. Starr et al. (2012, p. 439–446) studied the effect of the initial microstructure of 17-4 stainless steel powder on the microstructure of finished parts manufactured via powder bed fusion. Two powders with the same nominal chemical composition of 17 % Ni, 4 % Cr and 4 % Cu were gas atomized in different atmospheres, one in nitrogen (standard for 17-4 SS powder) and the other in argon. The powder atomized with nitrogen showed higher nitrogen content than the one atomized with argon (1500 versus 300 ppm). X-ray diffraction analysis showed that the nitrogen atomized powder had mostly austenitic structure and the argon atomized powder was mostly martensitic. Parts were manufactured from both powders with powder bed fusion in argon and nitrogen atmospheres, yielding mostly martensitic structures for the Ar atomized powders and mostly austenitic structures for N_2 atomized powders. The processing atmosphere had little effect on the microstructure of the finished parts, meaning that the initial chemical composition and microstructure of the powder controlled the microstructure of the finished parts, as other processing parameters were kept constant.

All of the above findings are important to note, as the optimized parameters for a given material that are usually provided by the AM machine manufacturer only produce the desired results on the finished part, if the properties of the used powder remain constant. For this reason some machine manufacturers also provide the powder, to guarantee that the finished parts have the desired properties. Parameter optimization for every batch of

powder with varying properties is not feasible and therefore to produce parts repeatedly with the desired properties the variations in the powder properties have to be minimized. Accurate characterization of the powder is therefore crucial.

4 KEY LITERATURE FINDINGS FOR PLANNING THE EXPERIMENTS

The findings from the literature review are used in planning the experimental methods of this thesis. This includes the selection of the waste streams subjected to recycling via powder preparation and the corresponding powder preparation processes. Approaches by previous authors to produce spherical powder from scrap feedstock are reviewed and taken into account when planning the experimental part.

Recycling scrap by making metal powder from it could provide significant environmental and economic benefits. For these potential benefits to come true, the process of turning the scrap metal into powder, usable in additive manufacturing, or even in some other PM application, has to be as simple as possible. In addition, the recycling has to be done alloy specific in a closed-loop instead of an open-loop recycling process, requiring alloy specific source separation at where the scrap is produced. Therefore, for the experimental part of this study, a waste stream is selected from a specific manufacturing process where the source separation is extremely easy to implement.

4.1 Potential scrap sources

Any metallic waste stream could be considered recyclable through powder preparation route, just as it would be recyclable via the conventional route. However, some waste streams and forms of scrap are more suitable raw material for powder preparation than others. For the mechanical milling together with further plasma spheroidization route scrap already in the form of powder close to the desired particle size would be ideal, whereas large bulky pieces require more size reduction. For atomization route the form of scrap is not so relevant if gas furnaces are used for melting. If induction furnaces are used, solid pieces instead of powder or granulate scrap is more suitable feedstock for efficient melting. There are numerous different manufacturing processes that produce different forms and quantities of metallic scrap as waste streams and it is therefore not possible to analyse all of the potential waste streams in detail in the scope of this thesis. Instead, different types of scrap in larger categories as shown earlier in figure 4 are discussed and common guidelines for selecting potential waste streams for AM powder preparation are given. In addition, a

specific waste stream deemed suitable for AM powder preparation is selected for a case study.

To produce powder from a metal or alloy scrap, without dilution and alloy additions, requires high purity from the initial scrap to achieve the strict requirements regarding chemical composition of engineering metals and alloys. Depending on the manufacturing process, impurities in various forms may be introduced to the scrap. Bulky scrap pieces without contamination are relatively easy to find, as these are mostly generated by mechanical or thermal cutting operations from high quality bar or plate feedstock during product manufacture. Even if the cutting surface would receive some contamination, the quantity would be insignificant as the bulk of the material remains pure.

The smaller forms of scrap with high amount of surface area in relation to the volume are more susceptible to significant quantities of contamination. This is the case with chip like scrap and powdered scrap that is produced as waste streams in many conventional subtractive manufacturing processes. As an example, machining chips pick up contaminants from the used processing media (cutting fluid), from physical contact with processing equipment (tool wear), from the ambient (oxidation) and from the machine as mixing of chips of another material to the waste stream. (Denkena et al. 2016, p. 480). In manufacturing processes where additional processing media like cutting fluids are needed, contamination from it is always a concern. Tool wear is always a concern when physical tool is used to subtract material to form products. The affinity towards oxygen pickup is material dependent, but usually becomes a problem in manufacturing processes where the scrap material is at elevated temperatures which significantly increase the oxide formation of metals. Mixing of different materials in the waste stream is a concern during production in manufacturing processes where more than one material is processed with the same machine without proper cleaning of the machine in between.

An example of a manufacturing process where all of the above contamination sources can be avoided is powder bed fusion additive manufacturing. In powder bed fusion thermal energy instead of physical tool is used to produce the desired product, eliminating the risk of tool contamination. As the metal is in molten state during the process, there is a risk of inducing impurities in the form of gases like oxygen from the atmosphere reacting with the

molten metal. To avoid this, inert gas shielding is always used in the building chamber. No other processing media is used during the process. In addition, powder bed fusion machines work with one specific material at a time and the machine has to be thoroughly cleaned prior changing to another material. As a result, high purity parts can be produced and as a bonus, the scrap generated in the process also avoids contamination.

The conventional metal production is actually limited in the scrap utilization as feedstock because of limited scrap availability in regards to the annual demand for new feedstock (Graedel et al. 2011, p. 17). In the case of steel, even if 100 % of the new scrap generated in the manufacturing phase of products were recycled to produce new products from semi-finished bulky feedstock with 100 % efficiency, this would only cover around 17 % of the global demand for new products (Cullen et al. 2012, p. 13051). The annual consumption of metal powders for additive manufacturing however is in the order of hundreds of metric tonnes, whereas the new scrap produced annually is measured in millions of metric tonnes. Therefore the demand for metal AM powders could be easily fully satisfied with powder produced from new scrap. Furthermore, as there is way more scrap available than required, only those material streams deemed most suitable for powder preparation need be selected. Ideally such a waste stream should come from a manufacturing process with at least the following properties:

1. No contamination of the scrap produced during the manufacturing process
2. No mixing of different scrap materials during production
3. The dimensions of the individual scrap particles produced are close to the desired particle size for AM powders, if mechanical milling is used for powder preparation.

The waste produced in powder bed fusion additive manufacturing, described in chapter 3.1.3, fits the criteria extremely well. The produced metal scrap is free of contaminants, there is no mixing of different materials in the machine and one of the waste streams is extremely close to the required particle size for new powder. Therefore for the experimental part of this study the waste stream generated in powder bed fusion in the form of support structures, defected parts and over-sized agglomerated sieve residue powder is used as the feedstock in an attempt to recycle scrap produced in the manufacturing phase of products back into powder usable in powder bed fusion. The sieve

residue represents a case of scrap in the form of powder, the support structures small solid pieces and the defected parts large bulky pieces.

4.2 Proposed recycling routes

Based on the literature review a flowchart is made of processing routes to recycle different forms of scrap into spherical metal powders for AM (figure 29). The estimated average and corresponding standard deviations for specific energy consumption of each route based on the values of table 1 and 2 is included. The section line shows the scope of the processes that are included in the SEC-values.

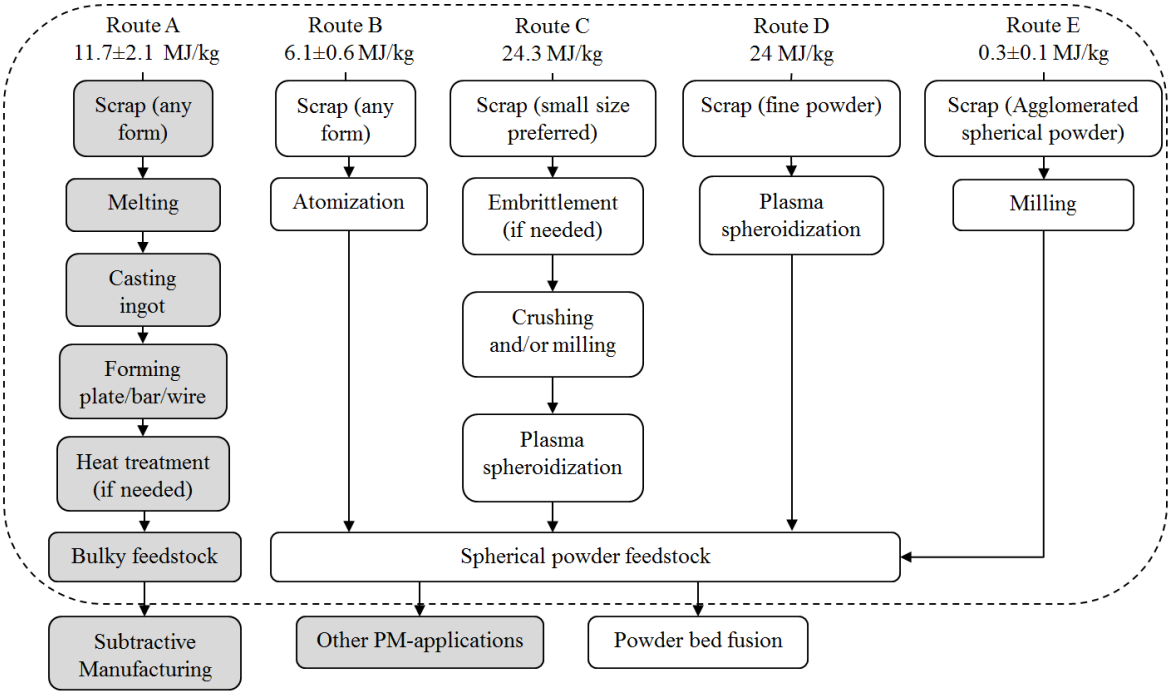

Figure 29. Processing routes for preparing spherical powder from scrap for powder bed fusion. The estimated specific energy consumptions are for steel, based on the values in table 1 and 2.

As we compare the SEC values of each route, gas atomization is the best choice of recycling scrap in the form of bulky pieces or small chips. Mechanical crushing/milling together with plasma spheroidization (route C) could produce spherical powders from scrap without some of the issues of gas atomized powders. However, as can be seen in figure 29, the SEC of plasma spheroidization is four times higher than with gas atomization. Both of these routes are tested in the experimental part. It should be noted that

if parts with sufficient properties from the gas atomized powder can be produced, then there is no justification for making higher quality powders with the cost of four times higher SEC. Furthermore, the mechanical milling prior to plasma spheroidization has to be extremely efficient so that it does not increase the SEC any further. The powder yield with the desired particle size has to be also clearly better, preferably close to 100 %, than with the gas atomization for there to be any sense in recycling through this route.

Mechanical milling can utilize scrap feedstock in any form, although less size reduction is needed for scrap consisting of small particles. For materials with high ductility some form of embrittlement treatment might be needed, further increasing the energy needed in the production. The SEC in the flowchart is based on the assumption that no such treatment is needed. After the scrap is milled into powder consisting of particles with the desired size for AM but with irregular morphology, it is further spheroidized to produce spherical powder. Scrap metal that is already in powder form can be recycled straight through plasma spheroidization route D, if the particle size distribution of the powder waste is close to the desired, regarded as fine powder in the flowchart.

A special case is route E where the scrap powder is such that nominally spherical particles with the desired particle size can be prepared from it with only milling, without the further plasma spheroidization. To produce spherical powders with only mechanical milling requires that the initial scrap material is powder. Furthermore, the powder has to consist of nominally spherical particles, which are agglomerated, bonded or sintered together in such a way that the individual particles still maintain their spherical shape and can be separated from each other without destroying the individual particles during the milling. However, as this requires a very specific form of scrap material it might be hard to find suitable waste streams in large enough quantities. This would be the most appealing recycling route as melting in the recycling process could be avoided and therefore the SEC is significantly reduced even from that of the gas atomization route. This is tested in the experimental part of this thesis with the sieve residue powder in hopes of avoiding the plasma spheroidization step, which would increase the SEC and also cost of the recycling route.

For comparison, the conventional recycling route A for producing bulky feedstock form scrap is included. Other powder metallurgy applications are also included at the bottom as

the same recycling methodology to produce powders with suitable characteristics for other powder metallurgy processes could be used. These are marked with a different colour as they are for reference only. If we compare the SEC of conventional recycling and the GA route, the difference is ~3–8 MJ/kg, taking into account lowest and highest scenarios based on the standard deviations. If we assume that the SEC related to the melting of the scrap is in both cases almost the same, the difference for the benefit of gas atomization comes from the replacement of casting, forming and possible heat treatment of bulky feedstock with just the actual atomization, which means blowing compressed gas to the melt.

In the study by Morrow et al. (2007, p. 938) for H13 tool steel, 1.0 MJ/kg is attributed to the actual atomization step in the powder production. In the case of plate production the ingot casting takes 3.31 MJ/kg, reheating 1.87 MJ/kg, hot rolling 1.45 MJ/kg, cold rolling 1.15 MJ/kg and annealing 1.19 MJ/kg, a total of 8.97 MJ/kg. The difference between all these steps and atomization is ~8 MJ/kg, which corresponds well to the highest difference between routes A and B, when taking into account the standard deviations. For bulky feedstock production from scrap this could be considered the worst case scenario. For hot rolled product made with continuous casting, therefore eliminating: reheating prior hot rolling, cold rolling, heat treatment and combining the casting and hot rolling, the SEC needed after the melting is reduced to ~3.6 MJ/kg (Arens, Schleich & Worrel 2012, p. 110). This is closer, but still higher than the 1.0 MJ/kg needed for just atomizing the melt into powder feedstock.

4.3 Current status of recycling via powder preparation

Water atomization in the recycling of iron and low alloy steel scrap to powders for conventional powder metallurgy applications, such as press and sinter, is done in industrial scale; however virgin materials are also added to the feedstock for dilution to achieve the desired alloy composition (Kruzhanov & Arnhold 2012, p. 14; Höganäs 2013, p. 82). In addition, water atomization does not produce powders with the desired spherical particle morphology for PBF AM and is not suitable for reactive materials.

Few authors have demonstrated the production of spherical powder from scrap feedstock following similar processing route as proposed. Yang et al. (2013, p. 2313–2316) demonstrated essentially the processing route C in figure 29 to prepare spherical titanium

powder from titanium machining scrap. They hydrogenated the titanium scrap to produce titanium hydride (TiH_2), which is extremely brittle, to be crushed easily in a ball mill into powder with irregular particle morphology and average particle size of around 30 µm. The ball-milled TiH_2 powder underwent a radio frequency (RF) plasma treatment, which effectively dehydrogenated and spheroidized the titanium particles into spherical powder with average particle size of around 20 µm.

Figure 30 shows that the PSD has become narrower with decreased mean average particle size and that all of the TiH_2 powder has dehydrogenated to titaium powder. The SEM images show how the plasma treatment resulted in spheroidized smooth particles. Such powder would most likely be usable in powder-based additive manufacturing, regarding physical properties such as flowability and packing density. Impurity levels for iron, chromium and nickel were minimal, however the amount of other possibly harmful impurities of carbon, oxygen, hydrogen and nitrogen in the finished powder were not discussed.

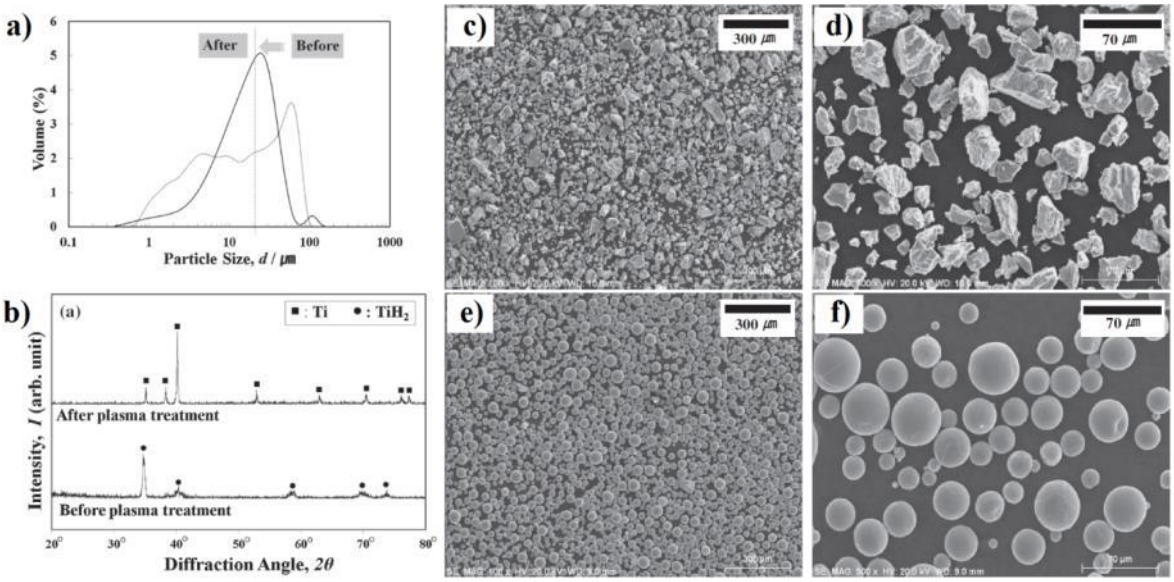

Figure 30. a) PSD, b) XRD and c–f) SEM images of TiH_2 powder and titanium powder, before and after RF plasma treatment, respectively (modified: Yang et al. 2013, p. 2315).

Han et al. (2015, p. 1507–1509) combined hydro- and physical metallurgy to prepare spherical tungsten powder from tungsten carbide-cobalt hard metal tool scrap. Their route consisted of multiple processing steps and the use of consumables like sodium hydroxide,

calcium chloride and hydrochloric acid. In addition, only tungsten was recovered and the cobalt (12 w-%) in the original scrap was discarded. At first the scrap was isothermally oxidized at 800 °C for 10 hours to transfer the dense scrap into porous WO_3 and $CoWO_4$ oxides. The resulting porous oxides are easily crushed by hammer mill and further milled into size of few microns with jet mill. The milled powder was then immersed in sodium hydroxide at 90 °C to selectively dissolve the tungsten from the oxides and receive cobalt hydroxide and sodium tungstate. The solid cobalt hydroxide was removed from the mixture by filtering. The remaining sodium tungstate was precipitated with calcium chloride to form calcium tungstate, which was then dissolved with hydrochloric acid to precipitate tungstic acid. The tungstic acid was dehydrated to receive solid tungsten trioxide powder, which was then reduced in hydrogen at elevated temperature to receive powder consisting of micron sized blocky tungsten particles. Finally, the powder was subjected to plasma spheroidization to receive spherical tungsten powder. Figure 31 shows the processing route used and the particle size distribution and SEM image showing spherical morphology for the resulting tungsten powder.

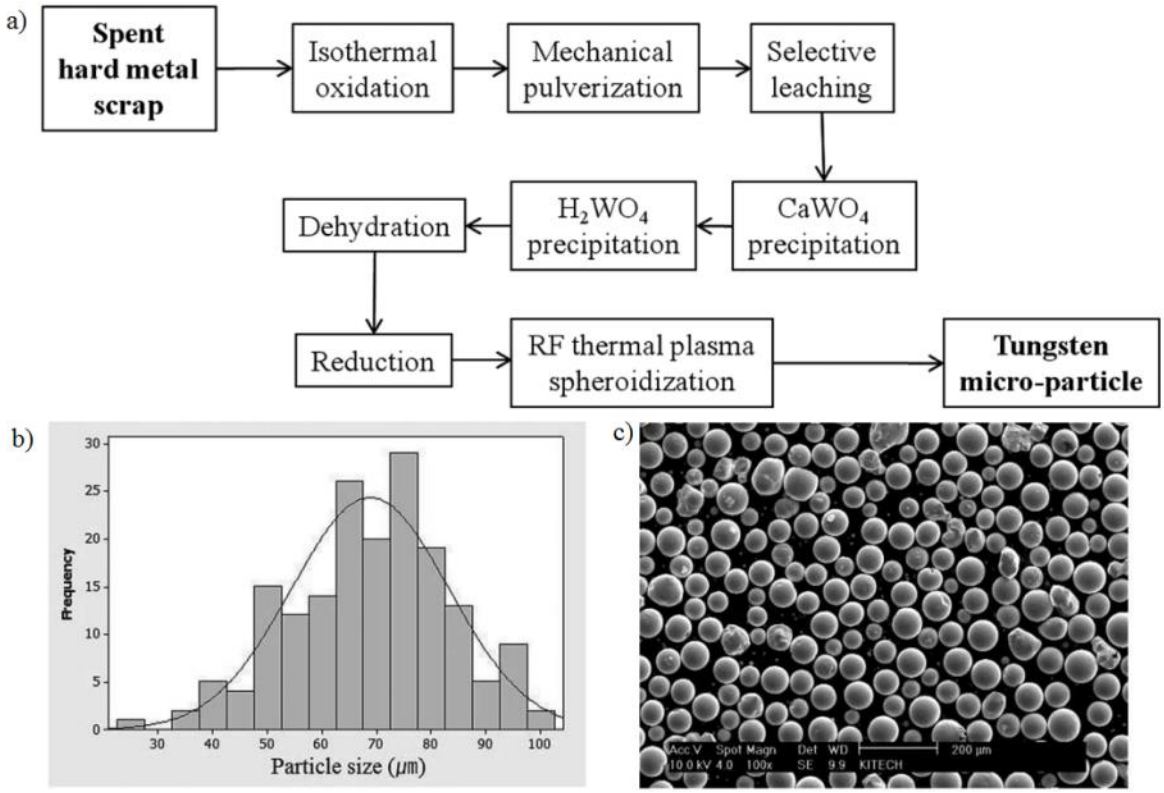

Figure 31. a) Recycling route to prepare b–c) spherical tungsten powder from tungsten carbide-cobalt tool scrap (modified: Han et al. 2015, p. 1508–1509).

In a recent study by Sun et al. (2016, p. 331–335) a novel method for producing spherical powder from Ti-6Al-4V scrap was proposed. First the scrap was cleaned and hydrogenated to produce brittle Ti-6Al-4V hydride which was then ball milled into fine (less than 10 µm) particles (figure 32a). After milling a thermoplastic binder was added to form slurry that was spray dried with argon gas to form spherical granules consisting of small Ti-6Al-4V hydride particles bound together by the thermoplastic binder (figure 32b). These granules were then debinded to remove the thermoplastic at 200–400 °C for 10 h and further sintered at 1200 °C for 4 h in argon atmosphere (figure 32c). Calcium oxide (CaO) powder was used as a separator to avoid sintering of the larger granules into each other. After sintering the CaO powder was removed with dilute hydrochloride acid and the spherical Ti-6Al-4V powder was de-oxygenated with calcium metal at 750 °C for 12 h in argon. Finally the powder was leached using dilute hydrochloric acid and dried in air at room temperature. Figure 32 shows the schematic representation of the process together with SEM images of the powder at each stage and the finished powder (a–d), cross-section showing completely solid particle (e) and the particle size distribution (f).

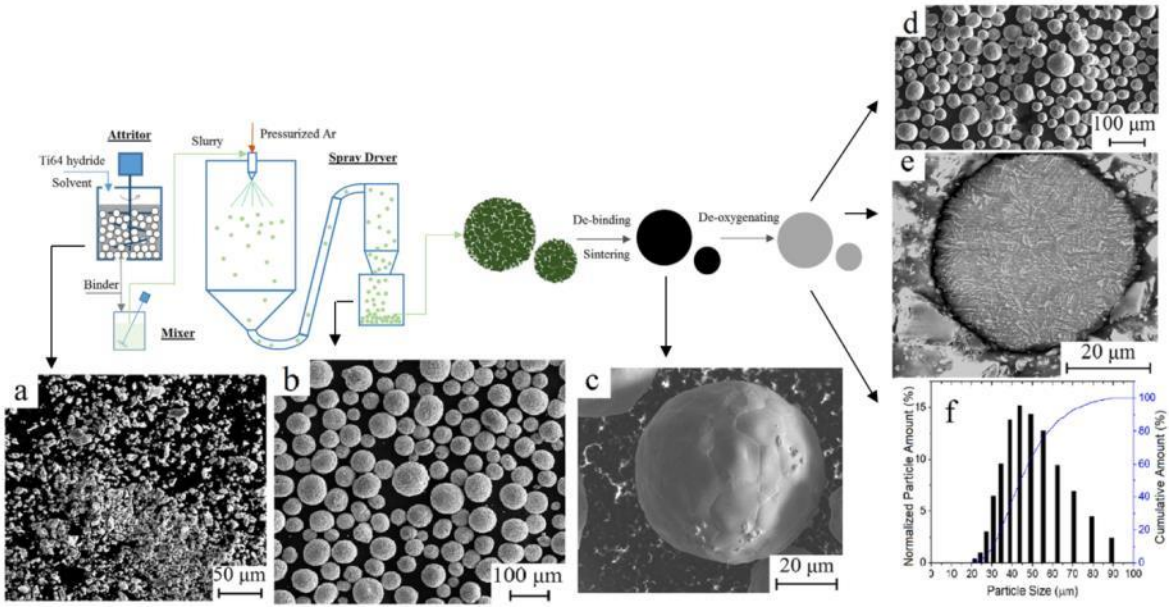

Figure 32. Recycling route to produce spherical Ti-6Al-4V powder from scrap feedstock (modified: Sun et al. 2016, p. 332).

Common for the studies above done by Yang et al. (2013, p. 2313–2316), Han et al. (2015, p. 1507–1509) and Sun et al. (2016, p. 331–335) is that only the powder is prepared and no actual parts or test pieces are manufactured with any powder metallurgy application from

that powder. As it was stated, validation of the powder to be probably usable in the AM machine is no guarantee that the parts produced from that powder have the desired properties. Therefore in the experimental part of this master's thesis the goal is to also manufacture test pieces from the prepared powder to see if parts can be actually manufactured and if so, do the mechanical properties differ from those manufactured from commercially available powders. The processing route by Yang et al. (2013, p. 2313–2316) is the most simple of those done by previous authors and avoids the multiple chemical treatments included in the routes by Han et al. (2015, p. 1507–1509) and Sun et al. (2016, p. 331–335). Each processing step and use of chemical consumables ads costs and degrades the feasibility of the recycling. The routes by Han et al. and Yang et al. relied on plasma spheroidization, which makes their routes energy intensive. The route by Sun et al. avoids melting of the metal, however the sintering and de-oxygenation are done at high temperatures for long times. The authors believe that their route uses less energy than atomizing methods, however it is stated that a detailed analysis of the SEC has not been done yet. In the following experimental part of this thesis the attempt is to further reduce the needed processing steps.

5 EXPERIMENTAL METHODS

From the selected waste streams, the sieve residue is tested to see if spherical powder can be prepared with only mechanical milling. The support structures are tested to see if they can be efficiently reduced to the desired particle size via mechanical milling, without embrittlement treatment, and then further plasma spheroidized to achieve spherical powder. Gas atomization is tested to see if usable spherical powder for powder bed fusion can be prepared from 100 % scrap feedstock without dilution with virgin materials.

5.1 Initial scrap materials

The materials used in the tests are H13 tool steel, which is relatively brittle, and 316L stainless steel, which is relatively ductile. Figure 33 shows SEM images of the initial H13 sieve residue powder. The powder consists of spherical particles agglomerated into larger satellites and also large individual spherical particles. Unlike agglomerates of extremely fine particles, held together by inter-particle forces, these agglomerates are sintered together. The agglomerates and individual particles are large enough that they cannot pass through the sieve with 90 micron opening, which was used when sieving the un-used powder after each build in the PBF machine. The sieve residue powder scrap is the part of the powder that did not pass the sieving operation. If the agglomerated particles can be just separated from each other without crushing the resulting individual particles during the milling, this could yield spherical powder with the desired size straight after milling without the need of further plasma spheroidization.

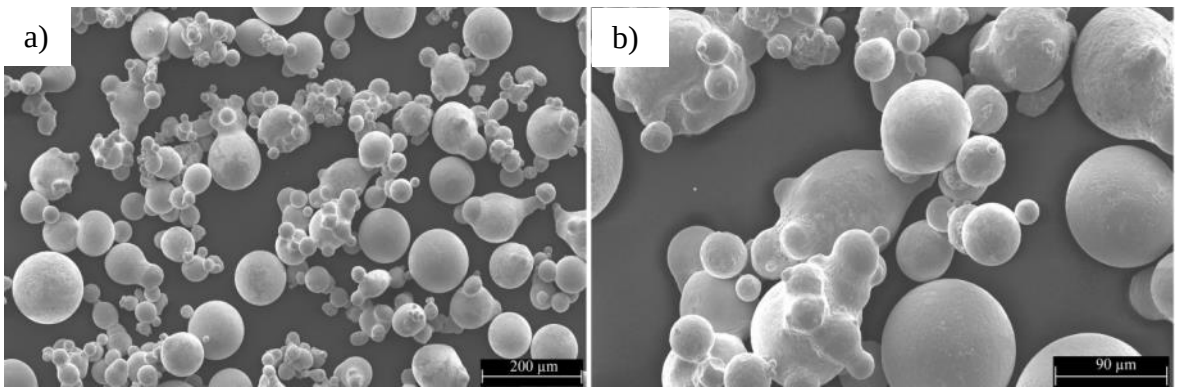

Figure 33. H13 new scrap in the form of sieve residue powder produced as a waste stream in SLM 125 HL PBF machine at a) 100x and b) 250x magnification.

Figure 34 shows SEM images of the 316L sieve residue powder, which also consists of agglomerated particles together with individual spherical particles. There are clearly more individual particles smaller than the 90 microns present than in the H13 sieve residue. These particles should have passed the sieving operation, so it might be that these particles have separated from the agglomerates after the sieving, for example when the sample for SEM analysis is taken. This would indicate that the bonds between the agglomerated particles are quite weak in comparison to those in the H13 powder. It can be further noted that the individual spherical particles are smaller and the overall particle size is smaller than in the H13 sieve residue.

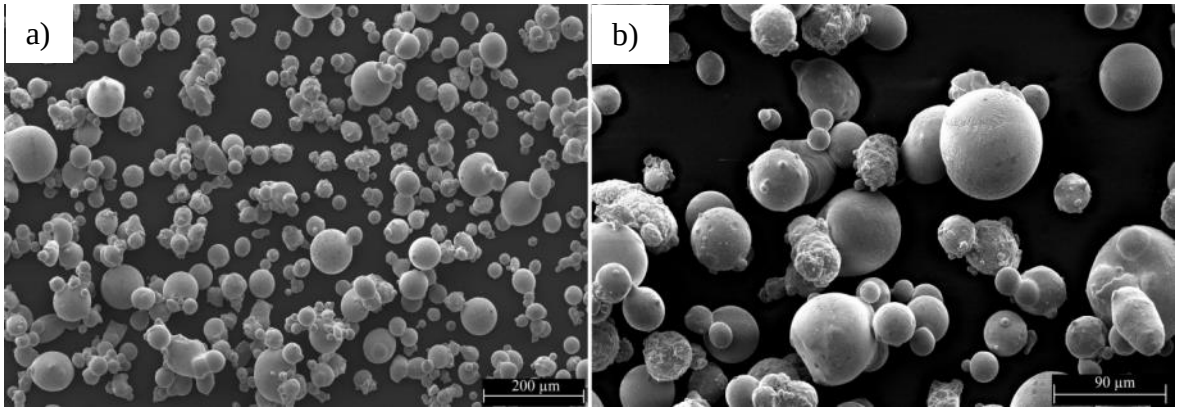

Figure 34. 316L new scrap in the form of sieve residue powder produced as a waste stream in SLM 125 HL PBF machine at a) 100x and b) 250x magnification.

The support structures that are removed during post-processing as scrap from additively manufactured parts are shown in figure 35a). The supports in this case are in the form of pillars and they have a lattice like structure, instead of being solid. This is beneficial for the mechanical milling; as such a porous structure should be more easily crushed and milled than a solid bulky piece. Prior milling the support structures were further cut into smaller pieces (figure 35b) to reduce the milling time.

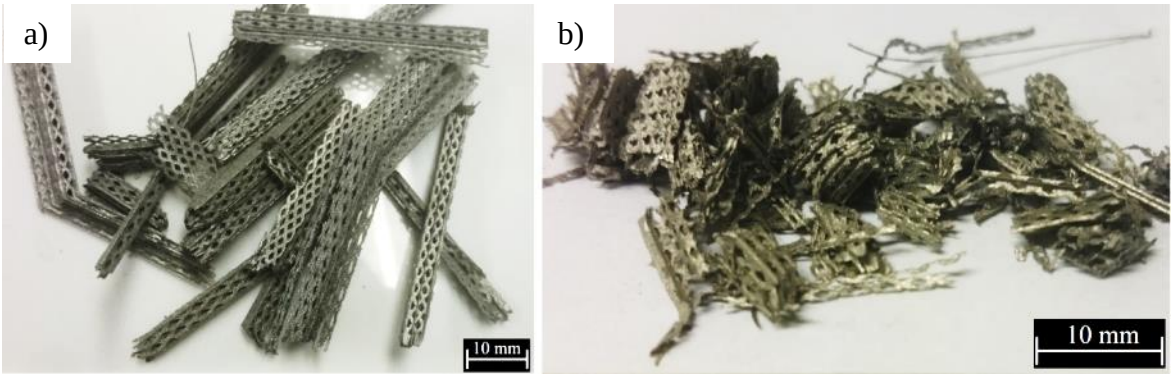

Figure 35. H13 new scrap in the form of support structures produced as a waste stream in SLM 125 HL PBF machine.

For gas atomization 316L stainless steel support structures together with rejected PBF parts that have been scrapped due to defects were used as the starting material (figure 36). The parts were sawed into pieces with dimensions of few centimetres, which is suitable size of feedstock for the induction furnace used to melt the material in the laboratory scale gas atomizer that is used in the experiments.

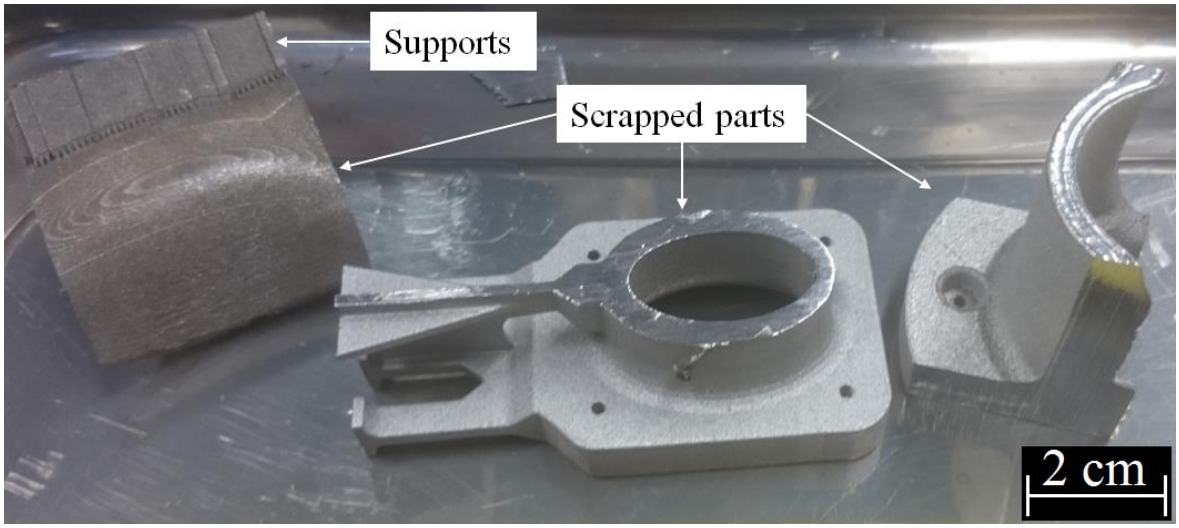

Figure 36. 316L new scrap in the form of support structures and defected parts (solid scrap) produced as a waste stream in SLM 125 HL and EOS M-series PBF machine.

EDS analysis was done for the initial scrap materials so that contamination that might be introduced during the powder preparation can be identified by comparing to the initial EDS spectrum. The weight percentages for each element that the EDS automatically provide cannot be considered reliable as the samples are neither flat nor polished and are therefore

not included. The presence and relative height of the peaks are compared to see if any differences occur as a result of contamination. The EDS spectrums are shown in appendix I. For H13 iron as the base metal shows the highest peaks and all the main alloying elements C, Cr, Mn, Si, V and Mo are distinguished. 316L also shows highest peaks for iron as the base metal and the main alloying elements Cr, Ni, Mo, Mn, and Si are distinguished. No contamination in the form of unwanted elements in the scrap is detected. In both cases C and O peaks are relatively high. The carbon peak is influenced by the carbon tape that is used as the base for the sample in the SEM equipment. The oxygen peak was expected as EDS is a surface sensitive method, therefore affected greatly by surface oxides formed by these materials.

5.2 Powder preparation

Few different types of mechanical mills were used for the experimental part of this thesis. Figure 37 shows the planetary ball mill that was used. The vial and grinding balls are made of low alloy hardened steel. The grinding balls have a diameter of 10 mm and an amount of balls equalling to 500 g of balls were used in all experiments. The vial capacity is 500 cm^3. Rotation speed, milling time and sample size was varied in the experiments. The tested parameter combinations are shown in table 3. Two separate vials were used to test simultaneously the milling of the sieve residue powder and support structures.

Table 3. Parameters used in the ball milling experiments of H13 sieve residue powder and support structures.

Parameter combination	Rotation speed [rpm]	Milling time [min]	Sample size [g]	Tested feedstock
1	150	60	5	both
2	250	30	5	both
3	150	5	5	sieve residue
4	200	5	5	sieve residue
5	150	120	5	sieve residue
6	300	60	5	supports
7	200	270	5	supports
8	200	5	25	sieve residue
9	200	5	100	sieve residue

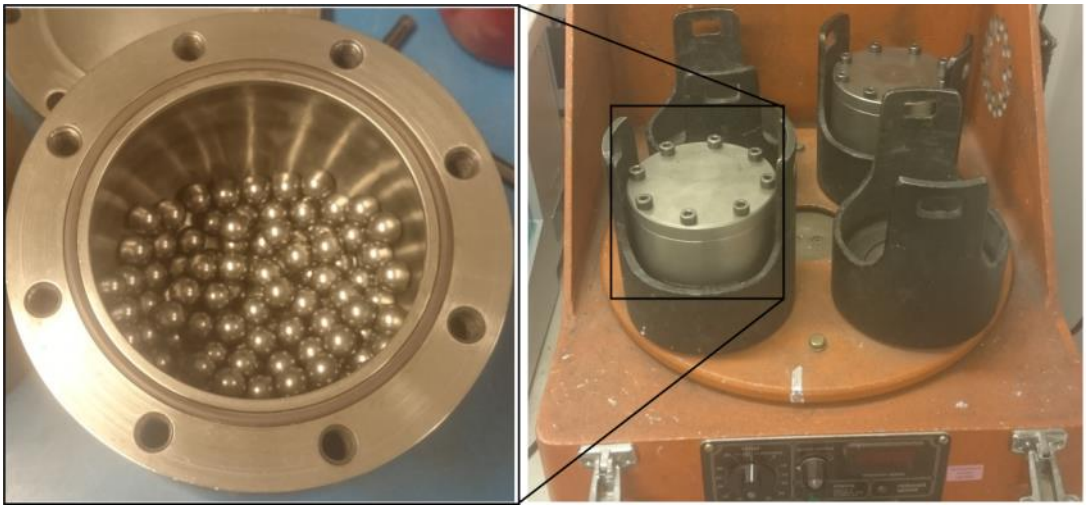

Figure 37. Fritsch pulverisette 5 planetary ball mill used for the experiments.

For the milling of the sieve residue powder also an air classifier jet mill was used (figure 38). The initial powder is fed into the processing chamber; where at the bottom jets of air fluidize the powder. The size reduction is a result of particle-particle collisions and by the impact with the rotating classifier wheel, located at the top of the processing chamber. Fine particles are carried through the classifier in the airflow and coarse particles are deflected and returned to the bottom of the chamber for further size reduction. In this study the attempt is only to separate the individual particles in the agglomerated sieve residue without further milling the particles into finer size. The assumption was that the agglomerated particles are relatively weekly bonded and by applying moderate energies during milling the bonds between the particles would break but the individual particles would not. The air classifier jet mill separates the powder lot into cuts of fine and coarse particles, but as the objective is to utilize all of the powder that was fed to the mill, the separate cuts are mixed back together after the milling. Table 4 shows the parameters used in jet milling both the H13 and 316L sieve residue powder.

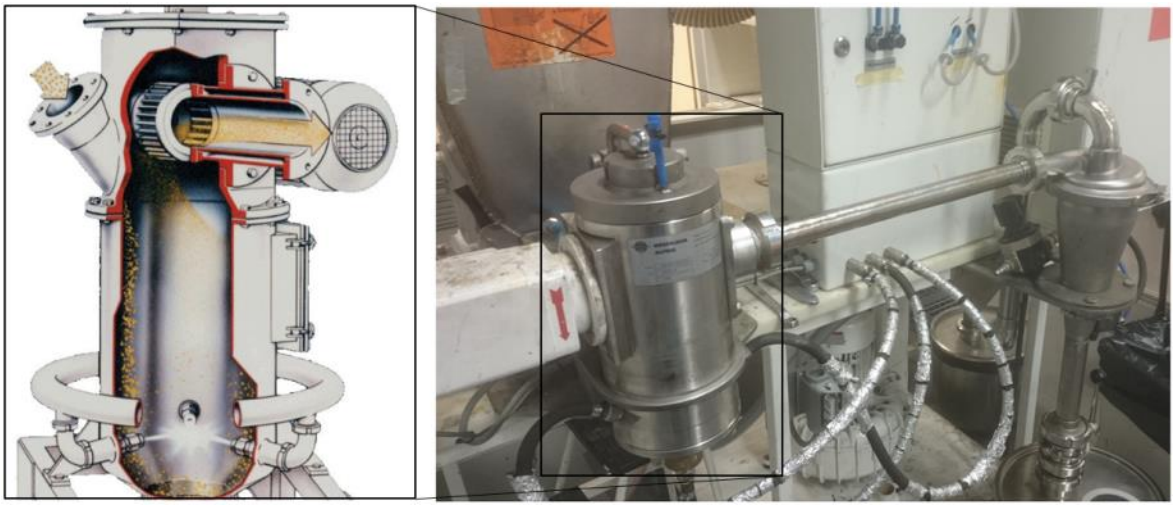

Figure 38. Schematic illustration of a fluidized bed air classifier jet mill and the Hosokawa Alpine 100 AFG jet mill used in the experiments (modified: Hosokawa Micron Powder Systems 2016).

Table 4. Parameters used in the jet milling of sieve residue powder.

Parameter	Value	Unit
Classifier wheel rotation speed	1510	rpm
Air jet pressure	0.62	MPa
Milling time (316L)	10	min
Milling time (H13)	40	min

In addition to ball milling of the support structures, a lab-made disintegrator mill was also used. Figure 39 shows a general schematic and the disintegrator mill used in the experiments. The parallel discs rotate at 10000 rpm in different directions relative to each other. The discs are equipped with cutting tools made of tungsten carbide. The supports are fed to the mill from the above and they are reduced to powder as a result of collisions with the cutting tools between the rotating discs. The resulting powder is ejected to the powder collector by the kinetic energy the particles receive from the rotating discs. 316L stainless steel was tested in the disintegrator mill, as it should be more suitable than the ball mill also for ductile materials (Kleis & Kulu, 2008, p. 178).

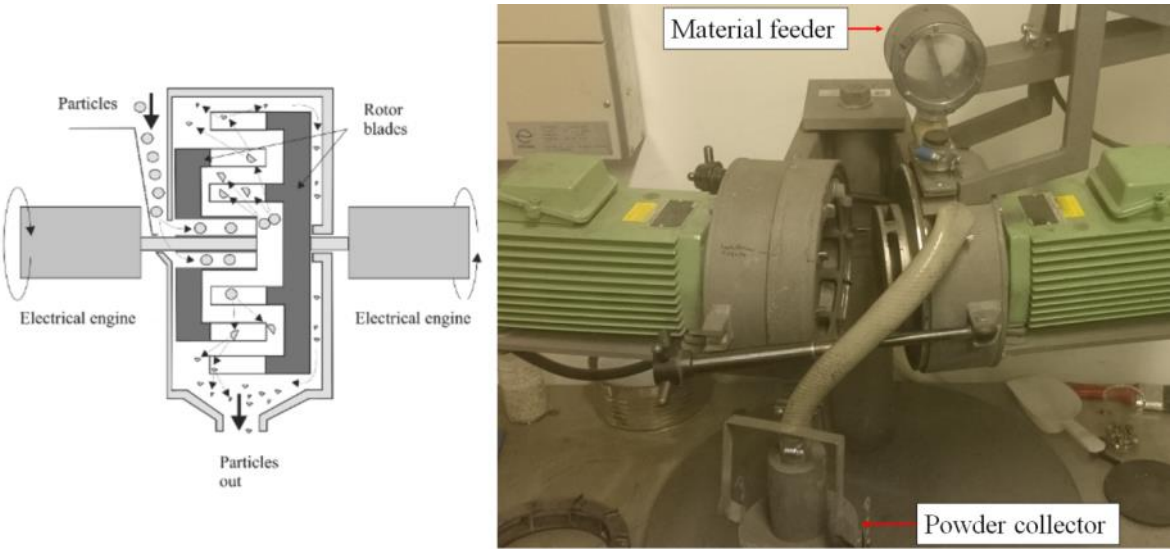

Figure 39. Schematic illustration of a disintegrator mill and the laboratory equipment used in the experiments (Kleis & Kulu 2008, p. 180).

The gas atomization of the support structures and scrapped defected parts was tested on the Hermiga 75/5VI equipment shown in figure 40. The schematic illustration of the working principle is shown in figure 6. A vacuum is generated both to the melt chamber and atomizing chamber prior starting the atomization procedure to remove any air and therefore oxygen from the process atmosphere. The temperature is increased with a speed of approximately one degree per 3 seconds. Both chambers were filled with argon once the melt chamber temperature was at 430 °C. The melt chamber was elevated to a slight overpressure. The scrap material is heated and melted in a ceramic (alumina) crucible by induction in the melt chamber. After reaching the melting temperature of the material the temperature of the melt is further increased to around 250 °C overheat to assure good flow through the atomizing nozzle. Once at the pouring temperature, the plug from the bottom of the crucible is removed and the melt flows through the nozzle via the force caused by the overpressure at the melt chamber and gravitation. Argon was used as the atomizing gas. The atomizing parameters are shown in table 5. Extremely fine particles or essentially dust that is produced during the atomization is carried to the cyclone and are not included in the powder batch that is collected for further analysis.

Figure 40. Gas atomizer used in the experiments.

Table 5. Parameters used in the gas atomization of 316L solid scrap.

Parameter	Value	Unit
Atomization gas pressure	6	MPa
Melt chamber over pressure	0.028	MPa
Melting point	1445	°C
Melt temperature at atomization	1705	°C
Nozzle diameter	2.5	mm

5.3 Powder analysis

Both the commercial powder used as a reference and the powder prepared from recycled new scrap were analysed with various methods. The particle morphology and chemical composition was analysed with Jeol JSM-6360LV scanning electron microscope coupled with energy-dispersive X-ray spectroscopy analysis. Scanning voltage of 15 kV was used and images with 100x and 250x magnification were taken. The particle size distributions were determined by laser diffraction analysis using Malvern Mastersizer 3000. The results were the average of three consecutive measures. Qualitative phase analysis was done with PANalytical Empyrean X-ray diffractometer using Cu-Kα radiation source and HighScore Plus software.

Hall flowmeter was used to measure the flowability, apparent and tap densities of the powders. The standardized apparatus used for the measurements is shown in figure 41. The opening of the orifice is 2.5 mm and the cup has a capacity of 25 cm^3. The powders were dried before the Hall flowmeter test in 80 °C for 2 hours to remove any moisture from the sample. The average from four measurements was taken. Stopwatch was used to measure the time it takes for 50 grams of powder to pass through the funnel. Apparent density is given by flowing powder through the funnel into the cup of know volume (25 cm^3), filling it precisely and measuring the mass of it. The packing density was measured by tapping the cup frequently onto the table and filling the cup with more powder as it packs more densely. Once the powder volume no longer decreased as a result of the tapping, the powder in the cup was weighted. Dividing the measured mass of the powders in the cup with the cup volume gives the densities.

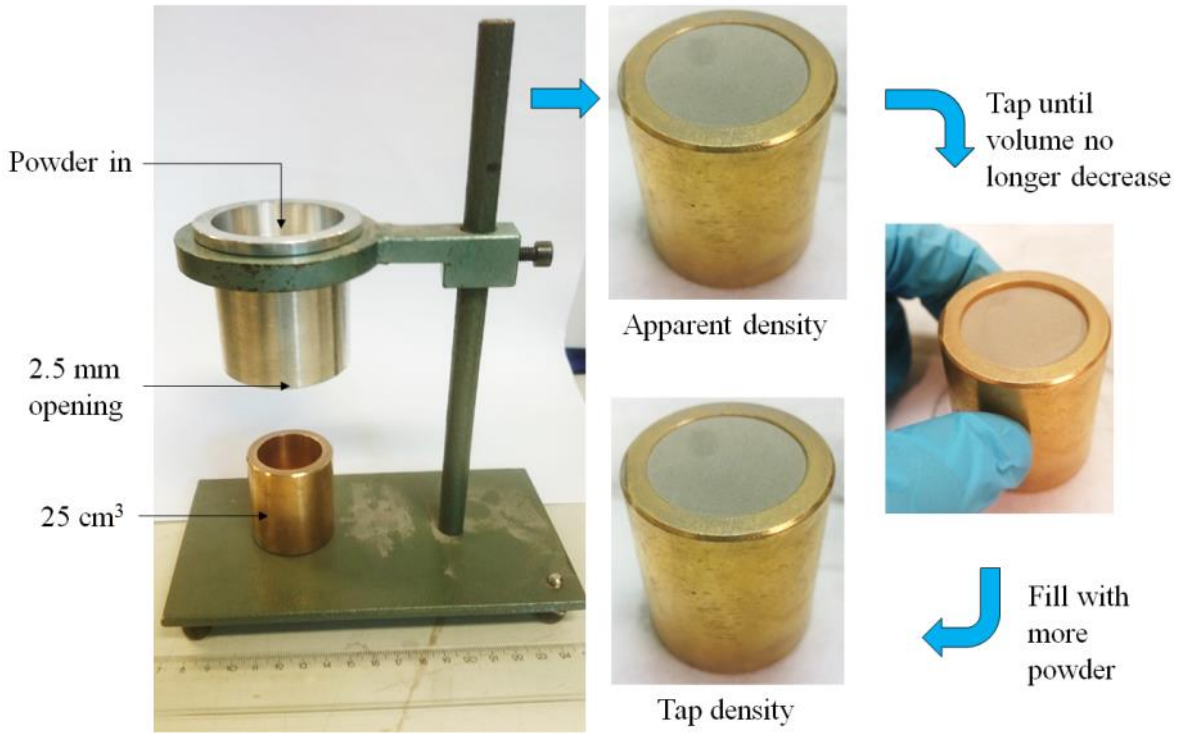

Figure 41. Hall flowmeter used to measure flowability, apparent and tap density.

5.4 Commercial reference powders

Commercial powders with the same nominal chemical composition as the scrap materials are used as reference for the powders that are prepared during the experimental part of this thesis, with the aim to prepare such powders that perform as good as the commercial powders. The first powder used as reference is gas atomized commercially available H13 tool steel powder provided by SLM Solutions GmbH. The powder is as-delivered virgin powder. Figure 42 shows SEM images taken from the H13 powder. The particle morphology is nominally spherical; however obvious and quite numerous irregularities are present such as elongated and elliptical particles. Some particles have also fused together to form so called satellites. These are both typical features of gas atomized powders.

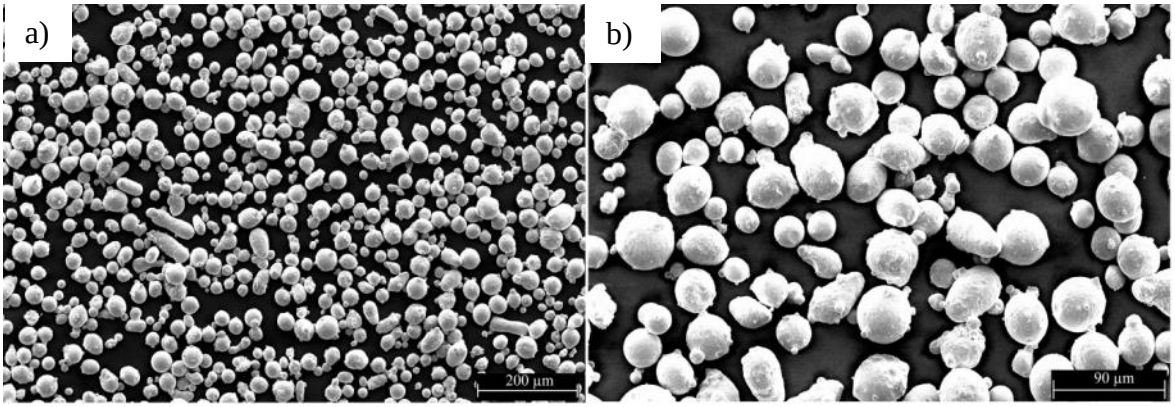

Figure 42. SEM images of as-delivered gas atomized H13 powder at a) 100x and b) 250x magnification.

The particle size distribution of the commercial gas atomized H13 powder was measured using the wet method (dispersion in water) with laser diffraction. This was done instead of dry method (dispersion in air) because the powder had a minor amount of fine particles (<10 µm) which did not properly show during analysis using air dispersion. Figure 43 shows the graphic particle size distribution. The corresponding D10, D50 and D90 values are 21.6 µm, 34.3 µm and 51.7 µm respectively. As can be seen from figure 43, the PSD is bi-modal with a slight peak of fine particles in the range of few to ten microns.

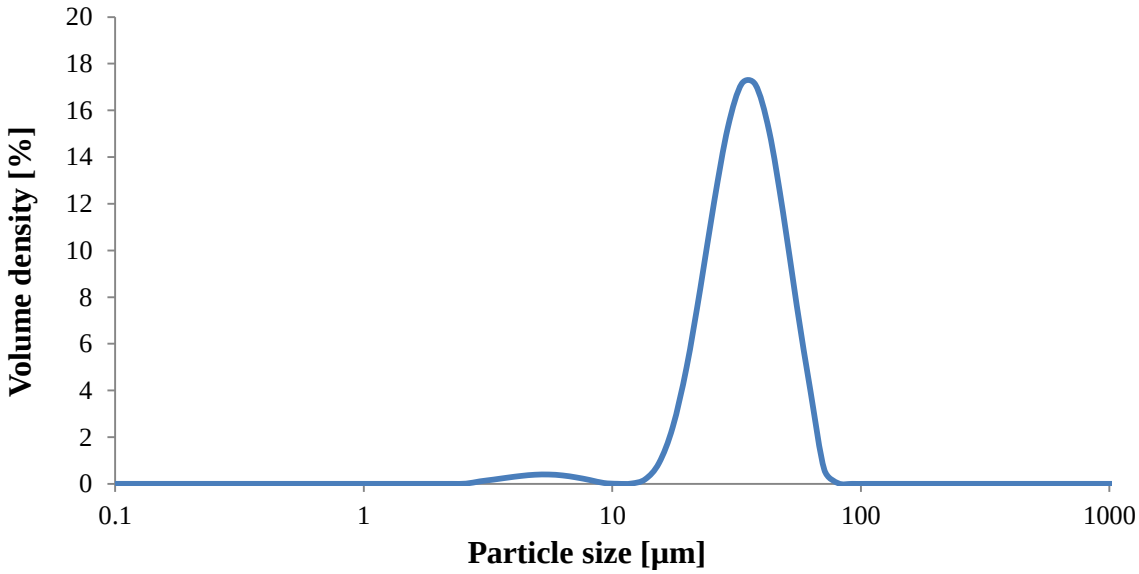

Figure 43. Particle size distribution of commercial gas atomized H13 powder.

The commercial H13 powder was not free-flowing, but required a single tap which is allowed to initiate flow in the Hall flowmeter. Table 6 shows the flowability, apparent and tap densities of the powder together with the corresponding standard deviations. If we use 7.80 g/cm^3 as the true density of H13 tool steel, the relative density of the powder is 50 % without compaction and 60 % after tapping.

Table 6. Flowability, apparent and tap densities of commercial GA H13 powder.

Flowability [s/50g]	Apparent density [g/cm^3]	Tap density [g/cm^3]
20.9±0.14	3.91±0.01	4.66±0.08

The second powder used as reference is commercially available 316L stainless steel powder also provided by SLM Solutions GmbH. Unlike the virgin H13 powder, the 316L powder has been used in the PBF machine and mixed with virgin powder after each build to account for the material that went into building the parts. Such recycled and mixed powder represents more accurately the case during production, as all of the powder that passes the 90 micron sieve is used again in the PBF machine. Figure 44 shows the SEM images of the 316L reference powder. The powder has quite similar morphology as the commercial H13 powder: nominally spherical particles with the presence of satellites and elongated or otherwise deformed particles.

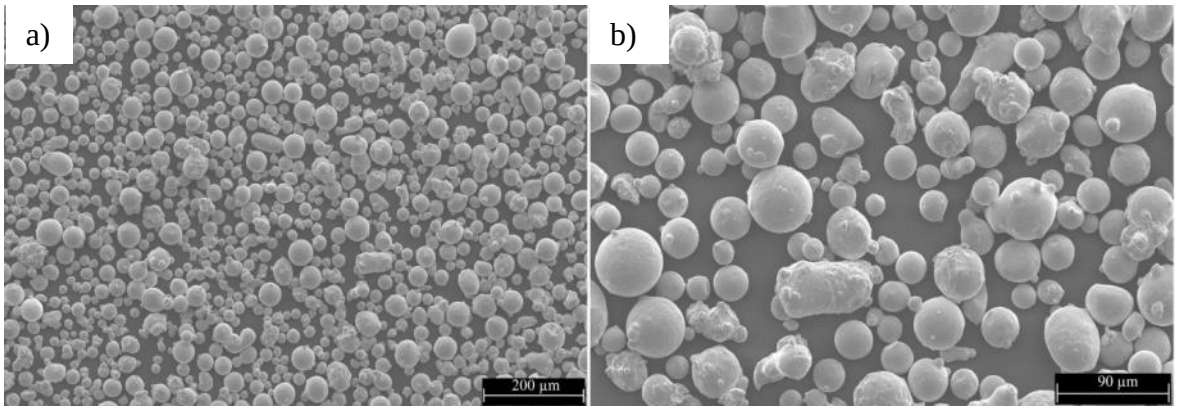

Figure 44. SEM images of used commercial 316L gas atomized powder at a) 100x and b) 250x magnification.

The particle size distribution of the commercial 316L powder was measured using the dry method (dispersion in air). This is a quicker method than the wet method (dispersion in water) and was suitable for this powder as it contains no extremely fine (<10 µm) particles. Figure 45 shows the graphic particle size distribution. The corresponding D10, D50 and D90 values are 22.5 µm, 35.8 µm and 56.0 µm respectively. The distribution is Gaussian and there is no additional peak at the range of 1–10 µm as was the case with the commercial H13 powder.

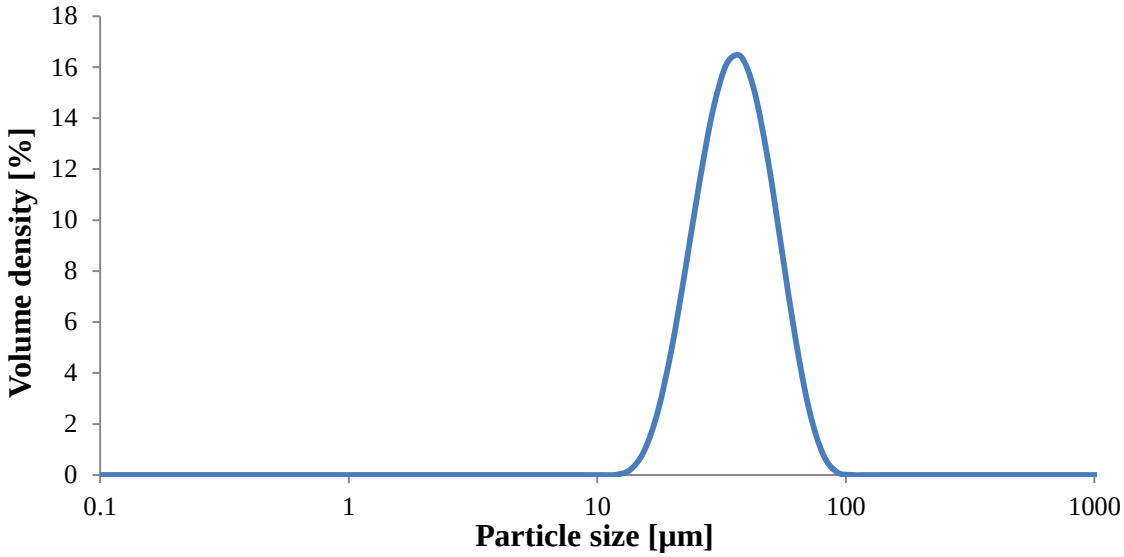

Figure 45. Particle size distribution of commercial gas atomized 316L powder.

Table 7 shows the flowability, apparent and tap densities of the commercial 316L powder. The powder was free flowing and no initial tap was needed. If we use 8.00 g/cm^3 as the true density of 316L stainless steel, the relative density of the powder is 54 % without compaction and 61 % after tapping.

Table 7. Flowability, apparent and tap densities of commercial 316L powder.

Flowability [s/50g]	Apparent density [g/cm^3]	Tap density [g/cm^3]
21.0±0.15	4.35±0.01	4.89±0.02

Comparison of the two commercial H13 and 316L powders reveals that the relative tapped densities are almost the same at 60 % and 61 % respectively. The relative apparent density

of the commercial H13 powder is only 50 % whereas for 316L it is 54 %. This difference is most likely due to the bi-modal distribution of the H13 powder. As seen from figure 20 the presence of small particles (in this case around few microns) should increase the packing density of the powder. In the commercial H13 powder there is only a small volume fraction of these fine particles, which is not enough to significantly increase the packing density. Instead the small amount of fines reduces the flowability (commercial H13 was not freely flowing, needed a single tap to initiate the flow) and because of this the apparent density remains low. As the powder fills the cup in the Hall flowmeter the particles assume a random position and a poorly flowing powder will have agglomerates, leaving larger pores to the powder bulk. Tapping separates these agglomerations and allows for the particles to arrange themselves more efficiently; hence a more significant increase is observed in the tapping density.

5.5 Powder bed fusion setup

SLM 125 HL powder bed fusion machine made by SLM Solutions GmbH, shown in figure 46, was used to manufacture test specimens from the prepared and commercial reference powder. The standard build volume 125x125x125 mm^3 of the machine was reduced to 50x50x50 mm^3 in order to decrease the amount of powder that is needed for each build. The powders were dried prior use in vacuum at 60 °C overnight to remove moisture. Once dried, the oven was backfilled with argon to seal the powder canisters in an inert atmosphere to be moved to the PBF machine. During operation the build chamber in the PBF machine is also filled with argon to avoid oxidation. The SLM 125 HL machine is equipped with single-mode continuous wave ytterbium fibre laser YLR-400 SM, producing a maximum laser power of 400 W at 1070 nm wavelength.

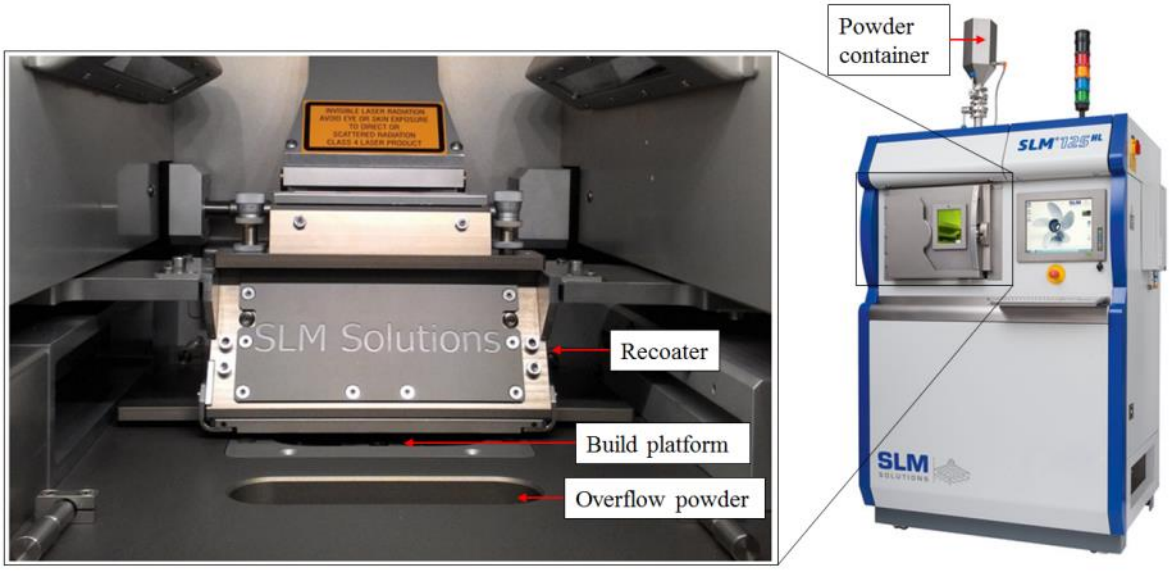

Figure 46. SLM 125 HL powder bed fusion machine with enlarged view on the build chamber (modified: SLM Solutions 2016).

Table 8 shows the processing parameters used for 316L stainless steel. The parameters were kept constant for each powder. Volumetric energy density combines the key parameters into a single parameter and it is often used when characterizing the L-PBF process and the resulting part properties. The volumetric energy density *VED* is calculated with the following equation:

$$VED = \frac{P}{v \times h \times LT} \quad (1)$$

In equation 1 P is laser power, v is scanning speed, h is hatch spacing and LT is layer thickness.

Table 8. Parameters used to additively manufacture the test specimens with SLM 125 HL.

Parameter	Value	Unit
Laser power (P)	234.05	W
Scanning speed (v)	936.1	mm/s
Layer thickness (LT)	30	µm
Hatch spacing (h)	100	µm
Laser spot diameter at focus	80±6	µm

Table 8 continues. Parameters used to additively manufacture the test specimens with SLM 125 HL.

Parameter	Value	[-]
Substrate pre-heat temperature	30	°C
Scanning strategy	Stripes	-
Oxygen content in build chamber	0.13–0.22	%
Volumetric energy density (*VED*)	83.34	J/mm^3

5.6 Destructive testing

The dimensions of the test specimens and their orientation on the build platform are shown in figure 47. The tensile test specimens are smaller than those specified in standard SFS-EN ISO 6892-1. The gauge length is just 10 mm which is less than in standard test specimens and it is noted in SFS-EN ISO 6892-1 (2016, p. 14) that using a gauge length less than 20 mm increases the uncertainty of the result in elongation after fracture. Otherwise the geometry is similar to the flat tensile specimens defined in the standard. Only such small sized bars fit on the platform (50x50 mm^2) that is used in the reduced build volume chamber of the SLM 125 HL machine. Usage of the smaller build volume and therefore platform was necessary so that the prepared powder quantities were sufficient for a successful build.

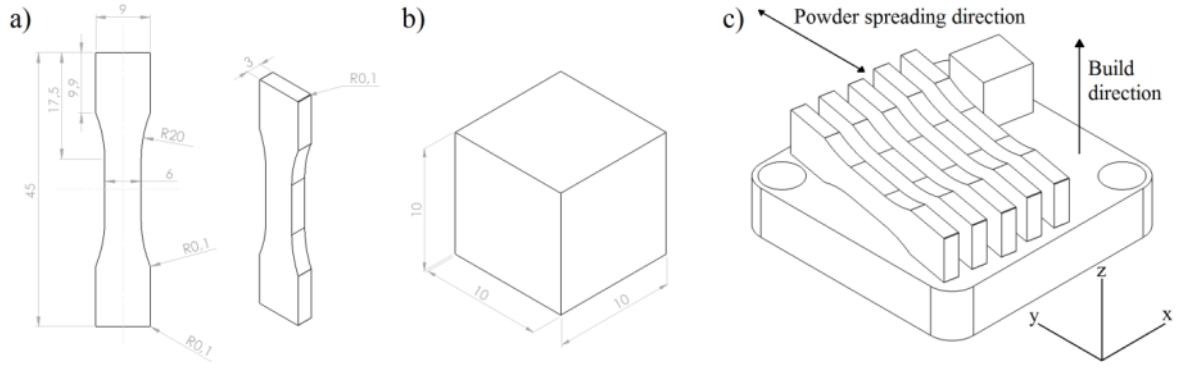

Figure 47. Test specimen a–b) dimensions and c) orientation on the build platform. The dimensions are in millimetres.

The size of the test cube for microstructural evaluation was selected at 10 mm^3 so that it would not further increase the height in the build direction (z-axis in figure 47) which was 14 mm with the addition of support structures beneath the tensile test specimens. These

small supports were included to ease the removal of the finished parts from the platform. The orientation of the tensile test bars was selected as such because of three factors: sufficient number (5) of specimens has to fit on the same platform, the height in the build direction has to be minimized for reduced need of powder and the contact area with the platform should be minimal for ease of removal.

The tensile testing was done on MTS 810 material testing system. Strain rate of 0.015 min^{-1} was used at the beginning of the testing to determine the yield strength ($R_{p0.2}$). The extensometer was removed at strains of around 10–15 % and after that the strain rate was increased to 0.4 min^{-1} for the rest of the test to determine tensile strength (R_m) and elongation after fracture (A). Such strain rates (with a relative tolerance of ±20 %) are recommended in standard SFS-EN ISO 6892-1 (2016, p. 18–19).

The test cubes for microstructural, porosity and hardness evaluation were cut from the middle parallel to the build direction and the cross-sections were polished using a semi-automatic Struers TegraForce-5/TegraPol-31 polisher. The first half was left in the mirror polished state and optical microscopy (OM) images were taken to see if any porosity is present. Microscopic images from three different locations at the test sample were taken. The relative porosity was calculated with ImageJ Fiji software and the result is the average from the three images. In the images of the polished samples the dense material appears bright and the pores dark. The relative porosity is calculated as the relation between bright and dark area in the image.

The other polished half was further etched using 10 % oxalic acid and applying a current (30V, 2A) for 30 seconds. OM images were taken with Olympus PME microscope from the etched surface to see the microstructure. The ferrite content in the test cubes was measured with Fischer Feritscope MP3. After the images were taken, Vickers hardness was measured from the cross-sections with Struers DuraScan equipment coupled with ecos Workflow software using a test force corresponding to the HV5 hardness, according to standard SFS-EN ISO 6507-1 (2005, p. 1–19). The results were the average of five consecutive measurements taken from the middle of the cross-sections with 1 mm intervals between the measuring points.

The chemical composition of the PBF parts was determined from the polished cross-sections with EDS, using UltraPLUS Thermal Field Emission Scanning Electron microscope (Carl Zeiss Microscopy GmbH) coupled with UltraDry EDS Detector (Thermo Fisher Scientific Inc.).

6 RESULTS

The first section of the results covers the preparation and analysis of the prepared powders in a chronological order, as the results from a previous experiment would show the way for the next. The resulting powders and their properties are compared to the commercial reference powders described in chapter 5.4. The latter section shows the mechanical properties of test specimens that were fabricated from those powders that were successfully prepared from recycled new scrap. Appendix III shows detailed results from all the tests done when determining the powder and part properties. For clarity, in this section the results are presented in tables, diagrams and graphs using average and corresponding standard deviations derived from the measurements.

6.1 Powders prepared from the sieve residue

Various parameter combinations were tested with the ball mill, most with poor results. Images were taken from all the resulting powders and for clarity not all of these are shown here in the results, but can be seen in appendix II. Figure 48 shows the effect of too high or low milling energy. With high rotation speed or milling time (figure 48a–b) the separated particles are crushed into flakes, whereas with low milling time and rotation speed (figure 48c) the energies are not enough to separate the agglomerations.

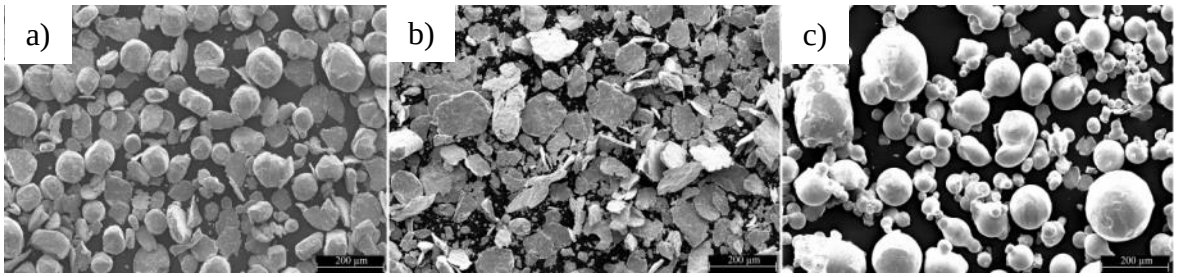

Figure 48. SEM images of ball milled H13 sieve residue powder: a) 60 min at 150 rpm, b) 30 min at 250 rpm and c) 5 min at 150 rpm.

Milling time of 5 minutes at 200 rpm resulted in best results during the ball milling tests as most of the particles were separated but only some were crushed into flakes, seen in figure 49a). However, as the first test runs were done at 5 g samples, next the amount of powder was increased as the goal is to produce enough powder that test specimens can be

manufactured with additive manufacturing. As seen from the SEM images at 100x magnification in figure 49, the increase in the sample size reduces the separation efficiency of the particles and shows that the parameter optimization in planetary ball mill should be done with the same sample size as in the intended production, which was deemed problematic.

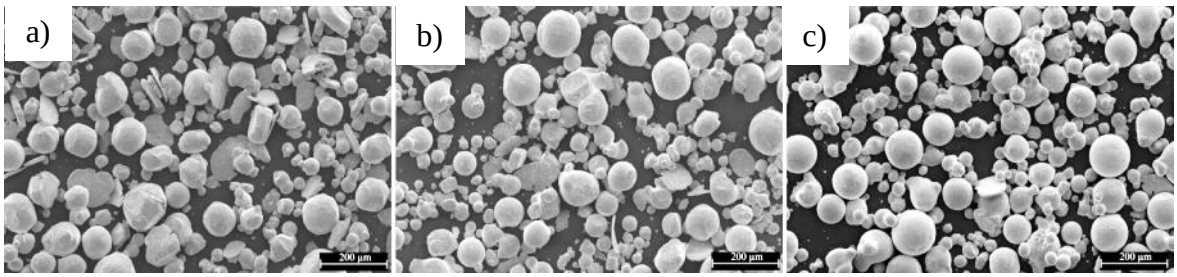

Figure 49. Effect of sample size a) 5g, b) 25g and c) 100g on the particle size and shape during ball milling of H13 sieve residue powder.

Therefore a different type of mill was tested next in an attempt to separate the agglomerates. Figure 50 shows the results from a test run with the air classifier jet mill. As can be seen almost every particle has been effectively separated, the spherical morphology is mostly retained and no particles are crushed into flakes. If we compare the jet milled sieve residue powder even to the best result from the ball mill it is clear that the jet milled powder consists of relatively more spherical particles, less agglomerates and no flakes. Therefore jet milling was selected for processing all of the sieve residue powder (H13 and 316L) to be further analysed.

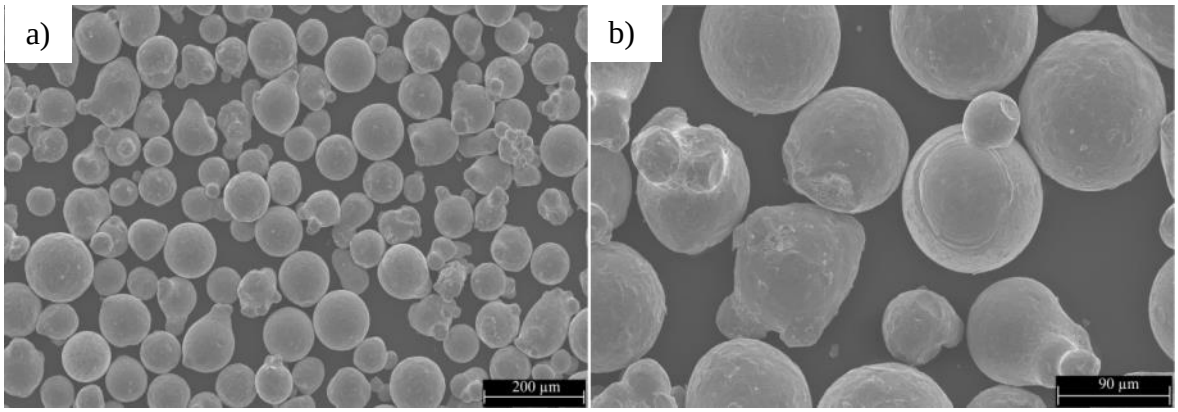

Figure 50. SEM images of the H13 sieve residue powder after jet milling at a) 100x and b) 250x magnification.

From the SEM images in figure 50 it can be already seen that the particles are relatively large compared to the commercial H13 powder. This is further confirmed by the laser diffraction analysis (dry method). Figure 51 shows the graphic particle size distribution for the jet milled H13 sieve reside powder. The corresponding D10, D50 and D90 values are 64.8 µm, 99.6 µm and 151 µm respectively. Such particle size distribution is not suitable for the L-PBF machine. Even if the layer thickness were increased to the maximum of 80 µm still more than half the particles would be larger than this. The increase in layer thickness would also make it harder to compare results with parts manufactured from the commercial powder, for which a layer thickness of 30 µm is typically used. Looking at the SEM images (figure 50) shows that the individual spherical particles are just too large, some clearly over 90 µm in diameter.

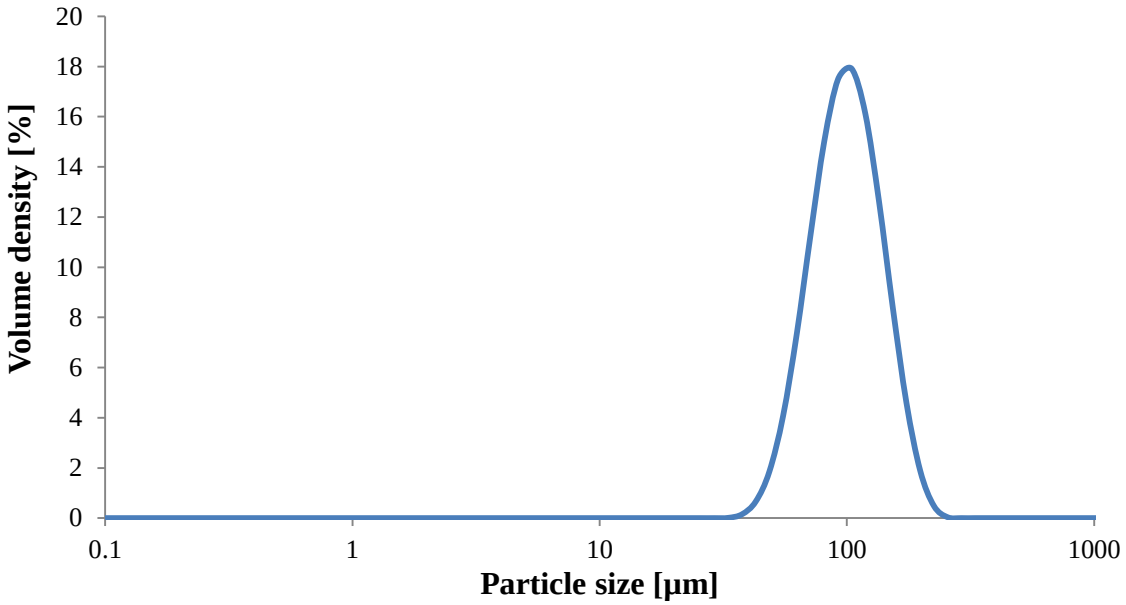

Figure 51. Particle size distribution of H13 powder prepared via jet milling the sieve residue powder.

Nevertheless, the powder has the desired quasi-spherical morphology and even if the particles are too large for L-PBF, the powder could be usable in other powder-based additive manufacturing, such as E-PBF or directed energy deposition. Manufacturing test specimens with one of these technologies is not in the scope of this thesis, but the flowability, apparent and tap densities of the powder were determined and are shown in table 9. Regarding these properties the jet milled H13 sieve residue powder performs better

than the commercial gas atomized H13 powder. The relative density of the powder is 56 % without compaction and 63 % after tapping. The better performance in the Hall flowmeter compared to the commercial H13 powder is due to the larger particle size; in powder with larger particles gravity becomes more substantial force and the powder flows more readily through the orifice. Increase in particle size also increases the packing density of the powder as there is less agglomeration.

Table 9. Flowability, apparent and tap densities of jet milled H13 sieve residue powder.

Flowability [s/50g]	Apparent density [g/cm^3]	Tap density [g/cm^3]
19.8±0.1	4.40±0.01	4.91±0.02

Figure 52 shows the SEM images of the jet milled 316L sieve residue powder. Almost all of the initial agglomerations have broken apart and the powder consists of individual quasi-spherical particles, as was the case with the H13 sieve residue. The smoothness of the particle surfaces have somewhat suffered as a result of particle-particle collisions and the separation of the sintered agglomerates via fracturing during the milling. It can be further seen that the bulk of the particles are significantly smaller than in the jet milled H13 sieve residue, with few large individual spherical particles.

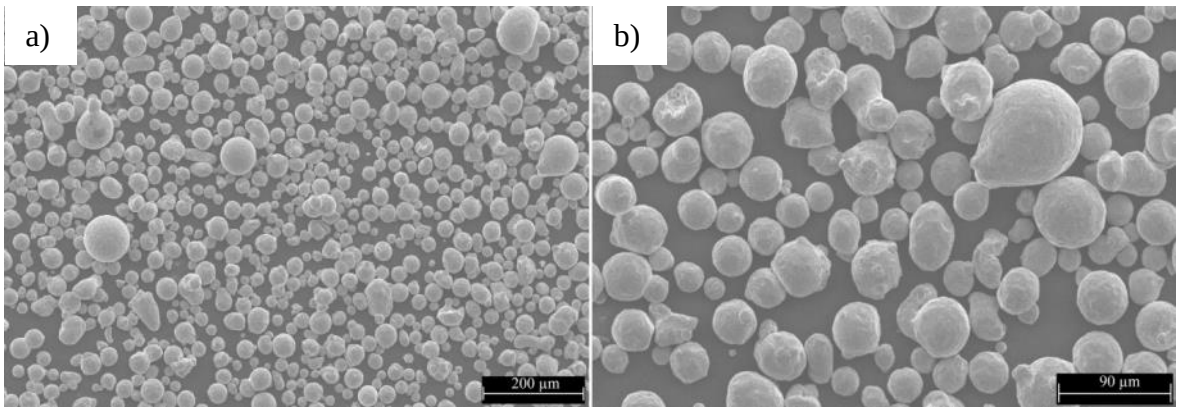

Figure 52. SEM images of the 316L sieve residue powder after jet milling at a) 100x and b) 250x magnification.

The particle size distribution of the jet milled 316L sieve residue powder scrap was measured using the dry method (dispersion in air). Figure 53 shows the graphic particle

size distribution, which is close to Gaussian distribution with slight asymmetry towards coarser particles. The corresponding D10, D50 and D90 values are 26.8 µm, 43.9 µm and 75.8 µm respectively. Unlike with the jet milled H13 sieve residue powder these results are more promising. Comparing to the commercial 316L powder the jet milled powder is coarser, but it should still be small enough for the PBF machine. Most of the particles (as indicated by the D90 value) are smaller than 90 µm, which is the opening of the sieve that is used between the builds to assure that particles larger than this are excluded from the PBF machine. Regarding particle size the jet milled 316L sieve residue powder was deemed suitable for L-PBF. The PSD shows that there is a small amount of particles larger than 90 microns, so the powder was passed through the 90 µm sieve before use in the PBF machine. Around 1 % of the powder was left on the sieve, meaning that jet milling the sieve residue powder resulted in a 99 % powder yield with suitable size for L-PBF.

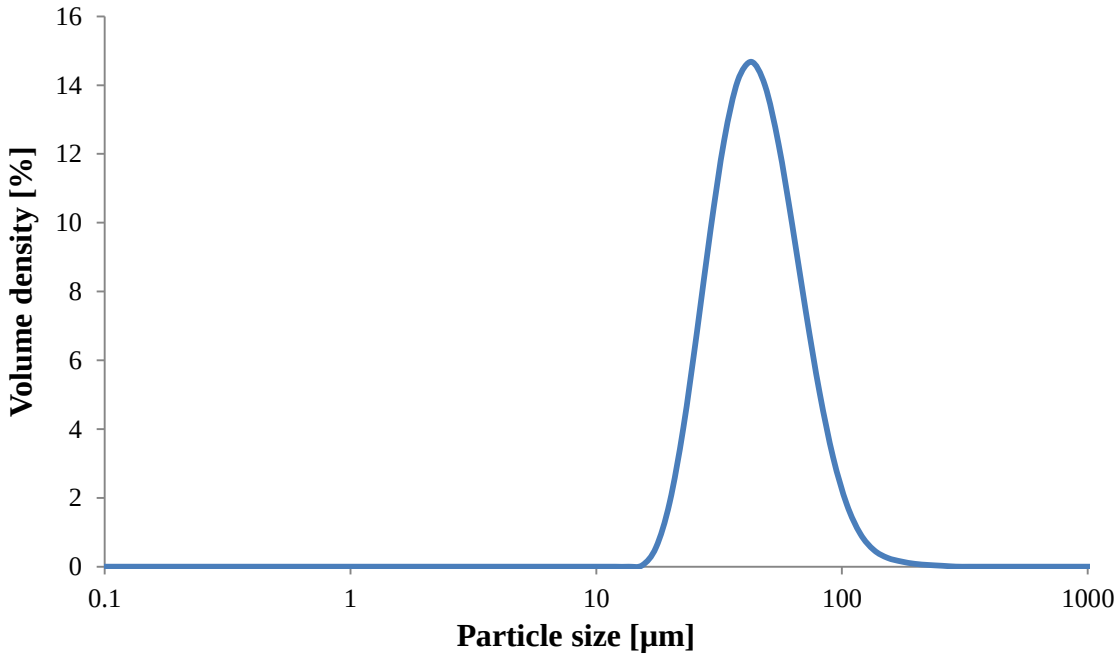

Figure 53. Particle size distribution of 316L powder prepared via jet milling the sieve residue powder.

Table 10 shows the results from the Hall flowmeter for flowability, apparent and tap densities together with the corresponding standard deviations of the 316L sieve residue powder after jet milling. The powder was free flowing and no initial tap was needed. The relative density of the powder is 56 % without compaction and 62 % after tapping. These results are comparable and further slightly better than those of the commercial reference

316L powder. The flowability is significantly (almost 10 %) better than in the commercial reference powder, because of the larger particle size of the jet milled sieve residue powder.

Table 10. Flowability, apparent and tap densities of jet milled 316L sieve residue powder.

Flowability [s/50g]	Apparent density [g/cm^3]	Tap density [g/cm^3]
19.1±0.05	4.45±0.01	4.93±0.04

Based on the quasi-spherical morphology, particle size distribution, flow and packing density properties the jet milled 316L sieve residue powder was determined suitable for L-PBF. EDS analysis was also done for the prepared powder to see if contamination occurs during the jet milling. The EDS spectrum in appendix I shows that no additional peaks in comparison to the commercial powder and the initial scrap material are present, indicating no contamination in the form of unwanted elements. This was expected, as the particles collide with each other and with the components of the jet mill, which are mostly made from 316L material. It was decided to proceed with the jet milled 316L powder into manufacturing test specimens with powder bed fusion.

6.2 Powders prepared from the support structures

Two separate processing routes were tested in an attempt to prepare powder from a more solid form of scrap (support structures and scrapped parts). At first H13 support structures were subjected to ball milling, to see if the material is brittle enough to be efficiently reduced into powder and then to be further plasma spheroidized. Various combinations of milling time and rotation speed were tested, however with poor results. Figure 54 shows the results after a) 60 minutes of milling at 150 rpm and b) 30 minutes at 250 rpm. It can be seen without the aid of microscope that most of the supports are not reduced into fine enough particles even after quite long milling time.

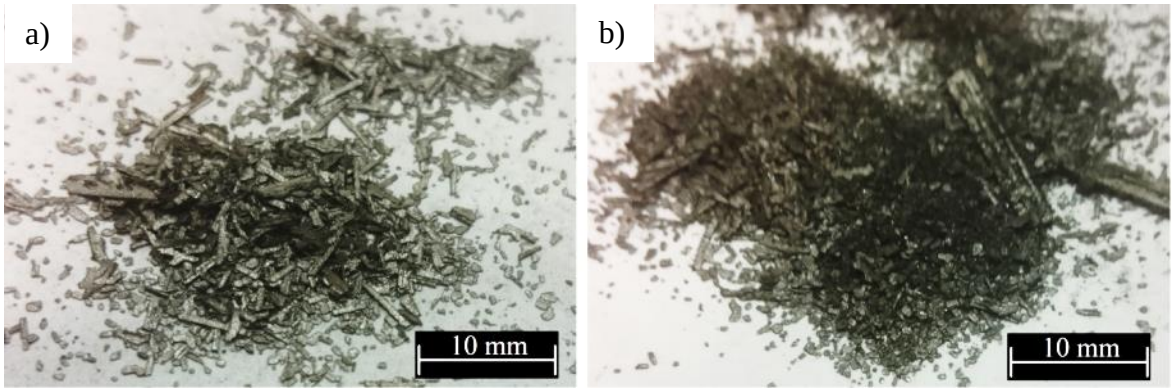

Figure 54. Ball milled H13 support structures: a) 60 min 150 rpm and b) 30 min 250 rpm.

After milling for 60 minutes at 300 rpm around half of the initial supports were reduced to powder, while the other half still remained in a particulate form visible to the naked eye. Furthermore, as seen from the SEM images in figure 55, the part of the supports that was reduced into powder mostly consists of particles in the size range of around few microns, which is already too small for PBF. Two extremely large particles are also visible in figure 55a). At this point ball milling was deemed unfeasible. It would take long time, meaning increased SEC, to achieve micron sized powder and furthermore, it was not possible to control the resulting particle size precisely enough. The particle size distribution is just too wide, as some particles remain close to the initial size of the feedstock, while others already reduce into particles too small for PBF.

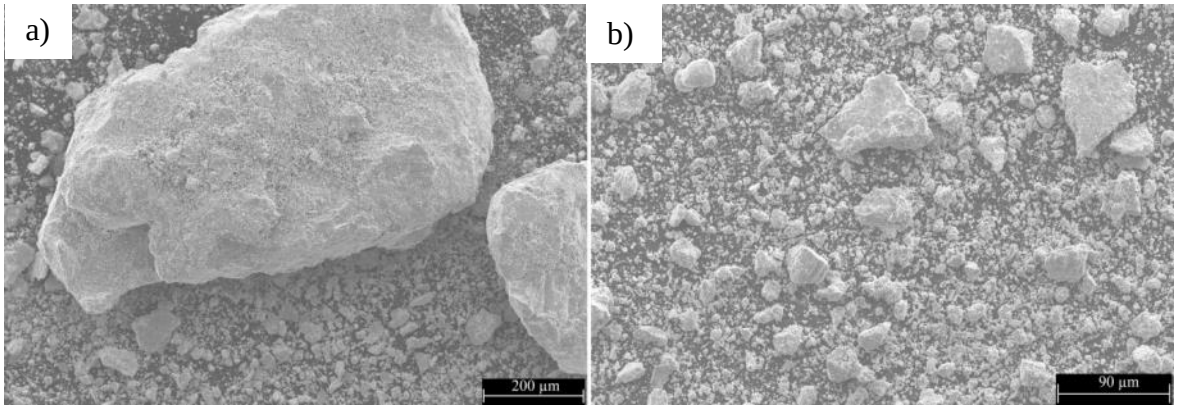

Figure 55. SEM images at a) 100x and b) 250x magnification of the resulting powder fraction after ball milling H13 support structures for 60 min at 300 rpm.

The disintegrator mill was tested next to reduce the 316L supports into micron sized powder more efficiently. Opposite to the ball mill where the particle size remained too

large after reasonable milling times, the disintegrator mill reduced all of the support structures essentially into dust in few minutes. The SEM images in figure 56 confirm that most of the particles are reduced into a size of around few microns or less which is too small for powder bed fusion. The powder was also severely oxidized because of the extremely small particle size and increased temperature of the material during milling, caused by the excessive energy that was transformed from the mill to the milled material. Based on this the powder was deemed unsuitable for L-PBF even if it were plasma spheroidized as the particle size distribution is not significantly altered by the plasma spheroidization process.

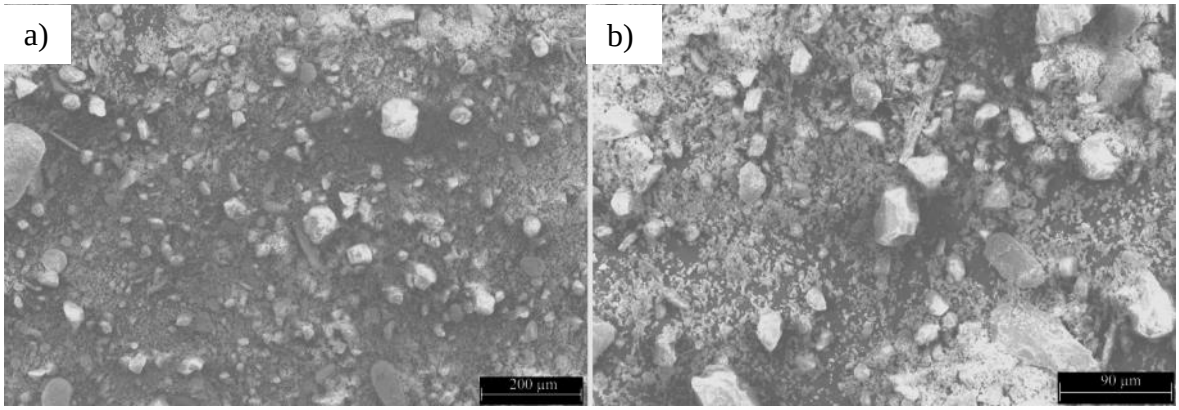

Figure 56. SEM images at 100x (a) and 250x magnification (b) of powder prepared with the disintegrator mill from 316L support structures.

Because it was not possible to achieve the desired PSD efficiently with the tested mills, the recycling route MM+PS was deemed unfeasible for these materials and mills. As it was already stated in the literature review, the milling step should be highly efficient for there to be any sense in regards of SEC in recycling through the MM+PS route. Furthermore, the milling step should have a powder yield close to 100 % with the desired particle size, which was not achieved in any milling test and hence there was no sense in further plasma spheroidization of the milled powders. Therefore the focus in the recycling of solid new scrap into powder was shifted to the GA route, which based on the literature review, has lower SEC than the MM+PS route and thus is a more appealing recycling route.

6.3 Powder prepared from the support structures and defected parts

As it was stated, GA also produces powder with quite wide PSD and only some portion of the produced powder has suitable size for L-PBF. However, the PSD is such that most of the powder that cannot be utilized in L-PBF is suitable for other PM applications. Unlike ball milling where half the particles remained in millimetre scale and the other half was reduced to dust, GA has close to 100 % yield of particles in the size range from few microns to few hundred microns, in other words powder. The powder prepared from solid scrap by GA was sieved (63 µm opening) and the fraction that passed was collected for analysis. Figure 57 shows SEM images of the sieved GA solid scrap powder. As could be expected, the particle morphology is similar quasi-spherical as the commercial GA powder, consisting of mostly spherical particles with some irregularities in the form of satellites and elongated or otherwise deformed particles. It can be noted that there is more fine (<10 µm) particles than in the commercial GA powder.

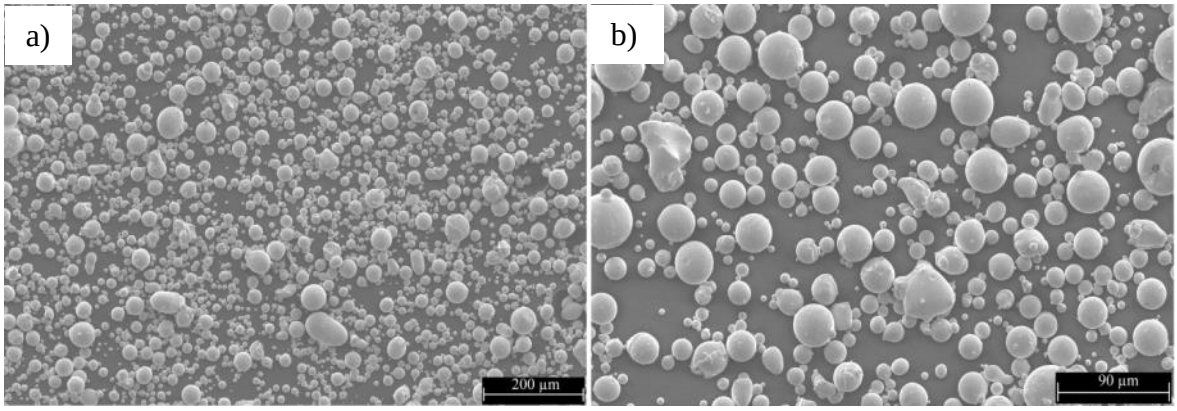

Figure 57. SEM images of gas atomized powder prepared from 316L support structures and scrapped parts at a) 100x and b) 250x magnification.

Figure 58 shows the graphic particle size distribution of the GA solid scrap powder after sieved with 63 µm sieve. The distribution is log-normal with clear asymmetry towards the finer particles, which is also seen in the SEM images. The corresponding D10, D50 and D90 values are 14.0 µm, 33.3 µm and 60.5 µm respectively. Comparing to the commercial reference powder, the D50 value is close but both the D10 and D90 values are further away from the mean. The asymmetry or tail towards the finer particles also is a clear difference. However, such PSD should be suitable for L-PBF, if the increased amount of fine particles is not too detrimental for the flowability of the powder.

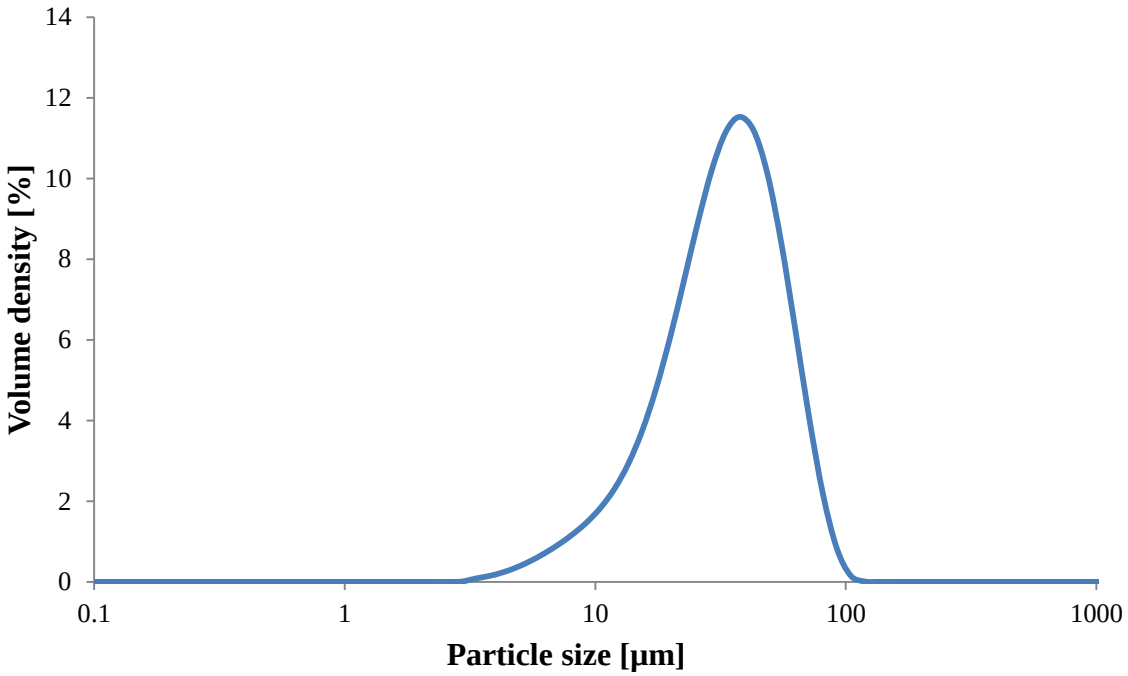

Figure 58. Particle size distribution of gas atomized 316L powder prepared from solid scrap. The powder has been passed through a sieve with 63 µm opening.

Table 11 shows the flowability, apparent and tap densities of the gas atomized powder prepared from 316L solid scrap. The powder was free flowing, except for one test were a single tap was needed to initiate flow. The relative density of the powder is 58 % without compaction and 64 % after tapping. Comparing to the commercial gas atomized 316L powder it can be seen that the powder atomized from scrap has slightly decreased flowability, but slightly increased apparent and tap densities. This is explained by the difference in PSD, as the higher amount of fine (<10 µm) particles in the GA solid scrap powder increases packing and decreases flowability.

Table 11. Flowability, apparent and tap densities of gas atomized sieved powder prepared from 316L solid scrap.

Flowability [s/50g]	Apparent density [g/cm^3]	Tap density [g/cm^3]
21.6±0.06	4.61±0.01	5.09±0.02

As both powders are gas atomized and should yield similar PSD's, most likely the particles under 10 µm have been separated from the commercial powder by the powder producer to

enhance flowability. However, as the difference in flowability is only around 3 %, it was decided not to separate the fine cut from the GA solid scrap powder. The separation process would decrease the powder yield and furthermore, cannot be achieved with sieving. To separate the fine cut from the powder more advanced and costly classification methods are needed, such as air classification, which would decrease the feasibility of the recycling route. As the GA solid scrap powder has a desirable PSD, quasi-spherical particle morphology, good packing properties and sufficient flowability after just sieving the coarse (over 63 µm) particles away, the powder was deemed suitable for PBF. Furthermore, the EDS analysis showed no contamination in the form of unwanted elements (see appendix I).

Initially 4195 g of scrap was loaded to the atomizer. Part of the scrap did not melt properly and therefore did not leave the melt chamber through the nozzle and was not atomized. This was caused by the scrap pieces sintering together at the upper part of the melt crucible, while the material at the bottom already melted. Most likely the heat provided by the induction coil was directed mostly to the already melted material and despite increasing the temperature of the melt, the upper part of the scrap did not melt. As the individual scrap pieces sintered together from the top edges they did not sink to the melt as they should have. Proper melting of all the material loaded to the melt crucible is achievable with a more thoughtful packing of the scrap pieces relative to each other in the melt crucible so that they would not sinter together from the top edges.

Table 12 shows the material flow from the atomization process. From the 2898 g of scrap that was successfully atomized, 1775 g was recovered as powder deemed suitable for L-PBF, providing a powder yield of 61 %. Compared to the as low as 20 % value from the literature, the yield is good. It should be highlighted that the coarse powder fraction, sieved between 63 and 125 µm, can be used in other PM applications and is not waste. The fraction regarded as loss is debris that is left on the atomizer walls and such, which are scrapped once the atomizer is cleaned after the production run. In this case the cyclone fraction, consisting of extremely fine powder around few microns, and the coarse debris, consisting of particles over 125 µm and up to millimetres, are also considered scrap.

Table 12. Material flow in the atomization of 316L solid scrap.

Material in	Mass [g]	Fraction
Initial scrap	4195	
Successfully atomized	2898	1
Cyclone	241	0.08
Loss	147	0.05
Collection chamber	2510	
Powder < 63 µm	1775	0.61
Powder 63–125 µm	529	0.18
Debris >125 µm	145	0.05
Samples for analysis	Remainder	Remainder

Powders deemed suitable for L-PBF were only successfully prepared from the 316L scrap so there were no need to manufacture any reference samples from the H13 material. Figures 59 and 60 summarizes the 316L powder properties of the commercial reference, jet milled sieve residue and gas atomized solid scrap powders. Note that in figure 60 a higher value for apparent and tap densities but a lower value for flowability is considered better. Comparing the prepared powders to the commercial reference, the packing properties are in both cases better. The jet milled sieve residue powder has clearly better flowability than the commercial reference, while the GA solid scrap powder has slightly poorer flowability. Figure 59 shows all three PSD's in the same graph. Comparing to the commercial reference powder, the jet milled sieve residue powder is shifted towards coarser particles and the GA solid scrap powder has a tail of finer particles. The commercial powder also has the most narrow particle size range. Even if all three powders were deemed suitable for L-PBF, these differences might cause some variations to the finished part properties.

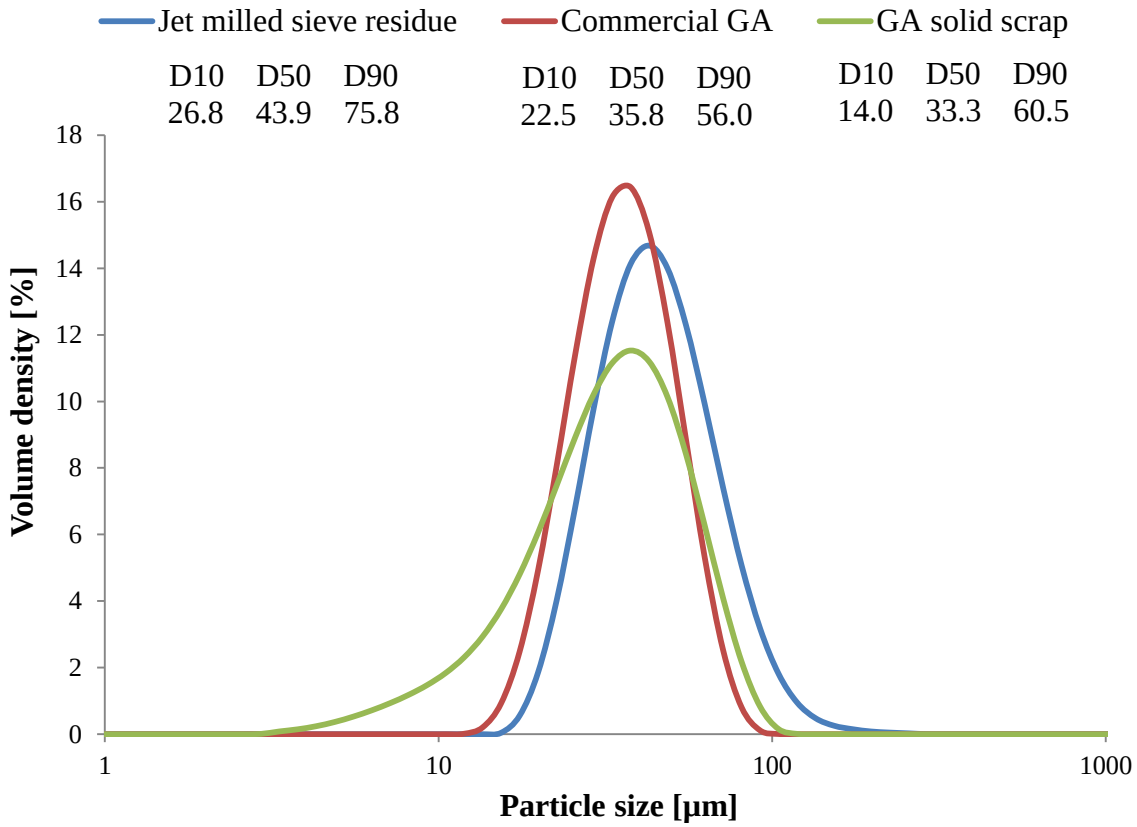

Figure 59. Particle size distributions of the 316L powders prepared from scrap, compared to the commercial powder used as reference.

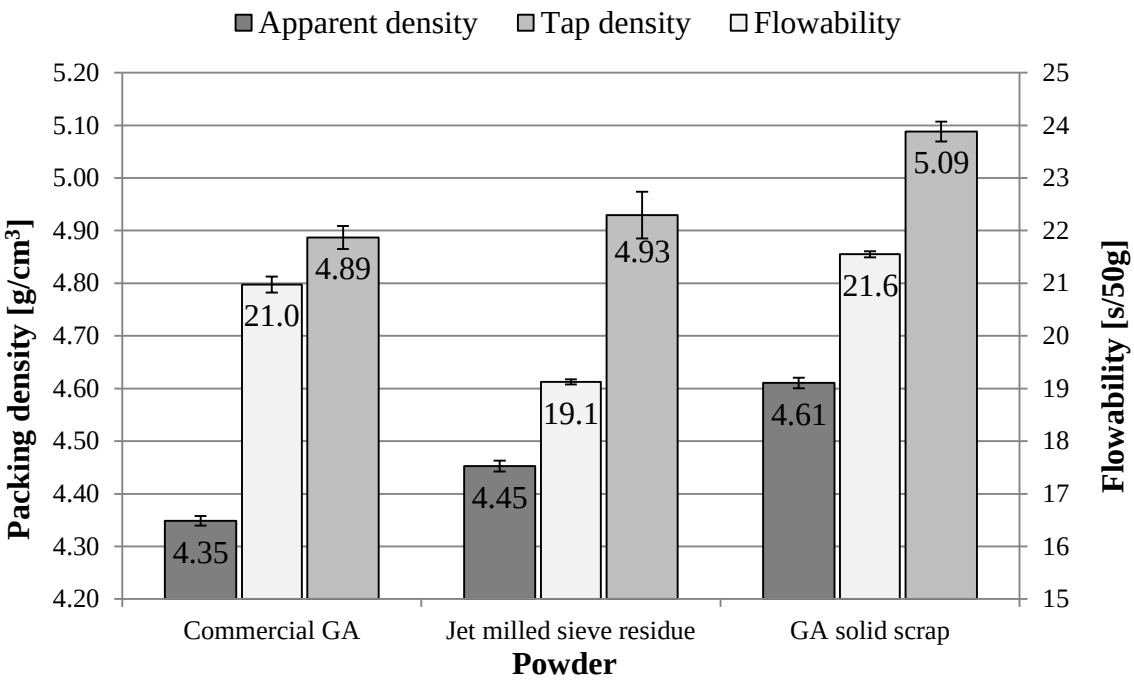

Figure 60. Flowability, apparent density and tap density of the 316L powders prepared from scrap, compared to the commercial powder used as reference.

XRD analysis was only done for the above three powders as they were the only powders from which test specimens were manufactured with PBF. Figure 61 shows the XRD spectrum for the 316L commercial GA, GA solid scrap and jet milled sieve residue powders. Two different crystal structures are distinguished in all three powders. The FCC structure is austenite, which is the dominant phase in all powders. The BCC structure is most likely ferrite, however based on the XRD spectrum alone it cannot be said with certainty whether the structure denoted as BCC is actually ferritic or martensitic.

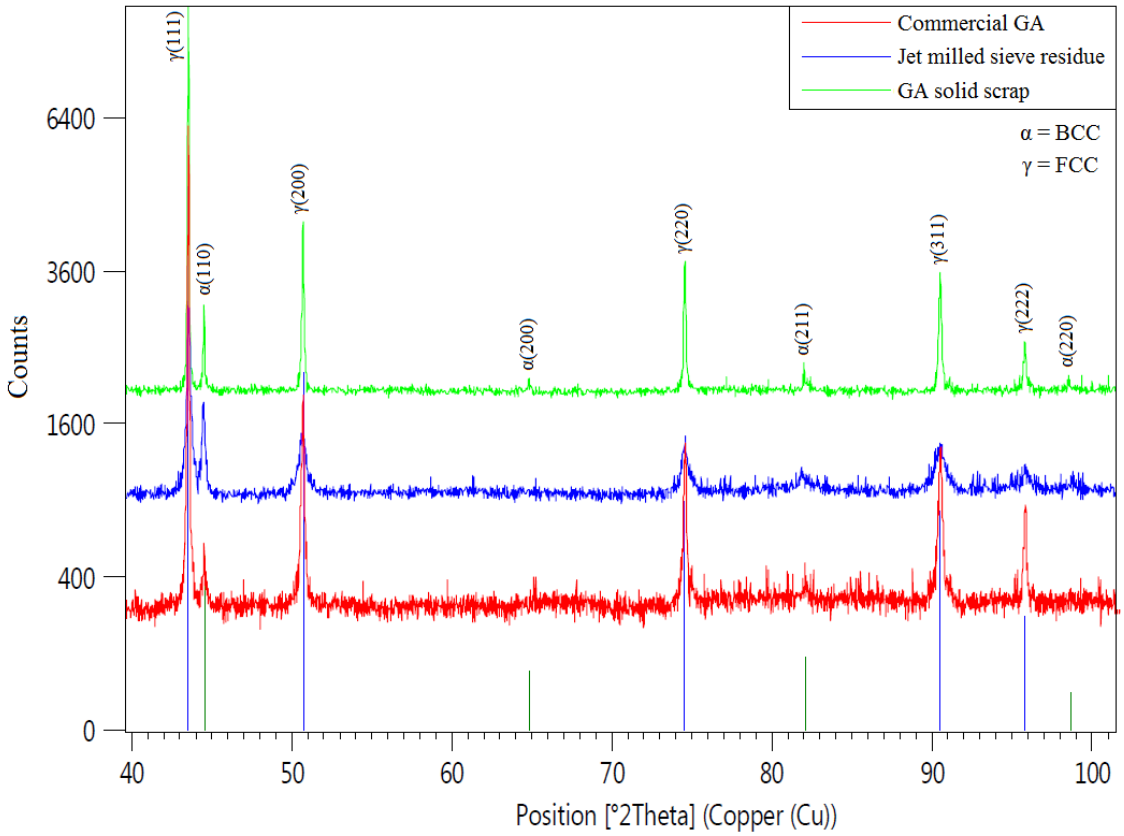

Figure 61. XRD spectrum of the 316L powders prepared from scrap, compared to the commercial powder used as reference.

Looking at the relative intensities of the peaks gives an indication to the ratio at which both the FCC and BCC structures are present. In the commercial GA powder (red) and GA solid scrap powder (green) the peaks corresponding to FCC structures show significantly higher intensities compared to the BCC structure, indicating that only minor quantities of the BCC structure is present. In the jet milled sieve residue powder the intensity of the peaks corresponding to FCC structure are still higher than the intensities of the BCC peaks,

however the difference between the intensities is reduced and the FCC peaks are broader than in the two gas atomized powders. The jet milled sieve residue powder is originally gas atomized powder, which has been used in the PBF machine and there subjected to heat cycles and after that jet milled, which has induced plastic deformations in the powder. Both of these processes may have contributed to the change in the phase structure. The broadening of the peaks indicates smaller grain size and/or residual stresses which are most likely induced by the plastic deformations during jet milling. As all of the powders are melted and solidified again during the manufacturing of the test specimens with PBF in a similar manner, the differences in the phase structure in the jet milled sieve residue powder compared to the other two should be eliminated.

6.4 Powder bed fusion test specimens

Figure 62 shows the as-fabricated 316L test specimens from the commercial gas atomized powder and from the powders prepared from recycled scrap. All of the builds were successful and no defects were visually detected in the samples. Visually one cannot distinguish whether the part has been manufactured from the commercial powder or from the powders prepared from recycled scrap.

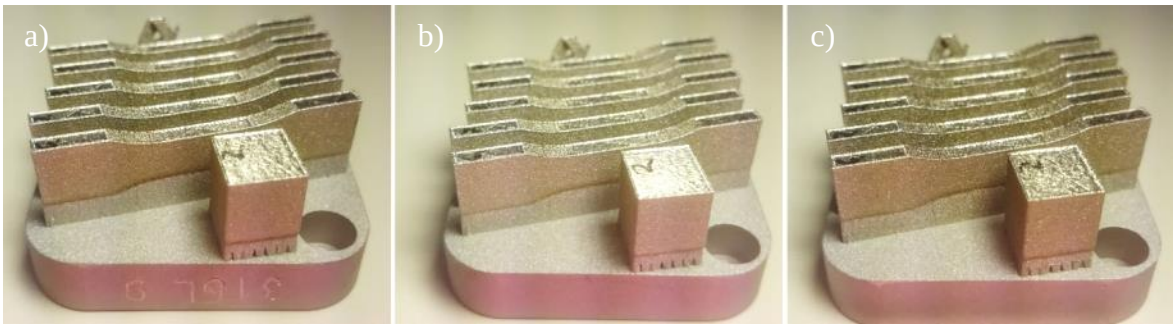

Figure 62. As-fabricated 316L test specimens additively manufactured from a) commercial GA, b) GA solid scrap and c) jet milled sieve residue powder.

The specimens were removed from the build platform by sawing and the remaining support structures beneath the specimens were removed manually with pliers and file. The cubes were further cut in half from the middle for metallographic examinations. Figure 63 shows the tensile test specimens (45 mm in length) after support removal. The samples were subjected to tensile testing in such state without any other post-processing.

Figure 63. As-fabricated 316L tensile test specimens after supports removal, manufactured from a) commercial GA, b) GA solid scrap and c) jet milled sieve residue powder.

Figure 64 shows the polished cross-sections under optical microscope of all three test specimens made from the different 316L powders. From each sample three images from different locations around the middle of the cross-section were taken, the porosities measured and the average value calculated. The dark spots are pores in otherwise dense material. Comparing the samples there is no significant difference in the amount of the pores present. Based on the image analysis the measured porosities are between ~0.06–0.18 %. As seen from the quite large standard deviations, the porosities are not evenly distributed in different locations of the test specimens. The differences in the measured porosities between the samples made from different powders fall under the experimental uncertainty, which is quite large in the image analysis. The extremely small pores that are hardly visible in the images are not included in the calculated porosities. Tan et al. (2016, p. 197–204) reports porosities of ~0.1–0.2 % based on image analysis of 316L L-PBF parts manufactured with SLM 250 HL machine, which is the larger version of the SLM 125 HL

used in this study. They further measured the porosity of the same samples based on the Archimedes principle, receiving porosities of ~0.75–0.9 % respectively.

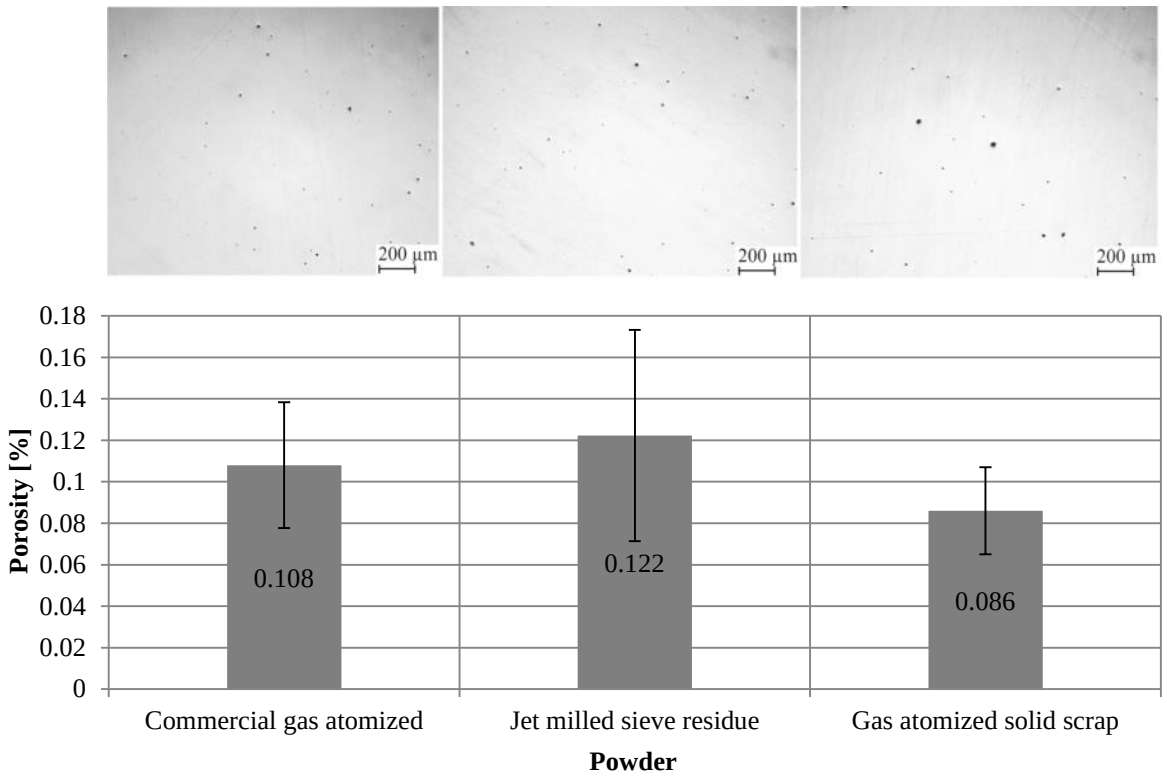

Figure 64. OM images and measured porosities of the polished cross-sections of test cubes made from a) commercial GA, b) jet milled sieve residue and c) GA solid scrap powder.

The microstructures of the three test specimens after etching the polished cross-sections are shown in figure 65. The phase structure in all three samples is austenitic, further confirmed by measuring the ferrite content with the Feritscope MP3, which showed 0 % ferrite for all three test specimens. The grain structure shows the outlines of the individual melt pools that have formed and solidified during the L-PBF process. Grains elongated over several such melt pools in the build direction can be seen. In all three samples dark patches in the microstructure are seen, but in the part made from the GA solid scrap powder (figure 65c) these dark patches are more evident. The areas seen as dark patches in the OM images were further investigated with SEM and EDS while determining the bulk chemistry of the samples.

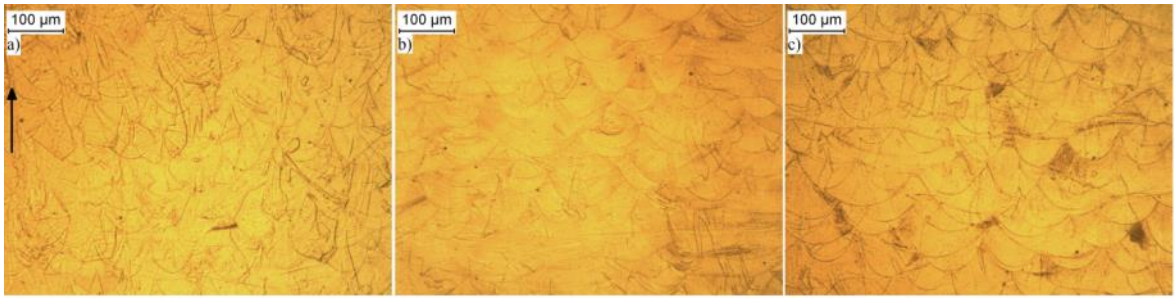

Figure 65. Microstructures of 316L test specimens made from a) commercial GA, b) jet milled sieve residue and c) GA solid scrap powders. The arrow marks the build direction.

In table 13 is shown the bulk chemistry for the main alloying elements of the samples made from the three different 316L powders. The GA solid scrap powder has higher chromium and nickel concentrations than the other two; however the composition of all three samples is in the limits set for 316L stainless steel (UNS S31603) parts manufactured with powder bed fusion by ASTM. It should be noted that for proper validation of the chemical composition, chemical analysis has to be performed with methods specified in the standard ASTM F3184-16. EDS analysis cannot be used to measure the amount of trace elements (such as carbon, sulphur and phosphorous) in the material which would be of interest in this case as maximum limits for these elements are also stated in the standard. However, there is no reason to assume that there would be an increased amount of these trace elements present, as no contamination of the powders was observed.

Table 13. Chemical composition of the 316L PBF parts based on EDS analysis. ASTM specification is included for reference (ASTM F3184-16 2016, p. 4).

	Cr [w-%]	Fe [w-%]	Mn [w-%]	Mo [w-%]	Ni [w-%]	Si [w-%]
Commercial GA	17.5	bal.	1.1	2.6	11.4	0.5
Jet milled sieve residue	17.4	bal.	1.2	2.7	11.3	0.6
GA solid scrap	17.9	bal.	1.2	2.8	13.5	0.6
ASTM F3184-16 (UNS S31603)	16.0–18.0	bal.	<2.0	2.0–3.0	10.0–14.0	<1.0

The dark patches that were evident in the OM images of the microstructures in figure 65 were analysed with EDS and SEM to determine what these are. Figure 66 shows a SEM

image of one such dark patch together with EDS analysis comparing the chemical composition of two different regions in the sample. From the SEM image it seems that the dark patches seen in the OM images are sub-grains that are oriented perpendicular to the surface of the sample and have therefore etched in a different manner from the bulk of the sample, thus differentiating as dark patches in the OM images. In the bulk of the samples, such as the area 1 in figure 66, these sub-grains are oriented more parallel to the surface of the sample and appear as a line of stripes. The EDS analysis further shows that there is no significant difference in the chemistry between the two areas in the sample. This indicates that the different etching behaviour of these areas in the samples is due to the difference in the sub-grain orientation, rather than the result of some secondary phase.

	1	2
	[w-%]	[w-%]
Cr	18.1	17.8
Fe	bal.	bal.
Mn	1.5	1.8
Mo	3.0	3.0
Ni	14.1	13.4
Si	0.6	0.6

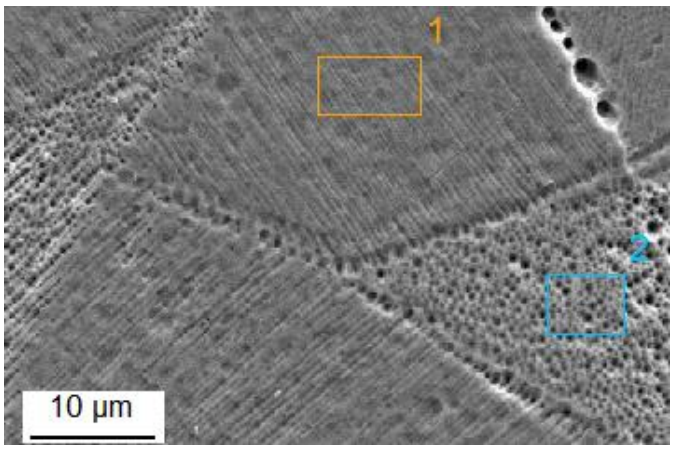

Figure 66. SEM image and chemical composition of one of the dark patches (bottom right corner) seen in figure 65c.

Vickers hardness test results for all the three test samples made from the different 316L powders are shown in figure 67. There are no significant differences in the hardness values, the variations observed falling under the experimental uncertainty. No significant difference in the hardness of the test samples further indicates similar grain structures for all three samples manufactured from the different powders. Slightly higher Vickers hardness values (~215–220 HV) for 316L L-PBF parts manufactured with comparable volumetric energy densities as in this study have been reported in other studies (Tan et al. 2016, p. 197–204; Cherry et al. 2015, p. 869–879).

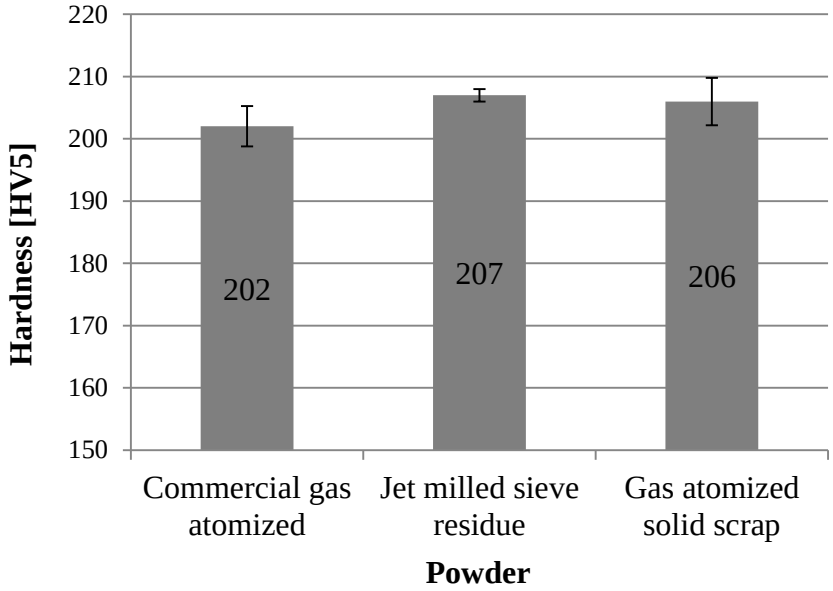

Figure 67. Vickers hardness measured from the cross-sections of the 316L test specimens made from commercial GA, jet milled sieve residue and GA solid scrap powders.

Five tensile test specimens were tested for each powder, from which the average was calculated together with the corresponding standard deviations unless otherwise stated. The results are shown in figure 68. The horizontal lines mark the minimum requirements for R_m=515 MPa, $R_{p0.2}$=205 MPa and A=30 % set in ASTM F3184-16 (2016, p. 5). Detailed results for all the tensile test specimens can be seen in appendix III. One test specimen manufactured from the GA solid scrap powder had some misalignment during setting the specimens between the grippers, resulting in unreliable results and was therefore excluded from the measurements. Therefore the result shown in figure 68 for GA solid scrap powder is the average and standard deviation for four measurements. The tensile strengths for all three powders show good consistency between test specimens and there is no significant difference between the powders either. In elongation after fracture there are quite large variations between individual test specimens. This is most likely due to the use of just 10 mm gauge length specimens and/or localized defects in the individual test specimens, which has been suggested in previous studies to be the cause for scatter that is observed in elongations measured from PBF parts (Casati, Lemke & Vedani 2016, p. 738–744).

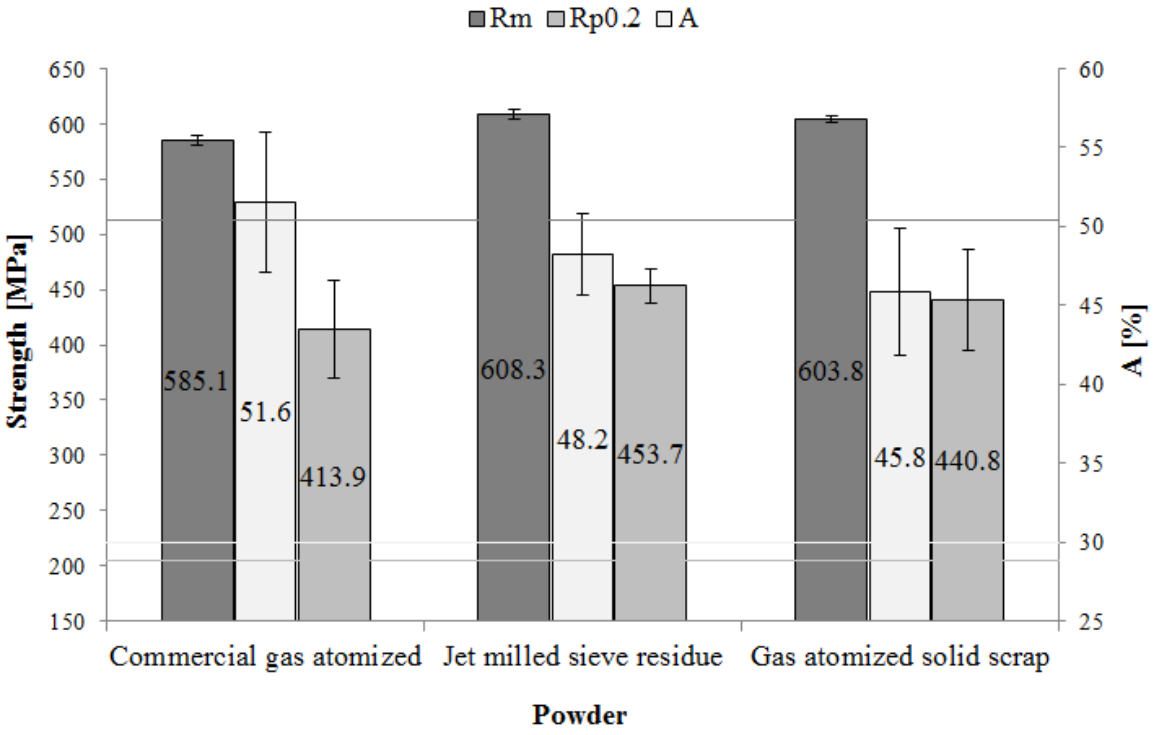

Figure 68. Tensile test results of the 316L test specimens made from commercial GA, jet milled sieve residue and GA solid scrap powders.

The yield strength shows higher variation between individual test specimens than the tensile strength. Similar results have been reported by Karnati et al. (2016, 592–604) for 304L stainless steel PBF parts. In this study there is more variation in the tensile strength of parts made from commercial GA and GA solid scrap powders (SD ~45 MPa) than in the jet milled sieve residue powder (SD ~15 MPa). The higher SD in the commercial GA and GA solid scrap measurements is in both cases caused by one specimen deviating substantially (~20 % lower) from the others. If these two samples are excluded from the results, shown in figure 69, the consistency in the yield strength between the remaining specimens is significantly improved.

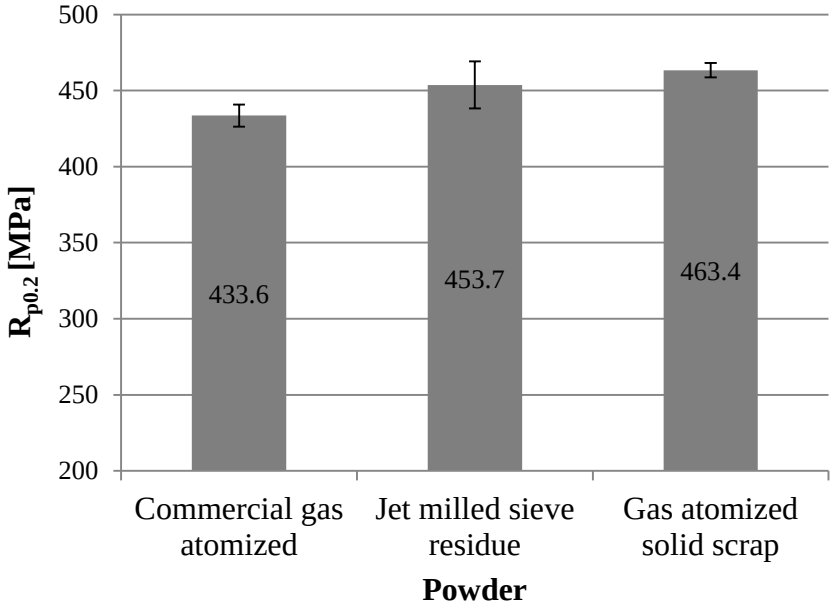

Figure 69. Average yield strength and corresponding standard deviations after excluding the two specimens that substantially deviate from the others.

The deviation in the yield strength of the two poor performing specimens is either caused by a flaw during testing or some local defect in the specimens. The tensile strengths and elongation at fracture for these specimens were comparable with the rest of the specimens (see appendix III) and only the yield strength was reduced. It could be argued based on the findings of Casati et al. (2016, 738–744) that if a local fault such as unmolten particles or inclusions in the specimen caused the earlier yielding, such a fault would also cause premature fracture and would show as reduced elongation. In their study, from the three tensile specimens that showed premature yielding, two also had reduced elongation after fracture, but one specimen had comparable elongation to the properly behaving specimens. In this study none of the specimens with premature yielding showed significantly reduced elongation, so the indication is more towards a fault during testing these specific specimens.

As it was stated, one specimen was completely excluded from the results because of noticeable misalignment of the test specimen while positioning between the grippers, which causes initial bending or torsion stress on the specimen. Similar, but not as severe misalignment and the resulting initial stress on the test specimen once the grippers take hold could be the reason for premature yielding during the actual tensile test. During the

tensile testing it was also noted that positioning the extensometer was challenging because of the short gauge length in the specimens, which could result in inaccurate strain values around the yield point and thus affect the calculated yield strength. This is all speculative and for definite answers, additional test such as analysis of the fracture surfaces should be performed. However that is not in the scope of this thesis, as the goal is just to define whether the powder that was used causes variation to the mechanical properties.

All tensile test specimens from all three powders exceed the minimum requirements set for PBF 316L parts in ASTM F3184-16 standard. The scatter in the elongation and yield strengths are variations between individual test specimens, observed in parts made from the same powder, in the same build with identical parameters. This means that the observed variations are not powder depended. Furthermore, the parts manufactured from the commercial powder had similar scatter in the measured elongation and yield strengths than the powders prepared from scrap. Based on these results the powder that was used, commercial or prepared from scrap, has no significant effect on the tensile properties of the parts.

7 DISCUSSION

In the attempts to recycle H13 and 316L sieve residue powder and solid scrap in the form of support structures and defected parts back into powder usable in L-PBF, successful results were obtained by jet milling 316L sieve residue and gas atomization of 316L solid scrap. Furthermore, no significant variations in the mechanical properties of the 316L PBF parts manufactured from GA solid scrap, jet milled sieve residue, and commercial reference powder were observed. However, there were some differences in the powder properties such as PSD, flowability and packing density of these powders. Based on the literature review such variations should have resulted in variations on the mechanical properties of PBF parts manufactured from the powders with identical parameters and conditions. Regarding mechanical properties, the earlier studies reviewed already provided inconsistent conclusions on whether the PSD of the powder has an effect on the tensile properties of the parts manufactured with PBF or not. The results from this study suggest towards the argument that variations, within the vicinity as in this study, in the powder PSD has no significant effect on the tensile properties, at least not in 316L stainless steel. As the microstructure ultimately determines the tensile properties (in samples with similar porosity levels) the focus should be in determining the relationship between PSD and microstructure of PBF parts. In this study there were no significant differences in the microstructures and as the porosity levels were similar, the hardness and tensile properties showed no powder related variations either.

The reviewed studies were unanimous that variations in the PSD results in variations in the finished part porosities in L-PBF, coarser powders yielding increased porosity. In this study there were variations in the PSD's of the powders, yet no significant difference in the porosity were observed. The results suggest that variations in PSD such as between the 316L powders in this study have no significant effect on the finished PBF part porosity with the parameters that were used. The PSD has an effect on the powder bed density and via this it may cause variations to the finished part porosity. The jet milled sieve residue and GA solid scrap powders had higher apparent and tap densities than the commercial reference powder and therefore should yield denser powder beds and less finished part porosity. As the parameters used in this study were selected based on what has been shown

to produce acceptable results with commercial 316L powder, it could be argued that the set of parameters used provide acceptable results with powders with at least the packing properties of the commercial reference powder used in this study. As the resulting porosities were already very small (<0.2 %) for the commercial powder, no further decrease in the porosity for the jet milled sieve residue and GA solid scrap powders is seen because a threshold has been reached.

It has been proposed that small amount of residual porosity will always be present in as-fabricated PBF parts made from gas atomized powders as the GA powder particles have some initial porosity which is transferred to the finished parts. Small extremely spherical pores in the as-fabricated PBF parts are believed to be the result of such powder induced gas porosity. The pores seen in the parts manufactured in this study fit the description as they were small, from few to 20 µm diameter, and extremely spherical. The other source of these gas pores might be soluble gases, such as oxygen, entrapped in the part once the melt solidifies. (Tammas-Williams et al. 2015, p. 47–61; Bauereiß, Scharowsky & Körner 2014, p. 2522–2528.) The oxygen content in the build atmosphere varied during the builds between 0.13–0.22 %, which is higher than typically achieved oxygen level in the PBF machine that was used for the experiments. The higher than usual oxygen content in the build chamber was caused by the use of the smaller build platform, as there were some challenges in the sealing associated with the platforms piston seal.

7.1 Feasibility

In general it would make more sense to recycle new scrap produced in the manufacturing industry as raw material for metal powder production rather than for the production of bulky feedstock (ingot/bar/plate/wire). Let’s consider the two scenarios of recycling scrap metals via the conventional route to make semi-finished bulky feedstock or the proposed method of recycling scrap to make powder feedstock. Let’s also assume that all of the produced scrap during the manufacturing of products can be, and therefore is recycled to make new semi-finished feedstock materials. In the conventional scenario all of the scrap is recycled to make bulky feedstock, which in the case of steel would cover only 17 % of the needed raw material, therefore virgin materials would account for 83 %. The other scenario is that the scrap is used to produce metal powders, where the demand is less than the available scrap quantities. Therefore all of the global metal powder demand could be

satisfied with the scrap material, leaving still most of the scrap to be used as raw material for the conventional metal production. In both scenarios the global need for virgin ore is the same. However, if all of the new scrap is used to produce bulky feedstock, then the demand for powder feedstock has to be satisfied by making powder from the bulky feedstock as there is no scrap available for this, adding an unnecessary processing step. Such indirect atomization where the feedstock has first gone through the conventional bulk production route and then produced into powder should be avoided as the SEC to produce such powder feedstock is the sum of both (bulk and powder) production routes (Morrow et al. 2007, p. 937). Such indirect atomization also is one of the reasons for high metal powder prices for AM, as the feedstock (ingot/bar/wire) for powder production is already expensive, at least if compared into making the powder from scrap feedstock.

Recycling new scrap via powder production is less energy intensive than recycling via the conventional route. The specific energy consumption of gas atomizing scrap to make powder instead of conventional recycling to bulky feedstock is around 50 % less for steel and stainless steel and up to 90 % less for titanium. In case of aluminium the conventional route has only slightly higher SEC than GA. These are all cases where 100 % scrap feedstock is utilized without any dilution with virgin materials or alloy additions. Furthermore, it should be noted that the SEC of gas atomizing aluminium is most likely lower than the 6.1±0.6 MJ/kg used here, as this is based on atomizing materials with significantly higher melting points than aluminium. Furthermore, if we apply the reported ratio of 75 % scrap and 25 % virgin materials for the conventional aluminium recycling, the SEC is increased to around 50 MJ/kg. Compared to this value, the energy needed in the atomization of 100 % scrap feedstock even with the SEC of 6.1±0.6 MJ/kg is almost 90 % less.

In this thesis gas atomization was successfully applied to the recycling of 316L stainless steel using 100 % scrap feedstock in the form of support structures and defected parts from the PBF process back into powder suitable for L-PBF. No significant variations in the part properties were found in comparison to parts manufactured from commercial 316L powder. This recycling method should be applicable to other materials and forms or sources of waste, assuming high purity from the scrap as was the case in this study. The lower SEC needed to produce gas atomized powder rather than bulky feedstock further

promotes the environmental benefits of powder based additive manufacturing along with the significantly reduced generation of scrap in the first place.

Combining the two factors above with the possibility of AM to produce topology optimized lightweight structures that can significantly reduce the environmental burden of the product during the use phase, makes additive manufacturing an appealing technology towards a more sustainable manufacturing industry. Huang et al. (2016, 1559–1570) studied the energy and emissions saving potential of AM in the case of lightweight aircraft components. They showed that in the manufacturing phase of components the most significant energy savings were achieved due to reduced overall need and SEC of the powder feedstock when using additive manufacturing instead of conventional manufacturing from bulky feedstock. It was further shown that even more significant were the energy savings achieved during the use phase of the product, as the fuel consumption of an aircraft is reduced with light weight components made possible by AM.

The recycling route of jet milling agglomerated powder scrap into useable powder for additive manufacturing that was demonstrated in this thesis requires very low energies as no melting of the powder is needed. If we use the value of 0.4 MJ/kg from the literature for jet milling, the energy needed to recycle steel is only few percent of the 11.7±2.1 MJ/kg of conventional route. The energy consumption also is significantly less than the 6.1±0.6 MJ/kg of gas atomization route. Unfortunately, waste streams recyclable this way are extremely limited, as the scrap has to be in a form of agglomerated spherical powders which have not been contaminated. As of now, the author has identified only one such waste stream. The sieve residue powder used here as a case study is a relatively small waste stream, as only 2–5 % of the initial powder per build in the powder bed fusion machine ends up as sieve residue and therefore this could not completely cover even the feedstock powder need for powder bed fusion additive manufacturing. Nevertheless, the fact that this powder can be returned back to use in PBF with minimal specific energy consumption is a good method to further increase the overall raw material utilization efficiency of powder bed fusion close to 100 %. This is of course the case only with parts where support structures are not needed.

Because of the limited applicability of mechanical milling alone or even with further plasma spheroidization to produce spherical powders to only some materials and forms of waste, gas atomization is regarded as the most flexible recycling method to produce spherical powders for AM. Solid scrap, which is the most generated form of scrap by the manufacturing industry, was successfully recycled via gas atomization but could not be efficiently recycled through the MM+PS route. All forms of solid scrap should be suitable feedstock for gas atomizing. It should be highlighted that the scrap has to be of high purity and consist of only one particular metal or alloy like was the case here, to avoid the need of dilution and alloying with virgin materials and achieve the low SEC of 6.1±0.6 MJ/kg.

To recycle a waste stream consisting of mixed materials or a material with impurities via gas atomization results in the same challenges as with conventional recycling. Sorting and cleaning the scrap might be needed prior melting and dilution with virgin material might be needed during the melting phase to meet the demands for the chemical composition, decreasing the feasibility of the recycling. Nevertheless, the SEC of recycling mixed or contaminated scrap via gas atomization is still less than recycling the same scrap via the conventional route. In such case the additional steps needed such as sorting, cleaning and diluting with virgin materials are the same for both routes, but the actual feedstock production of gas atomization to powder uses less energy than casting and forming into bulky feedstock.

In this study 316L stainless steel was successfully recycled into usable powder for PBF. Reactive and therefore expensive materials, such as titanium based alloys, provide the highest energy saving potential and potential cost savings in the powder production by utilizing recycled scrap feedstock. Because of the reactivity and ductile behaviour of titanium alloys, they might be hard to recycle through the MM+PS recycling route, which was unsuccessful for the non-reactive, more brittle H13 material in this study. On the other hand, gas atomization of titanium based alloys is known to be problematic as the extremely reactive molten titanium tends to pick up contaminants from all of the typically used ceramic melt crucible and nozzle materials in gas atomization equipment. However, with special melt crucible and nozzle designs and materials the contamination can be limited to acceptable levels. (Heidloff et al. 2010, p. 35–41). Therefore it should be possible to

recycle titanium scrap into high purity powders via gas atomizers that are equipped with melting configurations specifically designed for the extremely reactive materials.

For titanium based alloys and also for any other ductile material that is susceptible to hydrogen induced brittleness, the recycling route proposed by Yang et al. (2013, p. 2313–2316), with the addition of the hydrogen embrittlement step to the proposed MM+PS recycling route in this study, seems a prominent production route for high purity powders without too much of an increase in SEC and production cost. If the lower SEC route of gas atomization cannot be used in the recycling of titanium based materials because of contamination, the hydrogen embrittlement, milling and plasma spheroidization route is still less energy intensive than the conventional way of recycling titanium via re-melting, casting and forming into bulky feedstock. As of now, the relatively high SEC of plasma spheroidization limits the feasibility of recycling via MM+PS route into such materials that cannot be recycled via the lower SEC gas atomization route. To assess the feasibility of the recycling route proposed by Sun et al. (2016, p. 331–335) requires information about the SEC and amount of consumables that are needed to produce the powder. Hopefully the authors are planning on carrying out such further studies, as it was noted that the recycling method should be applicable also for other metals and alloys.

7.2 Reliability

The specific energy consumption values in table 1 should not be taken as exact values, as there are differences in how they have been calculated in the original studies, indicated also by the quite high standard deviations. Factors contributing to the deviations include the type of energy sources used and the scope of processes included in the calculations of the original studies. The fact that bulky feedstock is produced in many different forms and delivery conditions, such as ingots, bars, plates, sheets, tubes with various different heat treatments contributes also to the deviation in the SEC values. Unfortunately, for example cold rolling and heat treatment cannot be eliminated from the process chain just to reduce SEC. These processes are applied to achieve a defined size and specific microstructure to the feedstock. This is required so that the finished product conventionally manufactured from that feedstock can have the desired geometry and microstructure. In this study the SEC values are used for comparing the energy consumption in the conventional recycling and in the proposed routes for recycling by producing powder feedstock. For this purpose

the values are reliable enough, as the differences are clear and not within the standard deviations. For the bulky feedstock in table 1 more than one value was found for all but conventional scrap titanium recycling.

For the SEC values for powder preparation in table 2 more than one value is included for atomization and mechanical milling. Unlike with conventional recycling of scrap, the SEC of gas atomizing titanium is close to the iron based alloys. This is because the fundamental process remains the same for both materials. For plasma spheroidization the author only found one value that could be considered being close to the true SEC during production, as all the other reviewed studies were done on laboratory scale equipment. It should be highlighted that the values for SEC used in this study are such that resemble the case of full scale production. Measurements that could have been done by the author for the specific laboratory scale equipment that was used in the experimental part of this thesis would not yield SEC values that are even close to the truth during production. The economies of scale are a major contributor to the specific energy consumption of these processes.

The results after the jet milling of H13 sieve residue powder are quite puzzling; where did the individual, spherical large particles come from? As seen from the commercial unused H13 powder the largest particles are around 50 µm in diameter. However, after the powder has been used in the PBF machine and the leftover powder is sieved, spherical particles three times larger (D90 value was at 151 µm) appear on the powder and are left on the sieve residue, seen in figure 50, as they cannot pass the sieve with 90 µm opening. These are clearly not just two or more smaller particles sintered into one larger, as the SEM images reveal them to be extremely spherical, which cannot be the result of particles sintering into each other. Nevertheless, as the particles appear after using the powder in the PBF machine, they must be generated during that process.

The most likely explanation for this is that the large spherical particles are produced as a result of spattering which takes place during the PBF process. Droplets of molten metal are ejected from the melt pool and during the freefall in the process chamber these droplets solidify into spherical particles in the same manner as in atomization processes. Simonelli et al. (2015, p. 3842–3851) have studied the spatter formation in PBF process in more

detail and they provide evidence for the same conclusion; large spherical particles are formed in the process as a result of spattering. In the 316L sieve residue powder in this study there was also few larger spherical particles (around 100 µm) present than in the commercial reference powder, in which the largest particles are around 50 µm.

However, even the largest spherical particles in the 316L sieve residue are not as large as in the H13 sieve residue. Furthermore, the H13 sieve residue consists mostly of these coarse particles, whereas the 316L sieve residue only has few coarse particles in otherwise finer powder. This implies that the material itself or the parameters used for the given material are the cause for the formation of more and larger spatter in the H13 material in this study. This is also supported by the findings by Simonelli et al. (2015, p. 3842–3851), where the spherical particles produced by the spattering were smaller with 316L material compared to AlSi10Mg and Ti-6Al-4V.

7.3 Conclusions

The results from the literature review indicate increased environmental benefits of recycling new scrap generated by the manufacturing industry via powder preparation for powder-based AM, compared to the conventional recycling route applied today. Additive manufacturing also inherently generates less waste than the conventional manufacturing of today. Therefore shifting from subtractive towards additive manufacturing will enhance the sustainability of the manufacturing industry via reduced waste generation and improved energy efficiency in the recycling of the unavoidable scrap. The experimental work demonstrated the technical feasibility of recycling new scrap into suitable powder for L-PBF via gas atomization of solid scrap and jet milling of agglomerated spherical residue powder. No significant powder-related differences in mechanical properties and microstructures of the parts manufactured from the powder made from scrap were detected, in comparison to parts manufactured from commercial powders. The answers for the research questions set at the beginning of the study are as follows:

1. What are the benefits of recycling metallic waste as powder for AM?
    - Compared to the conventional recycling route: specific energy consumption can be reduced, dilution losses and non-functional recycling avoided. Powders

prepared from scrap feedstock could also reduce the relatively high price of AM powders.

2. What type of waste streams are most suitable for recycling via the proposed routes?
    - Those that receive no contamination from the manufacturing process and there is no mixing of different scrap materials during production. All forms of scrap are suitable for gas atomization, whereas for MM+PS route scrap close to the desired particle size is preferred (granulate or powder). Gas atomization may require special atomizer design for the most reactive materials (such as titanium) and MM+PS route requires initially brittle material or material, which can be subjected to additional embrittlement treatment.
3. Can the powder prepared from the selected material waste stream be used in powder-based AM?
    - The jet milled H13 sieve residue powder has too coarse PSD and could not be used in L-PBF, but should be appealing for other PM applications, including E-PBF and directed energy deposition. The jet milled 316L sieve residue powder and the gas atomized powder prepared from 316L support structures and scrapped parts were both successfully used in L-PBF.
4. What differences are there between the prepared and commercially available powders with the same nominal chemical composition?
    - The jet milled H13 sieve residue powder consists of particles twice or more the size of the commercial powder. Otherwise the powder had comparable or enhanced properties. The jet milled 316L sieve residue powder consisted of slightly larger particles with otherwise comparable or enhanced properties. The larger particles are present in the initial sieve residue as the result of spattering during the PBF process. Gas atomization of solid 316L scrap yielded 61 % of powder with a suitable size for L-PBF, with additional 18 % of coarser powder usable in other PM applications. Other key properties of the powder were close to or enhanced compared to the commercial powder.
5. Are there differences in mechanical properties and microstructures of parts manufactured from the prepared powder, compared to commercial powder?
    - No significant difference in the porosity of the parts manufactured from the 316L commercial GA, jet milled sieve residue and GA solid scrap powders were observed. Based on the image analysis the porosities were <0.2 %.

Regardless of the powder, all parts had fully austenitic microstructure and no significant differences in hardness were observed. Parts manufactured from the GA solid scrap powder had higher Cr and Ni concentration than the commercial reference. However, in case of all three powders the chemical composition for all the elements reliably determinable by EDS analysis is inside the limits set in ASTM standard F3184-16 for 316L PBF parts. Tensile testing showed some specimen-to-specimen variations in yield strength and elongation, but there was no connection between the powder and tensile properties. All test specimens manufactured from all three powders exceeded the minimum requirements set in ASTM F3184-16 standard.

7.4 Further studies

In this thesis the environmental benefit and technical feasibility of recycling scrap via powder preparation instead of the conventional route is demonstrated. The next logical step would be a comprehensive life cycle analysis of the proposed recycling methods compared to the conventional route. This should be performed especially on the gas atomization route, as it is the most feasible of the routes proposed in this study. In this thesis the scrap materials studied were H13 tool steel and 316L, the latter being only one subjected to gas atomization. Other materials that are frequently used today in L-PBF such as titanium based alloy Ti-6Al-4V, aluminium based alloy AlSi10Mg and nickel based Inconel 625/718 could be tested, to see if these materials can also be successfully recycled back into powder for AM via gas atomization. The AM experiments on this study were done with a laser-PBF system, but also recycling new scrap for other powder based additive manufacturing technologies such as E-PBF and blown powder directed energy deposition could be tested. As these processes can work with larger particle sizes, it might be easier to produce such powders.

The chemical composition of the prepared 316L parts were analysed with EDS, which cannot be used to reliably measure light elements and small concentrations. The amount of potentially harmful trace elements (carbon, phosphorous and sulphur) in the 316L parts could be further determined with more suitable methods. This study focused on the mechanical properties of the manufactured parts, as variations in the feedstock powder has been shown to have an effect on these properties, regardless the material. In the case of

316L stainless steel the corrosion resistance of the material is just as important property and therefore the corrosion resistance of the parts manufactured from the prepared powders could be tested.

Few other topics for further studies were acknowledged during the thesis that are not directly related to the utilization of waste streams as raw material for powder based AM, but rather concerns in general the powders used in PBF:

- The effect of powder spreading mechanism on the powder bed density in PBF.
- The required flowability of a powder in PBF machines incorporating different powder storage and spreading mechanisms.
- What determines the size and quantity of the spherical particles generated as spatter during the PBF process?
- A comprehensive mapping of the effects of powder properties (particle size, shape, PSD, packing density and chemistry) on the finished part properties in PBF.

8 SUMMARY

The possibilities and potential benefits of recycling metallic waste streams produced by the manufacturing industry by preparing powder for powder bed fusion additive manufacturing were studied. The manufacturing industry is a major consumer of energy and raw materials and therefore a major producer of GHG emissions and waste. The manufacturing industry is estimated to account for 18.8 % of GHG emissions and 11 % of waste produced in the European Union. Today manufacturing of products from metals and alloys is typically accomplished by subtracting material from semi-finished bulk feedstock to achieve the desired shape. Therefore the manufacturing industry has significant side stream metallic waste consisting of machining turnings, cuttings, stampings etc. which are referred to as new scrap. The amount of new scrap generated has been estimated to be 14.6 % for steel, 13.7 % for aluminium and 55 % for titanium from the input material stream during manufacturing. Titanium is mostly used by the aerospace industry, where complex structures with low-weight but high strength are needed. As the complexity of the product increases, so does the amount of scrap generated during subtractive manufacturing.

Circular economy is a concept of preserving the value of products, materials and resources in the economy for as long as possible, thus minimizing waste generation and maximizing reuse and recycling. The primary objective in the sustainable material usage in circular economy is to prevent the formation of this new scrap. Novel manufacturing technologies with less waste generation than in the conventional subtractive manufacturing are needed. Additive manufacturing (AM) is a fundamentally different manufacturing methodology as material is added only where it is needed, instead of removed from where it is not needed. After minimizing the scrap generation with suitable manufacturing technology choices (such as additive manufacturing), the next step is efficient recycling of the unavoidable scrap that is produced in the process. Conventional open-loop recycling via re-melting and forming into semi-finished bulky feedstock is energy intensive and results in non-functional recycling and dilution losses of alloying elements. To avoid these issues, closed-loop recycling of new scrap into powder feedstock useable in powder based additive manufacturing was studied in this master’s thesis. Powders prepared from recycled scrap would also reduce the relatively high price of the powder feedstock used in AM.

In the experimental part the objective was to prepare powder from scrap to be used in powder bed fusion additive manufacturing. This requires spherical shape, proper size distribution and purity from the powder. Therefore the powder was analysed via Hall flowmeter, laser diffraction, XRD, SEM and EDS. Test specimens for tensile and hardness testing and microstructural evaluation were additively manufactured with SLM 125 HL machine. The results were compared to identical test specimens manufactured from commercially available powder. The materials, waste streams and powder preparation methods for the case study were selected based on the findings from the literature. High purity scrap produced in the powder bed fusion process in the form of support structures and agglomerated sieve residue powder were selected to be processed following two different recycling routes; gas atomization and mechanical milling coupled with further plasma spheroidization (if needed) were the studied powder preparation methods, as these can utilize scrap as feedstock. Gas atomization reduces the SEC of recycling by around 50 % for steel and even more for titanium and aluminium based materials, compared to the conventional recycling route. Plasma spheroidization can produce better quality powders, but at the moment with the penalty of higher SEC. Therefore for the sieve residue powder it was tested if only mechanical milling could be used to achieve suitable powder for PBF, as this would be the least energy intensive option as melting of the material is completely avoided.

The laboratory experiments showed that powders with comparable properties to commercially available powder can be prepared from 100 % scrap feedstock following the proposed recycling routes of gas atomizing solid scrap and jet milling agglomerated sieve residue powders. Furthermore, it was shown that parts manufactured via PBF from the powders prepared from scrap feedstock showed no inferior mechanical properties, compared to parts manufactured from commercial powder. The experiments demonstrate the technical feasibility of these recycling routes. Based on the literature findings it also seems that recycling via powder preparation uses less energy than the conventional route. Additive manufacturing also inherently generates less waste than the conventional manufacturing of today. Therefore shifting from subtractive towards additive manufacturing will enhance the sustainability of the manufacturing industry via reduced waste generation and improved recycling efficiency of the unavoidable scrap.

REFERENCES

Antony, L. V. M. & Reddy, R. G. 2003. Processes for production of high-purity metal powders. The Journal of The Minerals, Metals & Materials Society, 55: 3. P. 14–18.

Arcam AB. 2016. EBM Hardware [Arcam AB web page]. [Referred 14.7.2016]. Available: http://www.arcam.com/technology/electron-beam-melting/hardware/

Ardila, L. C., Garciandia, F., González-Díaz, J. B., Álvarez, P., Echeverria, A., Petite, M. M., Deffley, R. & Ochoa, J. 2014. Effect of IN718 recycled powder reuse on properties of parts manufactured by means of Selective Laser Melting. Physics Procedia, 56. P. 99–107.

Arens, M., Schleich, J. & Worrel, E. 2012. Energy efficiency improvements in the german steel sector – more than window dressing? European Council for an Energy-Efficient Economy (ECEEE) Summer Study on Energy Efficiency in Industry 2012. Arnhem, The Netherlands. 11-14.9.2012. Stockholm, Sweden: ECEEE. P. 101–113

ASTM F3184-16. 2016. Standard Specification for Additive Manufacturing Stainless Steel Alloy (UNS 31603) with Powder Bed Fusion. West Conshohocken, PA, USA: ASTM International. 9 p.

ASTM F3049-14. 2014. Standard Guide for Characterizing Properties of Metal Powders Used for Additive Manufacturing Processes. West Conshohocken, PA, USA: ASTM International. 3 p.

Atzeni, E. & Salmi, A. 2012. Economics of additive manufacturing for end-usable metal parts. The International Journal of Advanced Manufacturing Technology, 62: 9. P. 1147–1155.

Bauereiß, A., Scharowsky, T. & Körner, C. 2014. Defect generation and propagation mechanism during additive manufacturing by selective beam melting. Journal of Materials Processing Technology, 214: 11. P. 2522–2528.

Becker, A. F. A. 2016. Characterization and prediction of SLS processability of polymer powders with respect to powder flow and part warpage [web document]. St. Gallen: October 2015. [Referred 24.8.2016]. Doctoral Dissertation. Swiss Federal Institute of Technology in Zürich. 168 p. Available in PDF-file: http://e-collection.library.ethz.ch/eserv/eth:49138/eth-49138-02.pdf

Benson, J. M. & Snyders, E. 2015. The Need for Powder Characterisation in the Additive Manufacturing Industry and the Establishment of a National Facility. South African Journal of Industrial Engineering, 26: 2. P. 104–114.

Boley, C. D., Khairallah, S. A. & Rubenchik, A. M. 2015. Calculation of laser absorption by metal powders in additive manufacturing. Applied Optics, 54: 9. P. 2477–2482.

Boulos, M. 2016. The Role of Transport Phenomena and Modeling in the Development of Thermal Plasma Technology. Plasma Chemistry and Plasma Processing, 36: 1. P. 3–28.

Budding, A. & Vaneker, T. H. J. 2013. New strategies for powder compaction in powder-based rapid prototyping techniques. Proceedings of the 17th CIRP Conference on Electro Physical and Chemical Machining, 6. P. 527–532.

Caffrey, T., Wohlers, T. & Campbell, I. 2016. Wohlers Report 2016 – 3D Printing and Additive Manufacturing State of the Industry – Annual Worldwide Progress Report. Fort Collins, Colorado, USA: Wohlers Associates. 335 p.

Casati, R., Lemke, J. & Vedani, M. 2016. Microstructure and Fracture Behavior of 316L Austenitic Stainless Steel Produced by Selective Laser Melting. Journal of Materials Science & Technology, 32. P. 738–744.

Cherry, J. A., Davies, H. M., Mehmood, S., Lavery, N. P., Brown, S. G. R. & Sienz, J. 2015. Investigation into the effect of process parameters on microstructural and physical properties of 316L stainless steel parts by selective laser melting. The International Journal of Advanced Manufacturing Technology, 76: 5. P. 869–879.

Cheruvathur, S., Lass, E. A. & Campbell, C. E. 2016. Additive Manufacturing of 17-4 PH Stainless Steel: Post-processing Heat Treatment to Achieve Uniform Reproducible Microstructure. The Journal of the Minerals, Metals & Materials Society, 68: 3. P. 930–942.

Clayton, J., Millington-Smith, D. & Armstrong, B. 2015. The Application of Powder Rheology in Additive Manufacturing. The Journal of The Minerals, Metals & Materials Society, 67: 3. P. 554–548.

Cleary, P. W. & Sawley, M. L. 2002. DEM modelling of industrial granular flows: 3D case studies and the effect of particle shape on hopper discharge. Applied Mathematical Modelling, 26: 2. P. 89–111.

Cloots, M., Spierings, A. B. & Wegener, K. 2013. Assessing new support minimizing strategies for the additive manufacturing technology SLM. Proceedings of the 24th Annual International Solid Freeform Fabrication Symposium. Austin, Texas, USA. 12-14.8.2013. P. 631–643. Available in PDF-file: http://sffsymposium.engr.utexas.edu/Manuscripts/2013/2013-50-Cloots.pdf

Commission of the European Communities. 2008. on the Sustainable Consumption and Production and Sustainable Industry Policy Action Plan. COM(2008) 397 final [web document]. Bryssels: July 2008. [Referred 4.8.2016]. Communication from the Commission to the European Parliament, the Counsil, the European Economic and Social Committee and the Committee of the Regions. 12 p. Available in PDF-file: http://eur-lex.europa.eu/legal-content/EN/TXT/PDF/?uri=CELEX:52008DC0397&from=EN

Cullen, J. M., Allwood, J. M. & Bambach, M. D. 2012. Mapping the Global Flow of Steel: From Steelmaking to End-Use Goods. Environmental Science & Technology, 46: 24. P. 13048–13055.

Cullen, J. M. & Allwood, J. M. 2013. Mapping the Global Flow of Aluminium: From Liquid Aluminium to End-Use Goods. Environmental Science & Technology, 47: 7. P. 3057–3064.

Dawes, J., Bowerman, R. & Trepleton, R. 2015. Introduction to the Additive Manufacturing Powder Metallurgy Supply Chain. Johnson Matthey Technology Review, 59: 3. P. 243–256.

Denkena, B., Dittrich, M-A. & Jacob, S. 2016. Energy Efficiency in Machining of Aircraft Components. Procedia CIRP, 48. P. 479–482.

Dietmar, A. 2012. Energy Saving Processes for Dry & Wet Micronisation of Ultrafine Fillers. Industrial Minerals International Congress and Exhibition. Budapest, Hungary. 26-29.3.2012. Presentation available: http://www.indmin.com/events/download.ashx/document/speaker/6517/a0ID000000X0jNLMAZ/Presentation

Dubreuil, A., Young, S. B., Atherton, J. & Gloria, T. P. 2010. Metals recycling maps and allocation procedures in life cycle assessment. The International Journal of Life Cycle Assessment, 15: 6. P. 621–634.

EOS. 2013. EOS-Dental Crowns and Bridges, Dental Models and Removable Partial Dentures (RPD) Alter the Dental Industry [online article]. Additive Manufacturing 12.3.2013. [Referred 15.7.2016]. Available: http://additivemanufacturing.com/2013/03/12/eos-laser-sintering-is-replacing-traditional-processes-in-dental-industry/

European Commission. 2015. Closing the loop – An EU Action plan for the Circular Economy. COM(2015) 614 final [web document]. Bryssels: December 2015. [Referred 4.8.2016]. Communication from the Commission to the European Parliament, the Counsil, the European Economic and Social Committee and the Committee of the Regions. 21 p. Available in PDF-file: http://eur-lex.europa.eu/resource.html?uri=cellar:8a8ef5e8-99a0-11e5-b3b7-01aa75ed71a1.0012.02/DOC_1&format=PDF

Eurostat. 2015. Waste statistics [Eurostat web page]. Last updated September, 2015. Planned update November 2016. [Referred 10.8.2016]. Available: http://ec.europa.eu/eurostat/statistics-explained/index.php/Waste_statistics

Eurostat. 2016. Greenhouse gas emissions by industries and households [Eurostat web page]. Last updated 11.4.2016. Planned update February 2017. [Referred 10.8.2016]. Available: http://ec.europa.eu/eurostat/statistics-explained/index.php/Greenhouse_gas_emissions_by_industries_and_households

Ford, S. & Despeisse, M. 2016. Additive manufacturing and sustainability: an exploratory study of the advantages and challenges. Journal of Cleaner Production, 137. P. 1573–1587.

Frazier, W. E. 2014. Metal Additive Manufacturing: A Review. Journal of Materials Engineering and Performance, 23: 6. P. 1917–1928.

Froes, F. H. 2012. Titanium powder metallurgy: A review – Part 1. Advanced Materials and Processes, 170: 9. P. 16–22.

Gao, W., Zhang, Y., Ramanujan, D., Ramani, K., Chen, Y., Williams, C. B., Wang, C. C. L., Shin, Y. C., Zhang, S. & Zavattieri, P. D. 2015. The status, challenges and future of additive manufacturing in engineering. Computer-Aided Design, 69. P. 65–89.

German, R. M. 1989. Particle packing characteristics. Princeton, New Jersey: Metal Powder Industries Federation. 443 p.

Gibson, I., Rosen, D. W. & Stucker, B. 2015. Additive Manufacturing Technologies – 3D Printing, Rapid Prototyping, and Direct Digital Manufacturing. New York: Springer. 498 p.

Goonan, T. G. 2010. [Chapter Y:] Titanium recycling in the United States in 2004. In book: Sibley, S. F. (Editor). Flow studies for recycling metal commodities in the United States. Virginia: U.S. Geological Survey Circular. 1196 p.

Graedel, T. E., Allwood, J., Birat, J-P., Buchert, M., Hagelüken, C., Reck, B. K., Sibley, S. F. & Sonnemann, G. 2011. Recycling Rates of Metals – A Status Report [web document]. Paris: May 2011. [Referred 2.8.2016]. A Report of the Working Group on the Global Metal Flows to the International Resource Panel. United Nations Environment Programme

(UNEP). 44 p. Available in PDF-file: http://www.unep.org/resourcepanel/Portals/24102/PDFs/Metals_Recycling_Rates_110412-1.pdf

Grimes, S., Donaldson, J. & Gomez, G. C. 2008. Report on the Environmental Benefits of Recycling. Brussels: Bureau of International Recycling (BIR). 48 p.

Gu, H., Gong, H., Dilip, J. J. S., Pal, D., Hicks, A., Doak, H. & Stucker, B. 2014. Effects of Powder Variation on the Microstructure and Tensile Strength of Ti6Al4V Parts Fabricated by Selective Laser Melting. Proceedings of the 25th Annual International Solid Freeform Fabrication Symposium. Austin, Texas, USA. 4-6.8.2014. P. 470–483. Available in PDF-file: http://sffsymposium.engr.utexas.edu/sites/default/files/2014-040-Gu.pdf

Gürtler, F-J., Karg, M., Dobler, M., Kohl, S., Tzivilsky, I. & Schmidt, M. 2014. Influence of powder distribution on process stability in laser beam melting: Analysis of melt pool dynamics by numerical simulations. Proceedings of the 25th Annual International Solid Freeform Fabrication Symposium. Austin, Texas, USA. 4-6.8.2014. P. 1099–1117. Available in PDF-file: http://sffsymposium.engr.utexas.edu/sites/default/files/2014-087-Guertler.pdf

Han, C., Na, H., Choi, H. & Kim, Y. 2015. High Purity Tungsten Spherical Particle Preparation From WC-Co Spent Hard Scrap. Archives of Metallurgy and Materials, 60: 2. P. 1507–1509.

Heidloff, A. J., Rieken, J. R., Anderson, I. E., Byrd, D., Sears, J., Glynn, M. & Ward, R. M. 2010. Advanced gas atomization processing for Ti and Ti alloy powder manufacturing. The Journal of The Minerals, Metals & Materials Society, 62: 5. P. 35–41.

Horiba. 2016. A Guidebook to particle size analysis [web document]. [Referred 11.8.2016]. 29 p. Available in PDF-file: https://www.horiba.com/fileadmin/uploads/Scientific/eMag/PSA/Guidebook/pdf/PSA_Guidebook.pdf

Hosokawa Micron Powder Systems. 2016. Alpine AFG fluidized bed opposed jet mill [Hosokawa Micron Powder Systems web page]. [Referred 26.9.2016]. Available: http://www.hmicronpowder.com/products/product/alpine-afg-fluidized-bed-jet-mill

Huang, R., Riddle, M., Graziano, D., Warren, J., Das, S., Nimbalkar, S., Cresko, J. & Masanet, E. 2016. Energy and emissions saving potential of additive manufacturing: the case of lightweight aircraft components. Journal of Cleaner Production, 135. P. 1559–1570.

Höganäs. 2013. Material and powder properties [web document]. Sweden: December 2013 [Referred 11.8.2016]. Höganäs Handbook for sintered Components. Höganäs AB. 112 p. Available in PDF-file: https://www.hoganas.com/globalassets/media/sharepoint-documents/HandbooksAllDocuments/Handbook1Material_and_Powder_Properties_December_2013_0674HOGinteractive.pdf

Irrinki, H., Dexter, M., Barmore, B., Enneti, R., Pasebani, S., Badwe, S., Stitzel, J., Malhotra, R. & Atre, S. 2016. Effects of Powder Attributes and Laser Powder Bed Fusion (L-PBF) Process Conditions on the Densification and Mechanical Properties of 17-4 PH Stainless Steel. The Journal of The Minerals, Metals & Materials Society, 68: 3. P. 860–868.

Jankovic, A. 2003. Variables affecting the fine grinding of minerals using stirred mills. Minerals Engineering, 16. P. 337–354.

Johnson, J., Reck, B. K., Wang, T. & Graedel, T. E. 2008. The energy benefit of stainless steel recycling. Energy Policy, 36: 1. P. 181–192.

Juechter, V., Scharowsky, T., Singer, R. F. & Körner, C. 2014. Processing window and evaporation phenomena for Ti-6Al-4V produced by selective electron beam melting. Acta Materialia, 76. P. 252–258.

Karnati, S., Axelsen, I., Liou, F. F. & Newkirk, J. W. 2016. Investigation of tensile properties of bulk and SLM fabricated 304L stainless steel using various gage length

specimens. Proceedings of the 27th Annual International Solid Freeform Fabrication Symposium. Austin, Texas, USA. 8-10.8.2016. P. 592–604. Available in PDF-file: http://sffsymposium.engr.utexas.edu/sites/default/files/2016/045-Karnati.pdf

Kleis, I. & Kulu, P. 2008. Solid Particle Erosion – Occurrence, Prediction and Control. London: Springer. 206 p.

Kobryn, P. A., Ontko, N. R., Perkins, L. P. & Tiley, J. S. 2006. Additive manufacturing of Aerospace Alloys for Aircraft Structures. Meeting proceedings of Cost Effective Manufacture via Net-Shape Processing. Neuilly-sur-Seine, France. RTO-MP-AVT-139, paper 3. P. 3-1–3-14.

Krantz, M., Zhang, H. & Zhu, J. 2009. Characterization of powder flow: Static and dynamic testing. Powder Technology, 194: 3. P. 239–245.

Kruzhanov, V. & Arnhold, V. 2012. Energy consumption in powder metallurgical manufacturing. Powder Metallurgy, 55: 1. P. 14–21.

Kulu, P., Mikli, V., Käerdi, H. & Besterci, M. 2003. Characterization of disintegrator milled hardmetal powder. Powder Metallurgy Progress, 3: 1. P. 39–48.

Lindemann, C., Jahnke, U., Moi, M. & Koch, R. 2012. Analyzing Product Lifecycle Costs for a Better Understanding of Cost Drivers in Additive Manufacturing. Proceedings of the 23th Annual International Solid Freeform Fabrication Symposium. Austin, Texas, USA. 6-8.8.2012. P. 177–188. Available in PDF-file: http://sffsymposium.engr.utexas.edu/Manuscripts/2012/2012-12-Lindemann.pdf

Liu, B., Wildman, R., Tuck, C., Ashcroft, I & Hague, R. 2011. Investigation the effect of particle size distribution on processing parameters optimisation in selective laser melting process. Proceedings of the 22th Annual International Solid Freeform Fabrication Symposium. Austin, Texas, USA. 8-10.8.2011. P. 227–238. Available in PDF-file: http://sffsymposium.engr.utexas.edu/Manuscripts/2011/2011-18-Liu.pdf

LPW Technology. 2016a. Methods of Powder Production [LPW Technology web page]. [Referred 16.6.2016]. Available: http://www.lpwtechnology.com/technical-library/technical-information/methods-of-powder-production/

LPW Technology. 2016b. Plasma spheroidization [LPW Technology web page]. [Referred 29.6.2016]. Available: http://www.lpwtechnology.com/technical-library/plasma-spheroidisation/

Lütjering, G. & Williams, J. C. 2007. Titanium. Berlin: Springer. 442 p.

Maol. 2005. Maol-taulukot. Keuruu: Otavan Kirjapaino Oy. 167 p. In Finnish

McCracken, C., Motchenbacher, C. & Deeter, R. 2012. Plasma Spheroidized (PS) Titanium Powders. Proceedings of the TITANIUM 2012 Conference. Atlanta, Georgia, USA. 7-10.10.2012. Presentation available: http://c.ymcdn.com/sites/www.titanium.org/resource/resmgr/2010_2014_papers/McCrackenColin_2012.pdf

McWilliams, A. (Editor). 2016. Powder Metallurgy: Technologies and Global Markets. Wellesley: BCC Reseach. 138 p.

Morrow, W. R., Qi, H., Kim, I., Mazumder, J. & Skerlos, S. J. 2007. Environmental aspects of laser-based and conventional tool and die manufacturing. Journal of Cleaner Production, 15: 10. P. 932–943.

Nakamura, S., Kondo, Y., Matsubae, K., Nakajima K., Tasaki, T. & Nagasaka, T. 2012. Quality- and Dilution Losses in the Recycling of Ferrous Materials from End-of-Life Passenger Cars: Input-Output Analysis under Explicit Considerations of Scrap Quality. Environmetal Science & Technology, 46: 17. P. 9266–9273.

Nandwana, P., Peter, W. H., Dehoff, R. R., Lowe, L. E., Kirka, M. M., Medina, F. & Babu S. S. 2016. Recyclability Study on Inconel 718 and Ti-6Al-4V Powders for Use in Electron Beam Melting. Metallurgical and Materials Transactions B, 47: 1. P. 754–762.

Norgate, T. E., Jahanshahi, S. & Rankin, W. J. 2007. Assessing the environmental impact of metal production processes. Journal of Cleaner Production, 15: 8–9. P. 838–848.

Outokumpu. 2015. Sustainability report [web document]. [Referred 8.12.2016]. 75 p. Available in PDF-file: https://www.outokumpu.com/SiteCollectionDocuments/Outokumpu_Sustainability_report_2015.pdf

Piili, H., Happonen, A., Väistö, T., Venkataramanan, V., Partanen, J. & Salminen, A. 2015. Cost Estimation of Laser Additive Manufacturing of Stainless Steel. Physics Procedia, 78. P. 388–396.

Reck, B. K. & Graedel, T. E. 2012. Challenges in Metal Recycling. Science, 337: 6095. P. 690–695.

Reijnders, L., 2016. Conserving functionality of relatively rare metals associated with steel life cycles: a review. Journal of Cleaner Production, 131. P. 76–96.

Renvall, J. 2014. Performance of Additive Manufacturing in the Process Industry, Mechanical Seal as a Target Application [web document]. Vantaa: November 2014. [Referred 13.9.2016] Master's Thesis. Aalto University, School of Engineering. 78 p. Available in PDF-file [in Finnish]: https://aaltodoc.aalto.fi/bitstream/handle/123456789/14551/master_Renvall_Jani_2014.pdf?sequence=1&isAllowed=y

Reuter, M., Hudson, C., van Schaik, A., Heiskanen, K., Meskers, S. & Hagelüken, C. 2013. Metal recycling – Opportunities, Limits, Infrastructure [web document]. Paris: April 2013. [Referred 2.8.2016]. A Report of the Working Group on the Global Metal Flows to the International Resource Panel. United Nations Environment Programme (UNEP). 316 p. Available in PDF-file: http://www.unep.org/resourcepanel/Portals/24102/PDFs/Metal_Recycling_Full_Report.pdf

Rotmann, B., Lochbichler, C. & Friedrich, B. 2011. Challenges in Titanium Recycling – Do We Need a New Specification for Secondary Alloys? Proceedings of the European

Metallurgical Conference 2011. Düsseldorf, Gemany. 26-29.6.2011. Clausthal-Zellerfeld, Germany: GDMB. P. 1465–1480.

Sames, W. J., List, F. A., Pannala, S., Dehoff, R. R. & Babu, S. S. 2016. The metallurgy and processing science of metal additive manufacturing. International Materials Reviews, 61: 5. P. 315–360.

SFS-EN ISO 3923-1. 2008. Metallic powders. Determination of apparent density. Part 1: Funnel method. Helsinki: Finnish Standards Association SFS. 5 p.

SFS-EN ISO 3953. 2011. Metallic powders. Determination of tap density. Helsinki: Finnish Standards Association SFS. 4 p.

SFS-EN ISO 4490. 2014. Metallic powders. Determination of flow rate by means of a calibrated funnel (Hall flowmeter). Helsinki: Finnish Standards Association SFS. 4 p.

SFS-ISO/ASTM 52900. 2016. Additive manufacturing. General principles. Terminology. Helsinki: Finnish Standards Association SFS. 22 p.

SFS-EN ISO 6507-1. 2005. Metallic materials. Vickers hardness test. Part 1: Test method. Helsinki: Finnish Standards Association SFS. 19 p.

SFS-EN ISO 6892-1. 2016. Metallic materials. Tensile testing. Part 1: Method of test at room temperature. Helsinki: Finnish Standards Association SFS. 83 p.

Shi, Y. & Zhang, Y. 2008. Simulation of random packing of spherical particles with different size distributions. Applied Physics A, 92. P. 621–626.

Simonelli, M., Tuck, C., Aboulkhair, N. T., Maskery, I., Ashcroft, I., Wildman, R. D. & Hague, R. 2015. A Study on the Laser Spatter and the Oxidation Reactions During Selective Laser Melting of 316L Stainless Steel, Al-Si10-Mg, and Ti-6Al-4V. Metallurgical and Materials Transactions A, 46: 9. P. 3842–3851.

SJM Alloys & Metals Limited. 2014. Alloys [SJM Alloys & Metals Limited web page]. [Referred 2.8.2016]. Available: http://www.sjmalloysandmetals.com/alloys/

SLM Solutions. 2016. SLM®125HL [SLM Solutions web page]. [Referred 11.11.2016]. Available: https://slm-solutions.com/products/machines/slmr125hl

Slotwinski, J. A. & Garboczi, E. J. 2015. Metrology Needs for Metal Additive Manufacturing Powders. The Journal of The Minerals, Metals & Materials Society, 67: 3. P. 538–543.

Slotwinski, J. A., Garboczi, E. J., Stutzman, P. E., Ferraris, C. F., Watson, S. S., Peltz, M. A. 2014. Characterization of Metal Powders Used for Additive Manufacturing. Journal of Research of the National Institute of Standards and Technology, 119. P. 460–493.

Spierings, A. B., Herres, N. & Levy, G. 2010. Influence of the particle size distribution on surface quality and mechanical properties in additive manufactured stainless steel parts. Proceedings of the 21st Annual International Solid Freeform Fabrication Symposium. Austin, Texas, USA. 9-11.8.2010. P. 397–406. Available in PDF-file: http://sffsymposium.engr.utexas.edu/Manuscripts/2010/2010-33-Spierings.pdf

Spierings, A. B. & Levy, G. 2009. Comparison of density of stainless steel 316L parts produced with selective laser melting using different powder grades. Proceedings of the 20th Annual International Solid Freeform Fabrication Symposium. Austin, Texas, USA. 3-5.8.2009. P. 342–353. Available in PDF-file: http://sffsymposium.engr.utexas.edu/ Manuscripts/2009/2009-30-Spierings.pdf

Spierings, A. B., Voegtlin, M., Bauer, T. & Wegener, K. 2016. Powder flowability characterisation methodology for powder-bed-based metal additive manufacturing. Progress in Additive Manufacturing, 1: 1. P. 9–20.

Stacey, M. 2015. Aluminium Recyclability and Recycling – Towards Sustainable Cities. Cwningen Press. 281 p.

Starr, T. L., Rafi, K., Stucker, B. & Scherzer, M. C. 2012. Controlling phase composition in selective laser melted stainless steel. Proceedings of the 23th Annual International Solid Freeform Fabrication Symposium. Austin, Texas, USA. 6-8.8.2012. P. 439–446. Available in PDF-file: http://sffsymposium.engr.utexas.edu/Manuscripts/2012/2012-33-Starr.pdf

Strondl, A., Lyckfeldt, O., Brodin, H., Ackelid, U. 2015. Characterization and Control of Powder Properties for Additive Manufacturing. The Journal of The Minerals, Metals & Materials Society, 67: 3. P. 549–554.

Sun, P., Fang, Z. Z., Xia, Y., Zhang, Y. & Zhou, C. 2016. A novel method for production of spherical Ti-6Al-4V powder for additive manufacturing. Powder Technology, 301. P. 331–335.

Suryanarayana, C. 2001. Mechanical alloying and milling. Progress in Materials Science, 46. P. 1–184.

Tammas-Williams, S., Zhao, H., Léonard, F., Derguti, F., Todd, I. & Prangnell, P. B. 2015. XCT analysis of the influence of melt strategies on defect population in Ti-6Al-4V components manufactured by Selective Electron Beam Melting. Materials Characterization, 102. P. 47–61

Tan, X., Sun, Z., Tor, S. B. & Yeong, W. Y. 2016. Selective laser melting of stainless steel 316L with low porosity and high build rates. Materials & Design, 104. P. 197–204.

Tang, H. P., Qian, M., Liu, N., Zhang, X. Z., Yang, G. Y. & Wang, J. 2015. Effect of Powder Reuse Times on Additive Manufacturing of Ti-6Al-4V by Selective Electron Beam Melting. The Journal of The Minerals, Metals & Materials Society, 67: 3. P. 555–563.

The Bermet Company. 2016. Scrap Metal Recycling Solutions. Metals [The Bermet Company web page]. [Referred 2.8.2016]. Available: http://bermetco.com/metals/

The Economist. 2012. The third industrial revolution [online article]. The Economist 21.4.2012. [Referred 15.7.2016]. Available: http://www.economist.com/node/21553017

Thomas, D. S. & Gilbert, S. W. 2014. Cost and Cost-effectiveness of Additive Manufacturing – A Literature Review and Discussion [web document]. Gaithersburg: December 2014. [Referred 10.8.2016]. NIST Special Publication 1176. National Institute of Standards and Technology, U. S. Department of Commerce. 77 p. Available in PDF-file: http://nvlpubs.nist.gov/nistpubs/SpecialPublications/NIST.SP.1176.pdf

Thompson, S. M., Bian, L., Shamsaei, N. & Yadollahi, A. 2015. An overview of Direct Laser Deposition for additive manufacturing; Part I: Transport phenomena, modelling and diagnostics. Additive Manufacturing, 8. P. 36–62.

United States Environmental Protection Agency. 2016. Sustainable Manufacturing. [United States Environmental Protection Agency web page]. Last updated 21.2.2016. [Referred 1.8.2016]. Available: https://archive.epa.gov/sustainablemanufacturing/web/html/

Vilaro, T., Colin, C. & Bartout, J. D. 2011. As-Fabricated and Heat-Treated Microstructures of the Ti-6Al-4V Alloy Processed by Selective Laser Melting. Metallurgical and Materials Transactions A, 42: 10. P. 3190–3199.

Vlachos, N. & Chang, I. T. H. 2011. Investigation of flow properties of metal powders from narrow size distribution to polydisperse mixtures through an improved Hall-flowmeter. Powder Technology, 205: 1–3. P. 71–80.

VTT. 2015. Mineral Economy [VTT web page]. [Referred 15.9.2016]. Available: http://www.vttresearch.com/impact/new-innovations-are-here/innovation-programmes/mineral-economy

Williams, N. (Editor). 2012. Arcast Inc. offers new atomisation system for refractory and reactive metal powders. Powder Injection Moulding International, 6: 1. P. 18–19.

Wilson, B. P., Lavery, N. P., Jarvis, D. J., Anttila, T., Rantanen, J., Brown, S. G. R. & Adkins, N. J. 2013. Life cycle assessment of gas atomized sponge nickel for use in alkaline hydrogen fuel cell applications. Journal of Power Sources, 243. P. 242–252.

World Steel Association. 2016a. Life cycle assessment (LCA) [World Steel Association web page]. [Referred 1.8.2016]. Available: http://www.worldsteel.org/publications/position-papers/lca.html

World Steel Association. 2016b. About Steel [World Steel Association web page]. [Referred 1.8.2016]. Available: https://www.worldsteel.org/faq/about-steel.html

Yang, S., Gwak, J-N., Tae-Soo, L., Yong-Jin, K., Jung-Yeul, Y. 2013. Preparation of Spherical Titanium Powders from Polygonal Titanium Hydride Powders by Radio Frequency Plasma Treatment. Materials Transactions. Volume 54. Issue 12. P. 2313–2316.

Zaleski, A. 2015. GE's bestselling jet engine makes 3-D printing a core component [online article]. Fortune 5.3.2015. [Referred 2.11.2016]. Available: http://fortune.com/2015/03/05/ge-engine-3d-printing/

Zheng, B. & Lavernia, E. J. 2011. [Chapter 36:] Melt atomization. In book: Ashgriz, N. (Editor). Handbook of Atomization and Sprays – Theory and Applications. New York: Springer. 935 p.

Zou, R. P., Gan, M. L. & Yu, A. B. 2011. Prediction of the porosity of multi-component mixtures of cohesive and non-cohesive particles. Chemical Engineering Science, 66: 20. P. 4711–4721.

EDS spectrums of studied materials.

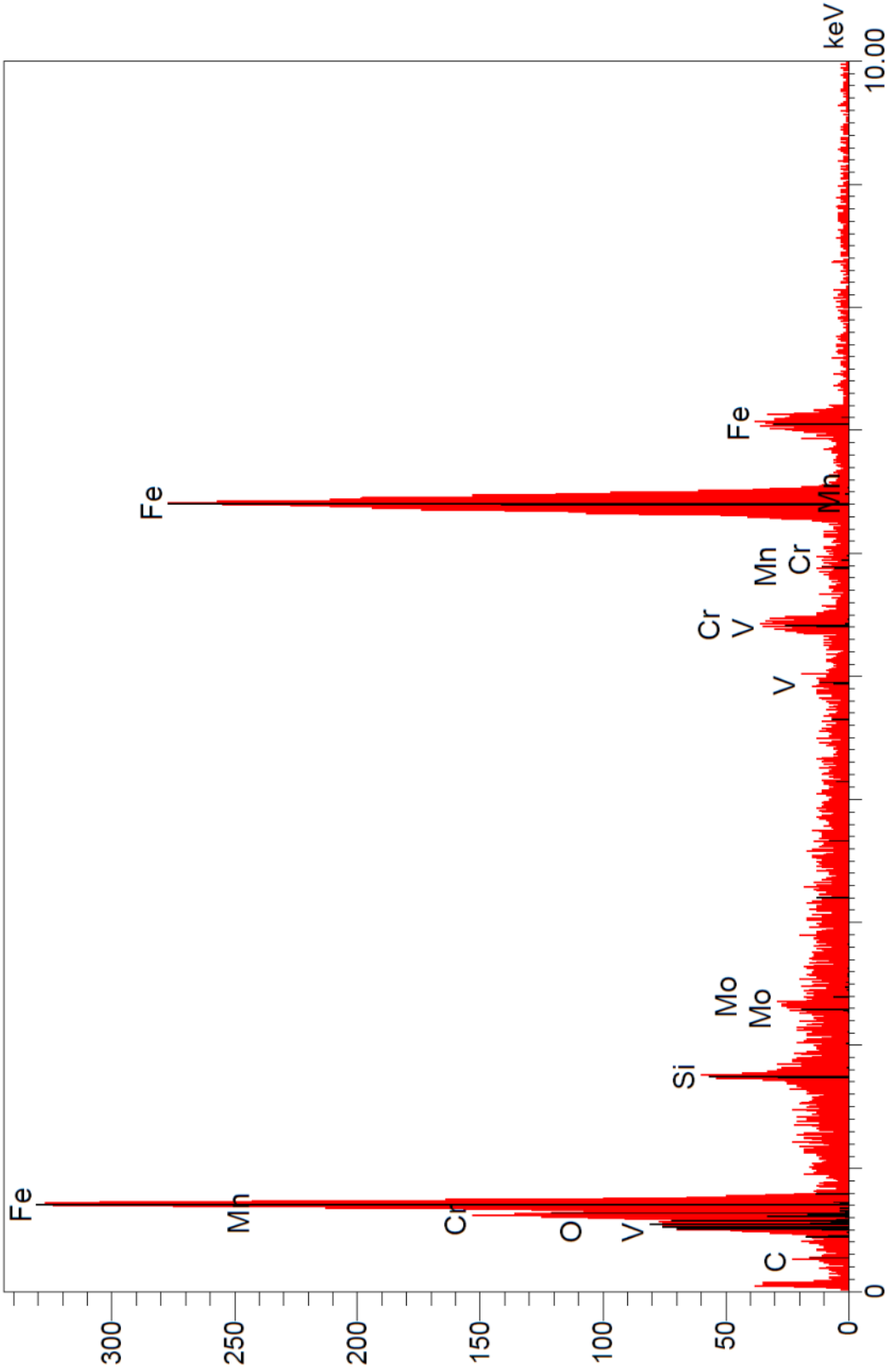

Figure I-1. EDS spectrum of H13 scrap.

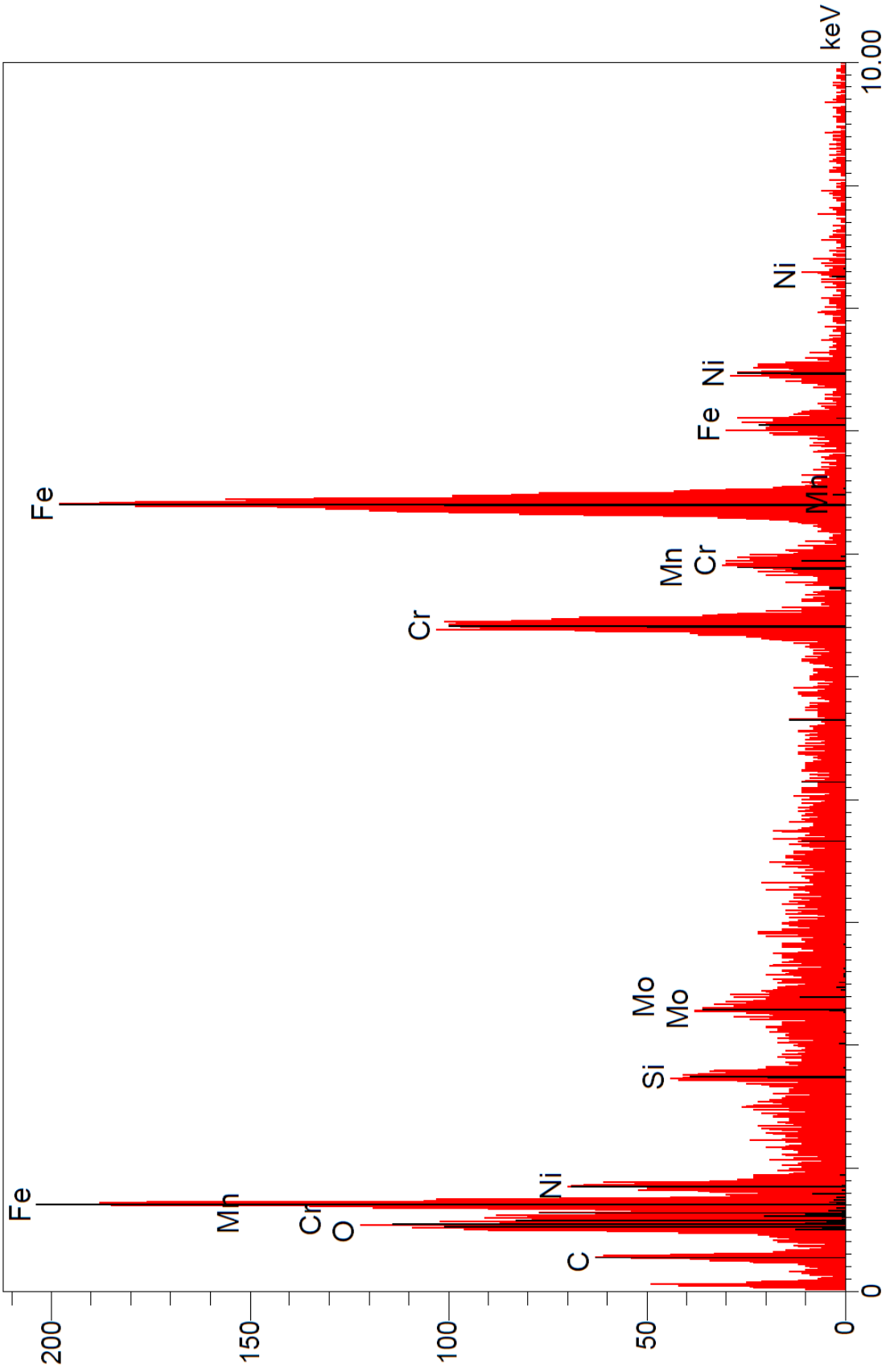

Figure I-2. EDS spectrum of 316L scrap.

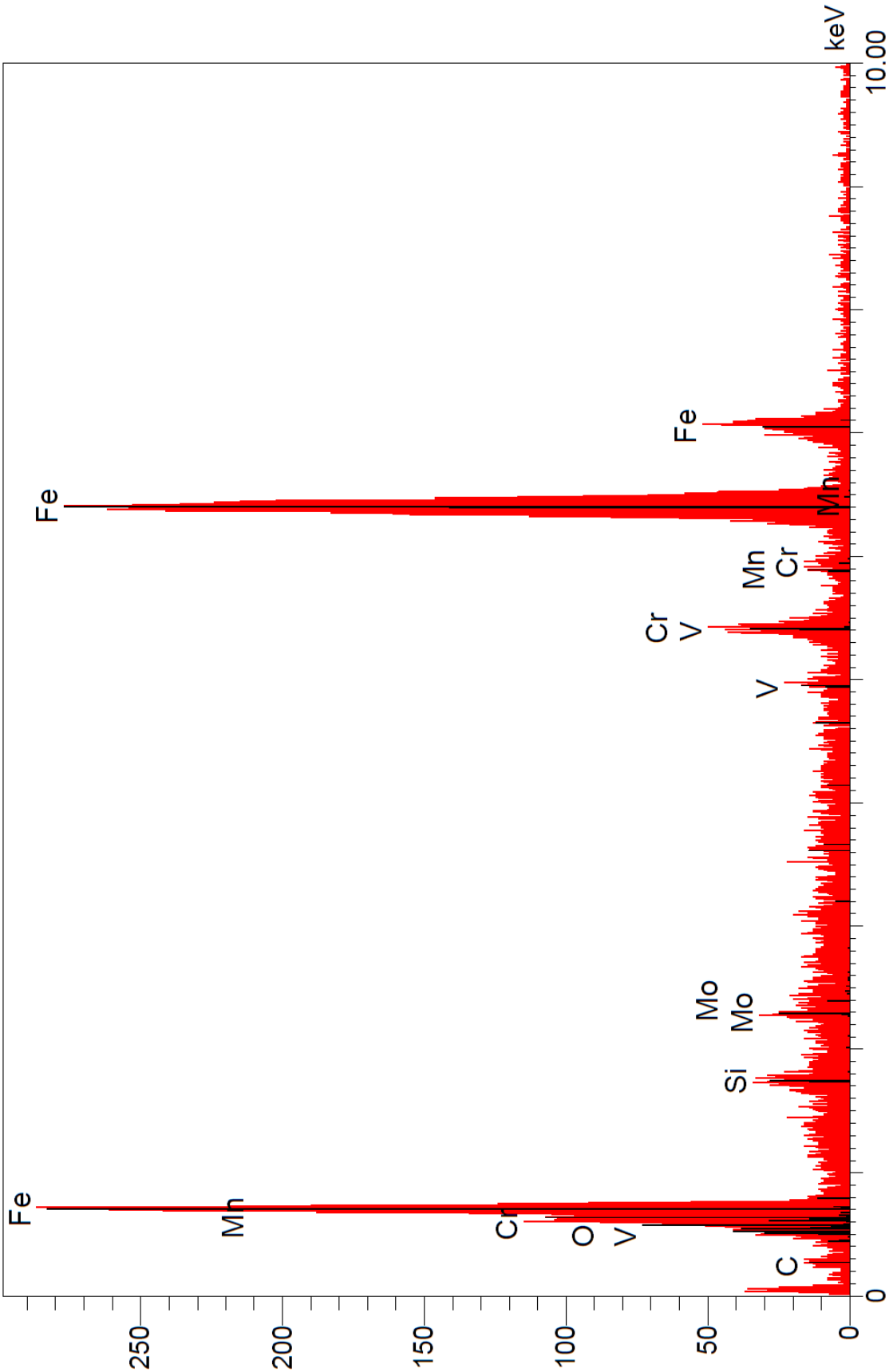

Figure I-3. EDS spectrum of commercial gas atomized H13 powder.

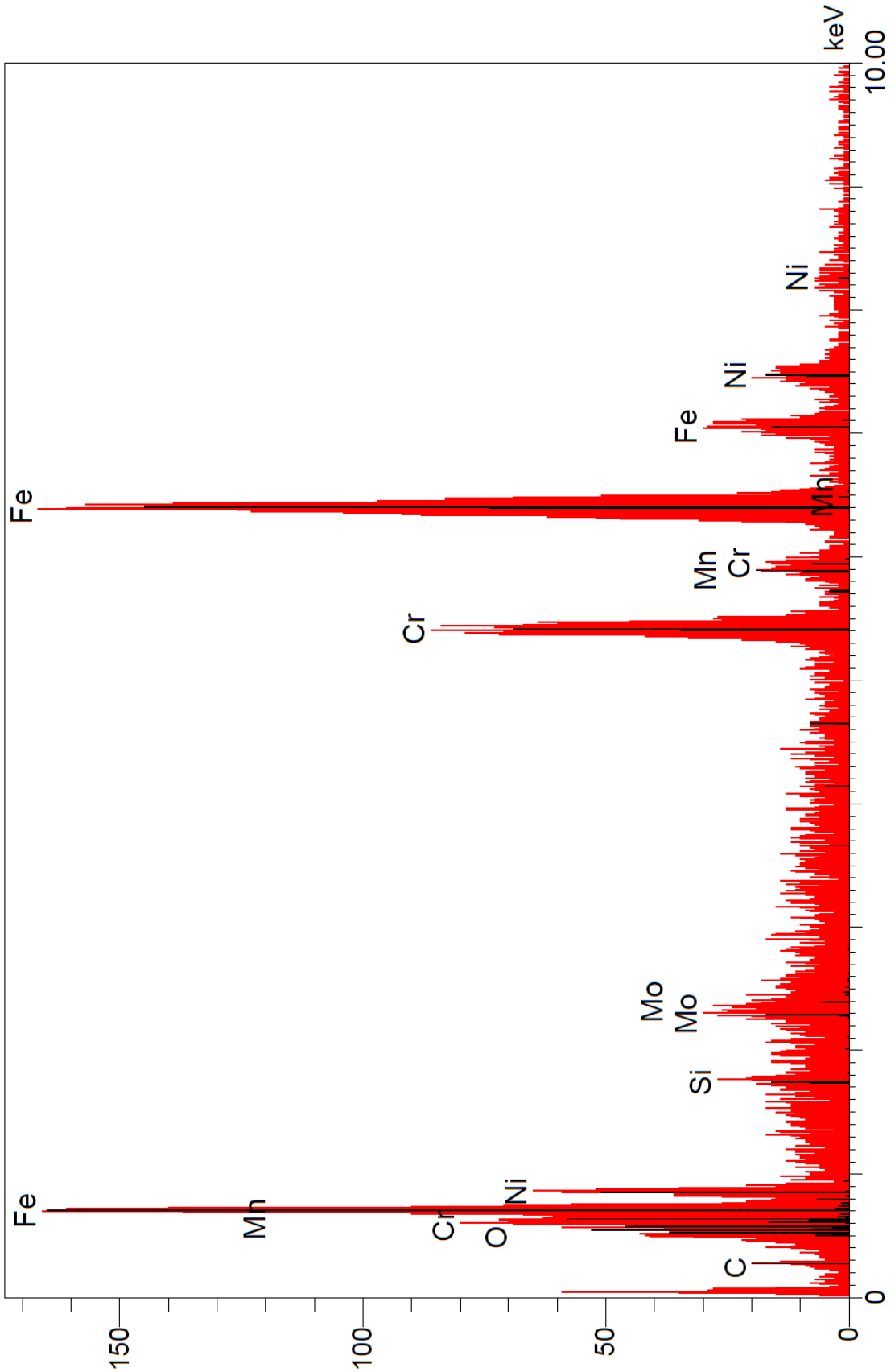

Figure I-4. EDS spectrum of commercial gas atomized 316L powder.

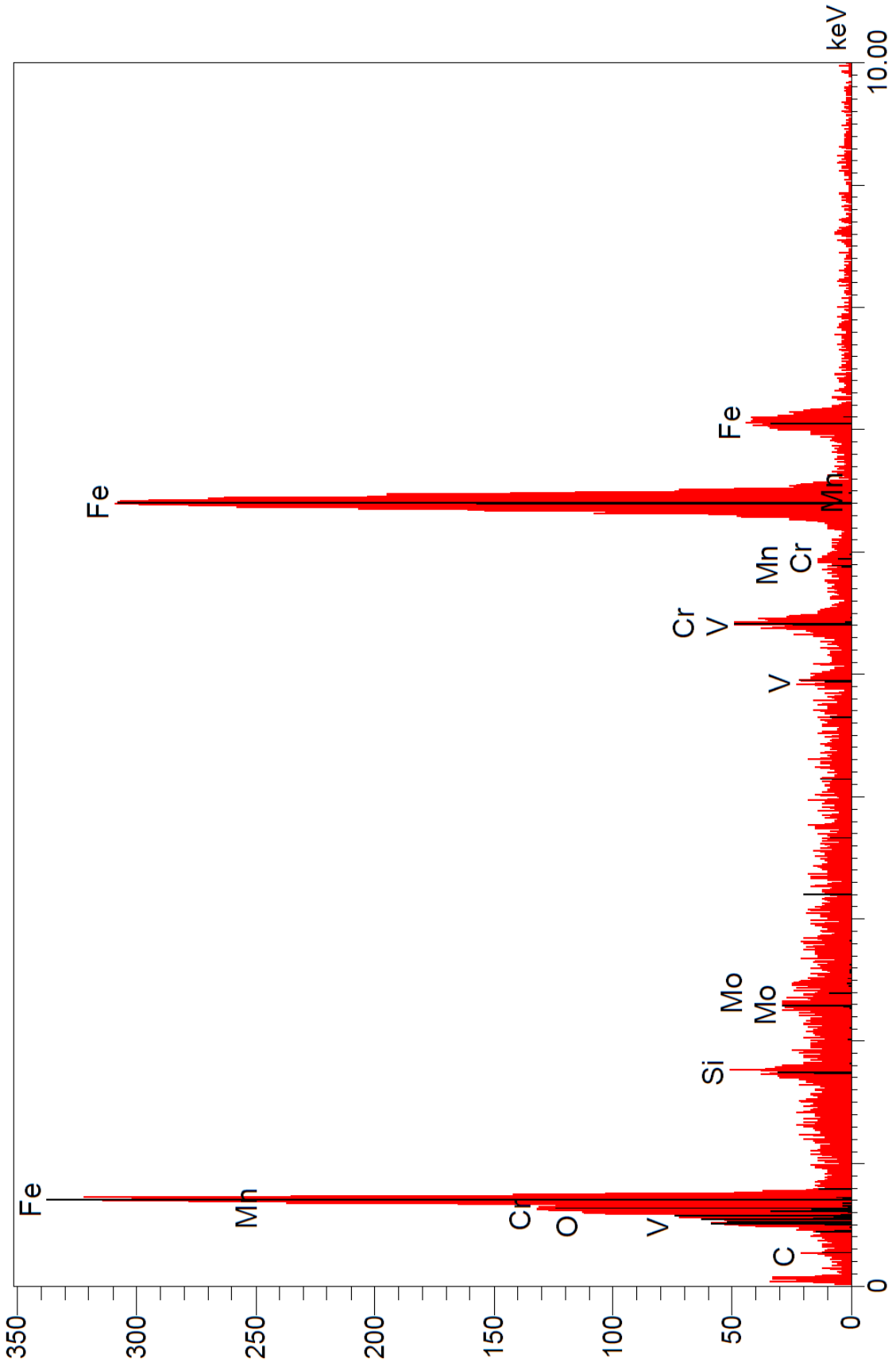

Figure I-5. EDS spectrum of jet milled H13 sieve residue powder.

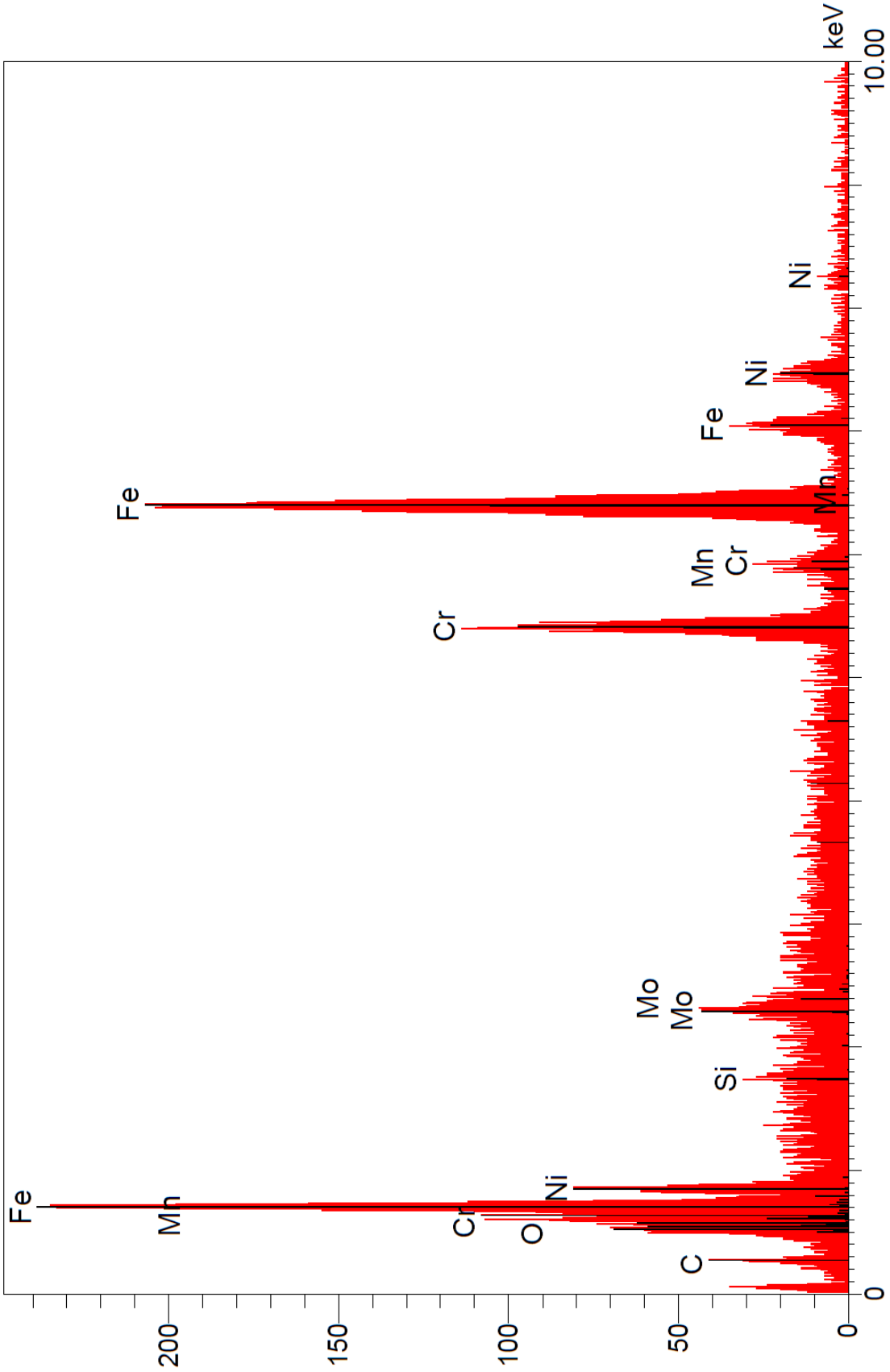

Figure I-6. EDS spectrum of jet milled 316L sieve residue powder.

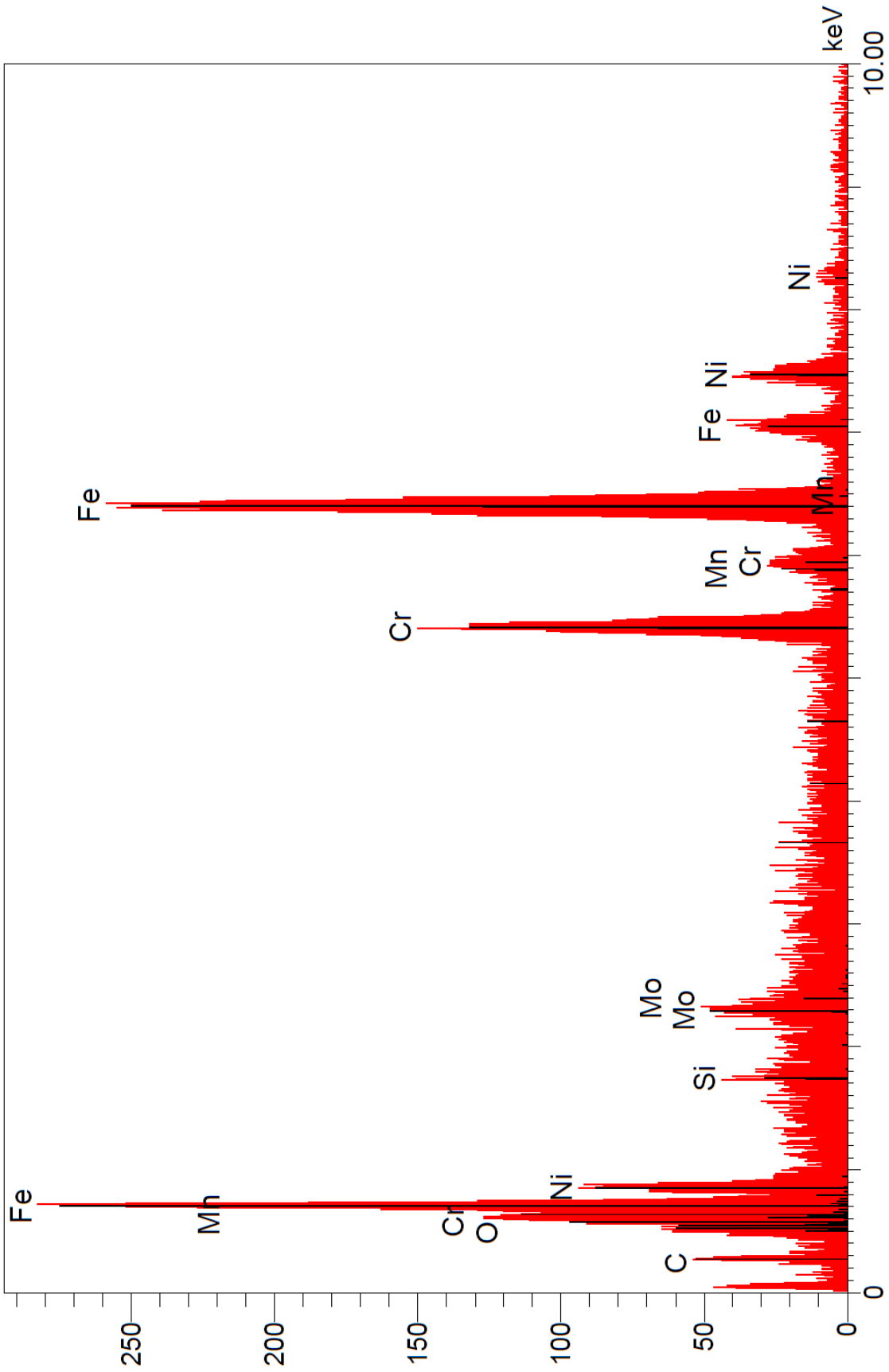

Figure I-7. EDS spectrum of 316L gas atomized powder prepared from solid scrap.

Appendix II

Results from all the ball milling tests.

Table I-1. Results from all the ball milling tests.

Parameter combination	Tested feedstock	Result
1	Sieve residue powder, support structures	See figure 48a, figure 54a
2	Sieve residue powder, support structures	See figure 48b, figure 54b
3	Sieve residue powder	See figure 48c
4	Sieve residue powder	See figure 49a
5	Sieve residue powder	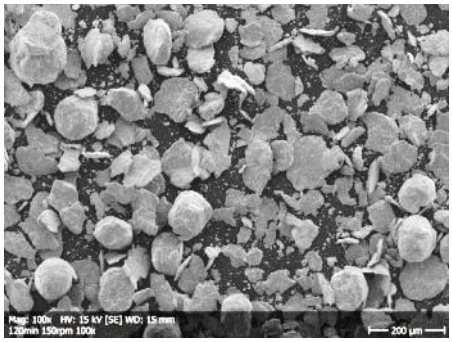 Particles crushed into flakes.
6	Support structures	See figure 55
7	Support structures	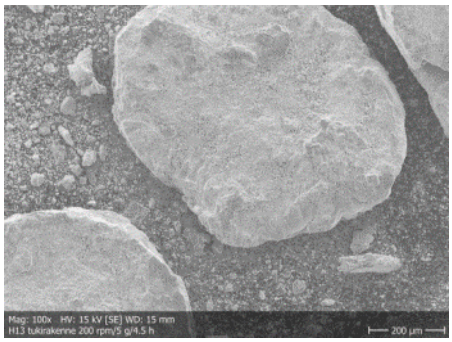 Extremely wide PSD, some particles reduced to dust, others remain visible to the naked eye.
8	Sieve residue powder	See figure 49b
9	Sieve residue powder	See figure 49c

Test results for powder and part properties.

Table III-1. Hall flowmeter test results.

Powder [-]	Measurement [-]	Flowability [s/50g]	Apparent density [g/cm^3]	Tap density [g/cm^3]
Commercial GA H13	1	21.0	3.90	4.56
	2	20.9	3.90	4.70
	3	21.0	3.90	4.75
	4	20.7	3.92	4.62
	Average	20.9	3.90	4.66
	SD	0.14	0.01	0.08
Commercial GA 316L	1	20.9	4.36	4.86
	2	21.2	4.35	4.92
	3	20.9	4.34	4.88
	4	20.9	4.34	4.89
	Average	21.0	4.35	4.89
	SD	0.15	0.01	0.02
Jet milled sieve residue H13	1	19.9	4.41	4.94
	2	19.7	4.40	4.92
	3	19.8	4.41	4.90
	4	19.7	4.40	4.88
	Average	19.8	4.40	4.91
	SD	0.10	0.01	0.02
Jet milled sieve residue 316L	1	19.2	4.44	4.96
	2	19.1	4.45	4.98
	3	19.1	4.47	4.89
	4	19.1	4.45	4.89
	Average	19.1	4.45	4.93
	SD	0.05	0.01	0.04
GA solid scrap 316L	1	21.6	4.62	5.10
	2	21.6	4.60	5.10
	3	21.5	4.60	5.06
	4	21.5	4.62	5.09
	Average	21.6	4.61	5.09
	SD	0.06	0.01	0.02

Table III-2. Particle size distribution analysis.

Powder [-]	Commercial GA H13	Commercial GA 316L	Jet milled sieve residue H13	Jet milled sieve residue 316L	GA solid scrap 316L
Size Classes [μm]	Volume Density [%]	Volume Density [%]	Volume Density [%]	Volume Density [%]	Volume Density [%]
<1.998886977	0	0	0	0	0
2.271061625	0.000134705	0	0	0	0
2.580296417	0.010351658	0	0	0	0.000092081
2.931637577	0.1055323	0	0	0	0.007992430
3.330818439	0.182950416	0	0	0	0.083029402
3.784353005	0.264469821	0	0	0	0.147736153
4.299642243	0.3395837	0	0	0	0.240339841
4.885094862	0.390063215	0	0	0	0.367482203
5.550264524	0.399567838	0	0	0	0.527334396
6.30600575	0.359554656	0	0	0	0.717071722
7.164651044	0.274461737	0	0	0	0.934781397
8.140212144	0.16106118	0	0	0	1.183830658
9.248608668	0.035743262	0	0	0	1.477110490
10.5079279	0.002504023	0.00011558	0	0	1.840211744
11.93871994	0.01358794	0.014571175	0	0	2.311307103
13.56433306	0.196449668	0.206262653	0	0.000225785	2.936375284
15.41129471	0.892358085	0.932387105	0	0.043161435	3.758866997
17.50974438	2.436485168	2.486107459	0	0.559167678	4.804577020
19.89392546	4.985824038	4.935414359	0	1.863698336	6.063807880
22.60274403	8.375104509	8.065087553	0	4.021830938	7.475159587
25.68040374	12.07178741	11.39869352	0	6.811287004	8.916985836
29.17712713	15.27277648	14.30082866	7.13E-05	9.784651508	10.212230451
33.14997522	17.13971789	16.1339351	0.010959786	12.39234173	11.150601125
37.66377863	17.10125113	16.43795768	0.1526962	14.13051316	11.528114374
42.7921955	15.09663296	15.08350137	0.658180595	14.67996087	11.198422448
48.61891352	11.63515463	12.34207149	1.860744943	13.9898911	10.123178264
55.23901552	7.630552503	8.83023194	4.078932946	12.27549296	8.403937629
62.76053114	3.946828001	5.327401188	7.360589672	9.931867548	6.280178923
71.30619965	0.600364448	2.526627112	11.29183395	7.404462483	4.086575307
81.01547288	0.027169384	0.806967936	15.01282147	5.071474511	2.177155644
92.04679085	0	0.11397251	17.48516636	3.17611275	0.829364969
104.5801673	0	0.005844294	17.91407255	1.813050871	0.153964395
118.8201271	0	4.41E-05	16.11344899	0.951901356	0.010092534
134.999044	0	0	12.60490407	0.480156378	0.000114478
153.3809324	0	0	8.401979806	0.254980012	0
174.2657557	0	0	4.586875224	0.150633526	0
197.9943213	0	0	1.892593181	0.082238672	0
224.953842	0	0	0.486850728	0.049288441	0

Table III-2 continues. Particle size distribution analysis.

Powder	Commercial GA H13	Commercial GA 316L	Jet milled sieve residue H13	Jet milled sieve residue 316L	GA solid scrap 316L
Size Classes [μm]	Volume Density [%]	Volume Density [%]	Volume Density [%]	Volume Density [%]	Volume Density [%]
255.5842545	0	0	0.035161848	0.0269342	0
290.3853991	0	0	0.000139148	0.002661495	0
329.9251753	0	0	0	3.80E-05	0
>374.8488101	0	0	0	0	0

Table III-3. Hardness tests.

Powder [-]	Measurement [-]	Hardness [HV5]	
Commercial GA 316L	1	201	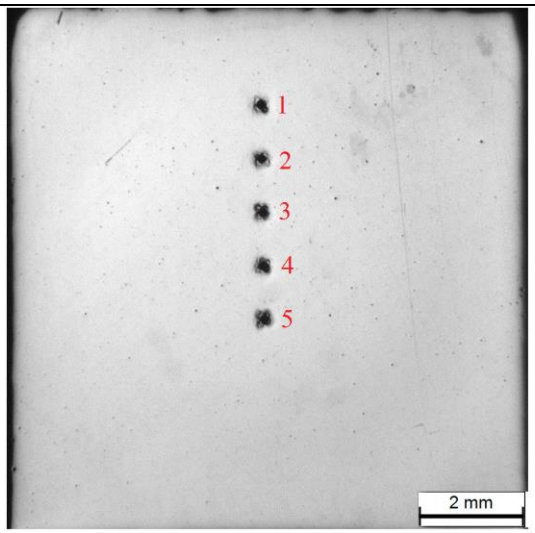
	2	198	
	3	202	
	4	202	
	5	207	
	Average	202	
	SD	3.2	
Jet milled sieve residue 316L	1	206	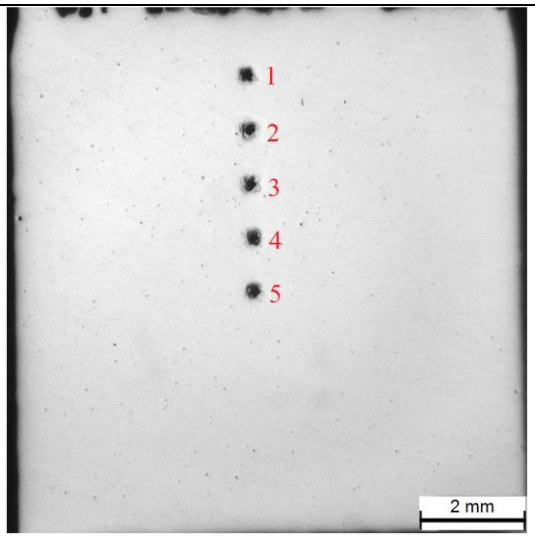
	2	206	
	3	207	
	4	208	
	5	208	
	Average	207	
	SD	1.0	
GA solid scrap 316L	1	212	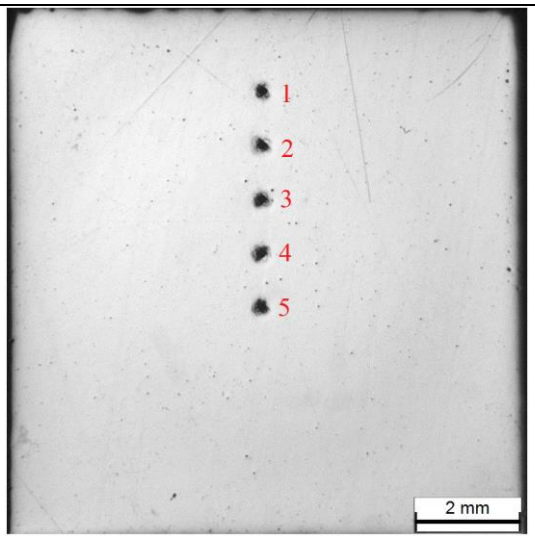
	2	205	
	3	202	
	4	207	
	5	204	
	Average	206	
	SD	3.8	

Table III-4. Porosity measurements.

Powder [-]	OM image [-]	Porosity [%]
Commercial GA 316L	1	0.092
	2	0.143
	3	0.089
	Average	0.108
	SD	0.030
Jet milled sieve residue 316L	1	0.078
	2	0.178
	3	0.111
	Average	0.122
	SD	0.051
GA solid scrap 316L	1	0.095
	2	0.101
	3	0.062
	Average	0.086
	SD	0.021

Table III-5. Tensile tests.

Powder	Specimen	R_m	$R_{p0.2}$	A
[-]	[-]	[MPa]	[MPa]	[%]
Commercial GA 316L	3	590.8	435.8	54.21
	4	579.5	424.1	51.68
	5	584.7	335.3	54.40
	6	586.4	432.9	43.86
	7	584.3	441.4	53.74
	Average	585.1	413.9	51.58
	SD	4.1	44.4	4.45
Jet milled sieve residue 316L	3	601.0	449.3	49.21
	4	611.6	470.6	52.00
	5	611.6	469.1	45.56
	6	609.7	442.4	46.11
	7	607.8	437.0	48.26
	Average	608.3	453.7	48.23
	SD	4.4	15.4	2.59
GA solid scrap 316L	3	602.0	465.7	48.87
	4	606.0	373.0	42.34
	5	-	-	-
	6	606.5	466.5	42.37
	7	600.5	457.87	49.76
	Average	603.8	440.8	45.84
	SD	3.0	45.3	4.03